Scattering Theory Approach to Electrodynamic Casimir Forces

by

Sahand Jamal Rahi

B.A., M.S. University of Pennsylvania (2005)

Submitted to the Department of Physics
in partial fulfillment of the requirements for the degree of

Doctor of Philosophy

at the

MASSACHUSETTS INSTITUTE OF TECHNOLOGY

June 2010

Author .....
Department of Physics
May 11, 2010

Certified by .....
Mehran Kardar
Professor
Thesis Supervisor

Certified by .....
Robert L. Jaffe
Professor
Thesis Supervisor

Accepted by .....
Krishna Rajagopal
Associate Department Head for Education

Scattering Theory Approach to Electrodynamic Casimir Forces

by

Sahand Jamal Rahi

Submitted to the Department of Physics
on May 11, 2010, in partial fulfillment of the
requirements for the degree of
Doctor of Philosophy

Abstract

We give a comprehensive presentation of methods for calculating the Casimir force to arbitrary accuracy, for any number of objects, arbitrary shapes, susceptibility functions, and separations. The technique is applicable to objects immersed in media other than vacuum, nonzero temperatures, and spatial arrangements in which one object is enclosed in another. Our method combines each object's classical electromagnetic scattering amplitude with universal translation matrices, which convert between the bases used to calculate scattering for each object, but are otherwise independent of the details of the individual objects. The method is illustrated by rederiving the Lifshitz formula for infinite half spaces, by demonstrating the Casimir-Polder to van der Waals cross-over, and by computing the Casimir interaction energy of two infinite, parallel, perfect metal cylinders either inside or outside one another. Furthermore, it is used to obtain recent results: the Casimir energies of i) a sphere or ii) a cylinder opposite a plate, all with finite permittivity and permeability, to leading order at large separation, iii) a parabolic cylinder opposite a plate, both representing perfect metal boundaries, and iv) a sphere or spheroid inside a cavity, where both the inside object and the cavity walls have realistic material properties.

We also examine whether electrodynamic Casimir forces can lead to stable levitation. Neglecting permeabilities, we find that any equilibrium position of objects subject to such forces is unstable if the permittivities of all objects are higher or lower than that of the enveloping medium; the former being the generic case for ordinary materials in vacuum.

Thesis Supervisor: Mehran Kardar
Title: Professor

Thesis Supervisor: Robert L. Jaffe
Title: Professor

Acknowledgments

I had a feeling that getting a PhD would not be easy. But I could not have fathomed the number of sleepless nights that I would endure to get to this point. The people, who consistently suffered with me, were my parents, Malihe and Hassan, and my sister Niloufar.

This thesis is dedicated to them.

It was absolutely not clear what I would do at MIT when I arrived. Many months before the start of my time here, during the MIT open house days, I had met and talked to the researcher I was most interested in working with, Prof. Mehran Kardar. Let us say that the conversation had not gone very well. In response to practically every future project I proposed, he suggested that I work with any number of other people at other universities. I did not understand at the time that this was him looking out for my best interest.

Given our first encounter, I actually felt more at ease to go to each and every office hour of Kardar's Statistical Mechanics class and ask any question I wanted; after all, he was clearly not interested in taking me as a student, I thought. Fate has it, though, that this is exactly what happened.

Now, having been Mehran Kardar's student for the past five years, I am not just happy I studied with him at MIT, I do not even know any other research group I would prefer. The physics questions that I was given to investigate were beautiful and relevant. His feedback was always thoughtful and useful, his record of responding to my questions and requests impeccable. I thank him for giving me room to define my own questions and to struggle with research, but investing time and energy to help me become a better instructor, speaker, and writer. I also thank him for his sense of responsibility toward me and for being my advocate when things got rough.

From today's perspective, what I had perceived to be a cool reception five years ago, was, in reality, Mehran Kardar being caring and honest; if I wanted to work on questions, which were not in his area of expertise, it would be best for me to go to those other places. But not only did Mehran Kardar always put his student's wishes

first, he also treated me with exceptional kindness and courtesy. From him I learned that even the most difficult situations with the outside world could be handled with tact and generosity.

As our research direction turned from biological and statistical physics to quantum fluctuation-induced forces, my interactions with Prof. Robert Jaffe intensified and he became my co-adviser. Robert Jaffe inspired me with his vast knowledge of physics and mathematical tricks and his emphasis on clarity in writing. I first met Robert Jaffe when he instructed my graduate quantum mechanics class. He, like Mehran Kardar, value and excel at lecturing effectively and pedagogically. The detailed properties of scattering matrices that he taught me seemed exotic and distant from my research at the time but turned out to be crucial for helping us solve the geometry problem in Casimir forces later.

Dr. Thorsten Emig was not only my most steady collaborator, he also paid for it by having to write upward of fifty letters of recommendation for me. I thank Thorsten for working with me and being a most pleasant company at work and at conferences.

From each of the other members of our group, Prof. Noah Graham, Mohammad Maghrebi, Alexander Shpunt, and Saad Zaheer I benefited through our various collaborations. Each of their individual styles made our team richer. Saad was still an undergraduate when he completed two research projects with me, which included very complicated calculations.

By working with Prof. Steven Johnson I learned how much ingenuity goes into numerical methods, and I was struck by his enthusiasm and energy.

Although Prof. Leonid Mirny and I only worked on one project, he was willing to go along with my dozens of requests for letters of recommendation. I am also indebted to Dr. Peter Virnau, who was a postdoc in our group and was instrumental in that joint project.

My friends and colleagues at MIT created an environment, in which pursuing our studies was a pleasure. Here, I met some of the most interesting people I have ever met, and I thank my friends and colleagues for our interactions over the past years: Masoud Akbarzadeh, Peyman Ahmadi, Daria Amin-Shahidi, Rana Amirtahmasebi,

Maissam Barkeshli, Orkideh Behrouzan, Hoda Bidkhori, Mihai Bora, Clement Chatelain, Davoud Ebrahimi, Hossein Fariborzi, John Frank, Alborz Geramifard, Pouyan Ghaemi, Tarun Grover, Nan Gu, Christoph Haselwandter, Hila Hashemi, Pedram Hekmati, Mark Hertzberg, Hamid Hezari, Tilke Judd, Florian Kämpfer, Vijay Kumar, Danial Lashkari, Alexander McCauley, Kaveh Milaninia, Ramis Movassagh, Shamim Nemati, Alejandro Rodriguez, Alberto Rosso, Mark Rudner, Saeed Saremi, Antonello Scardicchio, Reza Sharifi, Rouzbeh Shahsavari, Brian Swingle, Hadi Tavakoli Nia, Anahita Tafvizi, Abolhassan Vaezi, and Andrea Zoia.

Knowing that my uncle Reza, his wife Simin, my uncle Amir, and his girlfriend Feri were always there to help if I ended up in a non-academic disaster, on the other hand, helped my parents go to bed with fewer worries. I thank them for helping ensure that I had everything I needed.

Contents

List of Figures

List of Tables

Chapter 1

Introduction

Neutral objects exert a force on one another through electromagnetic fields even if they do not possess permanent multipole moments. Materials that couple to the electromagnetic field alter the spectrum of the field's quantum and thermal fluctuations. The resulting change in energy depends on the relative positions of the objects, leading to a fluctuation-induced force, usually called the Casimir force. Alternatively, one can regard the cause of these forces to be spontaneous charges and currents, which fluctuate in and out of existence in the objects due to quantum mechanics. The name 'Van der Waals force' is sometimes used interchangeably but it usually refers to the Casimir force in the regime where objects are close to one another so that the speed of light is effectively infinite. The Casimir force has been the subject of precision experimental measurements [1, 2, 3, 4, 5, 6, 7, 8, 9, 10, 11, 12, 13, 14, 15, 16, 17] and can influence the operation of nanoscale devices [5, 18], see reference [19] for a review of the experiments.

Casimir and Polder calculated the fluctuation-induced force on a polarizable atom in front of a perfectly conducting plate and between two polarizable atoms, both to leading order at large separation, and obtained a simple result depending only on the atoms' static polarizabilities [20]. Casimir then extended this result to his famous calculation of the pressure on two perfectly conducting parallel plates [21]. Feinberg and Sucher [22, 23] generalized the result of Casimir and Polder to include both electric and magnetic polarizabilities. Lifshitz, Dzyaloshinskii, and Pitaevskii

extended Casimir's result for parallel plates by incorporating nonzero temperature, permittivity, and permeability into a general formula for the pressure on two infinite half-spaces separated by a gap [24, 25, 26, 27, 28].

While these early theoretical predictions of the Casimir force applied only to infinite planar geometries (or atoms), the first precision experiments measured the force between a plate and a sphere. This geometry was preferred because keeping two plane surfaces parallel introduces additional challenges for the experimentalist. To compare the measurements with theory, however, a makeshift solution had to be used; the Casimir force in the so-called Proximity Force Approximation (PFA) is calculated by integrating the Casimir pressure of two parallel half spaces over the area that the sphere and the plate expose to one another [29]. In general, this simple approximation does not capture curvature corrections but in many experimental situations, it performs surprisingly well, as can be seen in Fig. 1, for example; at the small separations at which the force is typically probed in precision measurements the sphere and the plate surfaces are well approximated by a collection of infinitesimal parallel plates.

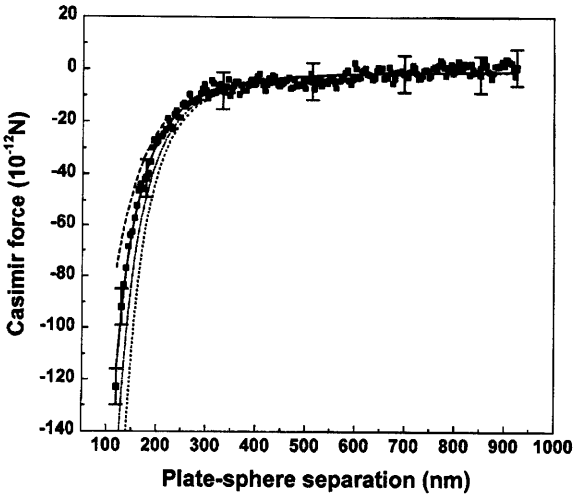

Figure 1-1: Force between a sphere of radius $\approx 100\mu$m and a plate, both coated with Au-Pd [2]. Square dots represent measurements, the solid line is a theoretical computation using the PFA approximation and taking into account roughness and finite temperature corrections as well as material properties. The other lines represent calculations, where some of these corrections are not taken into account.

Clearly, for larger separations and for surfaces that are not smooth the PFA must

fail. For example, in measurements of the Casimir force between a sphere and a trench array significant discrepancies were found [14]. And even for the regimes in which the PFA yields good estimates it would be desirable to know what the corrections to it are.

In order to study Casimir forces in more general geometries, it turns out to be advantageous to describe the influence of an arrangement of objects on the electromagnetic field by the way they scatter electromagnetic waves. Here, we derive and apply a representation of the Casimir energy, first developed with various limitations in Refs. [30, 31] and then fully generalized in Ref. [32], that characterizes each object by its on-shell electromagnetic scattering amplitude. The separations and orientations of the objects are encoded in universal translation matrices, which describe how a solution to the source-free Maxwell's equations in the basis appropriate to one object looks when expanded in the basis appropriate to another. The translation matrices depend on the displacement and orientation of coordinate systems, but not on the nature of the objects themselves. The scattering amplitudes and translation matrices are then combined in a simple algorithm that allows efficient numerical and, in some cases, analytical calculations of Casimir forces and torques for a wide variety of geometries, materials, and external conditions. The formalism applies to a wide variety of circumstances, including:

- n arbitrarily shaped objects, whose surfaces may be smooth or rough or may include edges and cusps;

- objects with arbitrary linear electromagnetic response, including frequency-dependent, lossy electric permittivity and magnetic permeability tensors;

- objects separated by vacuum or by a medium with uniform, frequency-dependent isotropic permittivity and permeability;

- zero or nonzero temperature;

- and objects outside of one another or enclosed in each other.

These ideas build on a range of previous related work, an inevitably incomplete subset of which is briefly reviewed here: Scattering theory methods were first applied to the parallel plate geometry, when Kats reformulated Lifshitz theory in terms of reflection coefficients [33]. Jaekel and Reynaud derived the Lifshitz formula using reflection coefficients for lossless infinite plates [34] and Genet, Lambrecht, and Reynaud extended this analysis to the lossy case [35]. Lambrecht, Maia Neto, and Reynaud generalized these results to include non-specular reflection [36].

Around the same time as Kats's work, Balian and Duplantier developed a multiple scattering approach to the Casimir energy for perfect metal objects and used it to compute the Casimir energy at asymptotically large separations [37, 38] at both zero and nonzero temperature. In their approach, information about the conductors is encoded in a local surface scattering kernel, whose relation to more conventional scattering formalisms is not transparent, and their approach was not pursued further at the time. One can find multiple scattering formulas in an even earlier article by Renne [39], but scattering is not explicitly mentioned, and the technique is only used to rederive older results.

Another scattering-based approach has been to express the Casimir energy as an integral over the density of states of the fluctuating field, using the Krein formula [40, 41, 42] to relate the density of states to the $\mathcal{S}$-matrix for scattering from the ensemble of objects. This $\mathcal{S}$-matrix is difficult to compute in general. In studying many-body scattering, Henseler and Wirzba connected the $\mathcal{S}$-matrix of a collection of spheres [43] or disks [44] to the objects' individual $\mathcal{S}$-matrices, which are easy to find. Bulgac, Magierski, and Wirzba combined this result with the Krein formula to investigate the scalar and fermionic Casimir effect for disks and spheres [45, 46, 47]. Casimir energies of solitons in renormalizable quantum field theories have been computed using scattering theory techniques that combine analytic and numerical methods [48].

Bordag, Robaschik, Scharnhorst, and Wieczorek [49, 50] introduced path integral methods to the study of Casimir effects and used them to investigate the electromagnetic Casimir effect for two parallel perfect metal plates. Li and Kardar used

similar methods to study the scalar thermal Casimir effect for Dirichlet, Neumann, and mixed boundary conditions [51, 52]. The quantum extension was developed further by Golestanian and Kardar [53, 54] and was subsequently applied to the quantum electromagnetic Casimir effect by Emig, Hanke, Golestanian, and Kardar, who studied the Casimir interaction between plates with roughness [55] and between deformed plates [56]. (Techniques developed to study the scalar Casimir effect can be applied to the electromagnetic case for perfect metals with translation symmetry in one spatial direction, since then the electromagnetic problem decomposes into two scalar ones.) Finally, the path integral approach was connected to scattering theory by Emig and Buescher [57].

Closely related to the work we present here is that of Kenneth and Klich, who expressed the data required to characterize Casimir fluctuations in terms of the transition $\mathbb{T}$-operator for scattering of the fluctuating field from the objects [58]. Their abstract representation made it possible to prove general properties of the sign of the Casimir force. In Refs. [30, 31], we developed a framework in which this abstract result can be applied to concrete calculations. In this approach, the $\mathbb{T}$-operator is related to the scattering amplitude for each object individually, which in turn is expressed in an appropriate basis of multipoles. While the $\mathbb{T}$-operator is in general "off-shell," meaning it has matrix elements between states with different spatial frequencies, the scattering amplitudes are the "on-shell" matrix elements of this operator between states of equal spatial frequency.[1] So, it is not the $\mathbb{T}$-operator itself that connects, say, outgoing and standing waves in the case of outside scattering but its on-shell matrix elements, the scattering amplitudes. In this approach, the objects can have any shape or material properties, as long as the scattering amplitude can be computed in a multipole expansion (or measured). The approach can be regarded as a concrete implementation of the proposal emphasized by Schwinger [59] that the fluctuations of the electromagnetic field can be traced back to charge and current fluctuations on

[1]Because of this relationship, these scattering amplitudes are also referred to as elements of the *T-matrix*. In standard conventions, however, the T-matrix differs from the matrix elements of the $\mathbb{T}$-operator by a basis-dependent constant, so we will use the term "scattering amplitude" to avoid confusion.

the objects. This formalism has been applied and extended in a number of Casimir calculations [60, 61, 62, 63, 64, 65].

The basis in which the scattering amplitude for each object is supplied is typically associated with a coordinate system appropriate to the object. Of course a plane, a cylinder, or a sphere would be described in Cartesian, cylindrical, or spherical coordinates, respectively. However, any compact object can be described, for example, in spherical coordinates, provided that the matrix of scattering amplitudes can be either calculated or measured in that coordinate system. There are a limited number of coordinate systems in which such a partial wave expansion is possible, namely those for which the vector Helmholtz equation is separable. The translation matrices for common separable coordinate systems, obtained from the free Green's function, are supplied in Appendix C. For typical cases, the final computation of the Casimir energy can be performed on a desktop computer for a wide range of separations. Asymptotic results at large separation can be obtained analytically.

The primary limitation of the method is on the distance between objects, since the basis appropriate to a given object may become impractical as two objects approach. For small separations, sufficient accuracy can only be obtained if the calculation is taken to very high partial wave order. (Vastly different scales are problematic for numerical evaluations in general.) In the case of two spheres, the scattering amplitude is available in a spherical basis, but as the two spheres approach, the Casimir energy is dominated by waves near the point of closest approach [66]. As the spheres come into contact an infinite number of spherical waves are needed to capture the dominant contribution (see Section 2.2 for further discussion). A particular basis may also be fundamentally inappropriate at small separations. For instance, if the interaction of two elliptic cylinders is expressed in an ordinary cylindrical basis, when the elliptic cylinders are close enough one may not fit inside the smallest circular cylinder that encloses the other. In that case the cylindrical basis would not "resolve" the two objects (although an elliptic cylindrical basis would; see Section 2.2). Finally, for a variety of conceptual and computational reasons, we are limited to linear electromagnetic response.

In spirit and in mathematical form our final result resembles similar expressions obtained in surface integral equation methods used in computational electrodynamics [67]. Using such a formulation, in which the unknowns are currents and fields on the objects, one can compute the Casimir energy using more general basis functions, e.g., localized basis functions associated with a grid or mesh, giving rise to finite element and boundary elements methods [63].

In addition to an efficient computational approach, the scattering formalism has provided the basis for proving general theorems regarding Casimir forces. The seemingly natural question whether the force is attractive or repulsive turns out to be an ill-defined or, at least, a tricky one on closer inspection. When, for example, many bodies are considered, the direction of the force on any one object depends, of course, on which other object's perspective one takes. Even for two objects, "attractive" forces can be arranged to appear as a "repulsive" force, as in the case of two interlocking combs [68]. To avoid such ambiguous situations one can restrict oneself to analyzing two objects that are separable by a plane. Even here, it has turned out that a simple criterium for the direction of the force could not be found. Based on various calculations for simple geometries it was thought that the direction of the force can be predicted based on the relative permittivities and permeabilities of the objects and the medium. Separating materials into two groups, with *(i)* permittivity higher than the medium or permeability lower than the medium ($\epsilon > \epsilon_M$ and $\mu \leq \mu_M$), or *(ii)* the other way around ($\epsilon < \epsilon_M$ and $\mu \geq \mu_M$), Casimir forces had been found to be attractive between members of the same group and repulsive for different types in the geometries considered. However, a recent counterexample [69] shows that this is not always true. A rigorous theorem, which states that Casimir forces are always attractive, exists only for the special case of mirror symmetric arrangements of objects. It was proven first with a $\mathbb{T}$-operator formalism [58], similar to our approach used here, and later using reflection positivity [70]. We have taken an alternative characterization of the force as fundamental, namely, whether it can produce stable equilibria [71]. Here, the categorization of materials into the two groups is meaningful since objects made of materials of the same type cannot produce stable levitation. One

practical consequence of this theorem is that it reveals that many current proposals for producing levitation using metamaterials cannot succeed.

To illustrate the general formulation, we provide some sample applications, including the closed-form expressions for computing the interaction of a plate and a sphere with finite, uniform, frequency-dependent electric permittivity and magnetic permeability. We present the Casimir interaction energy explicitly at asymptotically large separations in terms of the zero frequency permittivities and permeabilities of the objects. Although most experiments have centered around the sphere-plate configuration [1, 2, 3, 72, 5, 73, 74, 8, 9, 10, 12, 13], it is only recently that the force between a dielectric sphere and an idealized metallic plate has been obtained for all distances [75]. Subsequently, this result has been extended to the situation where both objects are described by the plasma model [76], or also the Drude model, taking into account finite temperature corrections [77, 78]. In addition, we present the Casimir interaction energy of a plate and a cylinder at asymptotically large distances in terms of the two objects' zero frequency permittivities and permeabilities. Results beyond the leading order using our closed-form formulation are not explicitly included, but all the essential formulas are contained here. These results extend the perfect metal cylinder and plate results presented in Ref. [79]. Furthermore, we analyze the Casimir effect for a parabolic cylinder opposite a plate when both represent perfect metal material boundary conditions [80]. We find that the Casimir force does not vanish in the limit of an infinitesimally thin parabola, where a half plate is arranged above an infinite plate, and we compute the edge effect.

Another class of geometries that is treated here consists of configurations, in which one object is enclosed inside another. We rederive results for one perfect metal cylinder inside of another one [81] (in addition to the result for two cylinders outside of one another [82]). Also, we consider the case of a finite sphere or a small spheroid inside a spherical cavity, and a small spheroid inside a slightly deformed spherical cavity [83, 84]. In these situations, we show that one can achieve stable levitation for a compact object due to the Casimir force alone, when the conditions of the theorem regarding instability are violated. We also find that Casimir torques exhibit an

unexpected and rich dependence on the electromagnetic properties of the materials.

The thesis is organized as follows: In Section 2.1 we review the derivation of the ground state energy of a field theory using path integrals. In Section 2.2 we expand the free electromagnetic Green's functions in terms of regular and outgoing waves, taking into account that the pairs of waves in the expansion are evaluated with respect to two different coordinate systems. This analysis yields the translation matrices. Section 2.3 provides an overview of elements of scattering theory we will use, including the connection between the $\mathbb{T}$-operator and the scattering amplitude. In Section 2.4 the path integral expression for the energy is re-expressed in terms of the results of the preceding two sections, yielding the main result, Eq. (2.4.13). The theorem regarding stability is derived in Section 3.1. In Section 3.2 sample applications are presented: A short derivation of the Lifshitz formula, the cross-over between van der Waals and Casimir regimes for two atoms, a general derivation of previous results for cylinders, and recent results for the energy between a dielectric sphere or cylinder and a dielectric slab, between a parabolic cylinder and a plate, as well as between an object and the surrounding cavity walls. Some future research directions are discussed in Section 4.1, finally.

Chapter 2

Methods

2.1 Casimir energy from field theory

2.1.1 Electromagnetic Lagrangian and action

We consider the Casimir effect for objects without free charges and currents but with nonzero electric and magnetic susceptibilities. The macroscopic electromagnetic Lagrangian density is

$$\mathcal{L} = \frac{1}{2}(\mathbf{E}\cdot\mathbf{D} - \mathbf{B}\cdot\mathbf{H}). \tag{2.1.1}$$

The electric field $\mathbf{E}(t,\mathbf{x})$ and the magnetic field $\mathbf{B}(t,\mathbf{x})$ are related to the fundamental four-vector potential A^μ by $\mathbf{E} = -c^{-1}\partial_t\mathbf{A} - \boldsymbol{\nabla}A^0$ and $\mathbf{B} = \boldsymbol{\nabla}\times\mathbf{A}$. We treat stationary objects whose responses to the electric and magnetic fields are linear. For such materials, the $\mathbf{D}$ and $\mathbf{B}$ fields are related to the $\mathbf{E}$ and $\mathbf{H}$ fields by the convolutions $\mathbf{D}(t,\mathbf{x}) = \int_{-\infty}^{\infty} dt'\,\epsilon(t',\mathbf{x})\mathbf{E}(t-t',\mathbf{x})$ and $\mathbf{B}(t,\mathbf{x}) = \int_{-\infty}^{\infty} dt'\,\mu(t',\mathbf{x})\mathbf{H}(t-t',\mathbf{x})$ in time. We consider local, isotropic permittivity and permeability, although our derivation can be adapted to apply to non-local and non-isotropic media simply by substituting the appropriate non-local and tensor permittivity and permeability functions. A more formal derivation of our starting point Eq. (2.1.1), which elucidates the causality properties of the permeability and permittivity response functions, is given in Appendix A. An alternative route to seeing that this Lagrangian density,

even for dispersive media, is the correct one for use inside a path integral is presented in Ref. [85].

We define the quantum-mechanical energy through the path integral, which sums all configurations of the electromagnetic fields constrained by periodic boundary conditions in time between 0 and T. Outside of this time interval the fields are periodically continued. Substituting the Fourier expansions of the form $\mathbf{E}(t,\mathbf{x}) = \sum_{n=-\infty}^{\infty} \mathbf{E}(\omega_n,\mathbf{x})e^{-i\omega_n t}$ with $\omega_n = 2\pi n/T$, we obtain the action

$$S(T) = \frac{1}{2}\int_0^T dt \int d\mathbf{x}\ (\mathbf{E}\cdot\mathbf{D} - \mathbf{B}\cdot\mathbf{H}) = \frac{1}{2}T\sum_{n=-\infty}^{\infty}\int d\mathbf{x}\left(\mathbf{E}^*\cdot\epsilon\mathbf{E} - \mathbf{B}^*\cdot\mu^{-1}\mathbf{B}\right), \tag{2.1.2}$$

where ϵ, $\mathbf{E}$, μ, and $\mathbf{B}$ on the right-hand side are functions of position $\mathbf{x}$ and frequency ω_n, and we have used $\mathbf{D}(\omega,\mathbf{x}) = \epsilon(\omega,\mathbf{x})\mathbf{E}(\omega,\mathbf{x})$ and $\mathbf{H}(\omega,\mathbf{x}) = \frac{1}{\mu(\omega,\mathbf{x})}\mathbf{B}(\omega,\mathbf{x})$.

From the definition of the fields $\mathbf{E}$ and $\mathbf{B}$ in terms of the vector potential A^μ, we have $\boldsymbol{\nabla}\times\mathbf{E} = i\frac{\omega}{c}\mathbf{B}$, which enables us to eliminate $\mathbf{B}$ in the action,

$$S(T) = \frac{1}{2}T\sum_{n=-\infty}^{\infty}\int d\mathbf{x}\left[\mathbf{E}^*\cdot\left(\mathbb{I} - \frac{c^2}{\omega_n^2}\boldsymbol{\nabla}\times\boldsymbol{\nabla}\times\right)\mathbf{E} - \frac{c^2}{\omega_n^2}\mathbf{E}^*\cdot\mathbb{V}\,\mathbf{E}\right], \tag{2.1.3}$$

where

$$\mathbb{V} = \mathbb{I}\,\frac{\omega_n^2}{c^2}\left(1-\epsilon(\omega_n,\mathbf{x})\right) + \boldsymbol{\nabla}\times\left(\frac{1}{\mu(\omega_n,\mathbf{x})} - 1\right)\boldsymbol{\nabla}\times \tag{2.1.4}$$

is the potential operator and we have restored the explicit frequency dependence of ϵ and μ. The potential operator is nonzero only at those points in space where the objects are located ($\epsilon \neq 1$ or $\mu \neq 1$).

In the functional integral we will sum over configurations of the field A^μ. This sum must be restricted by a choice of gauge, so that it does not include the infinitely redundant gauge orbits. We will choose to work in the gauge $A^0 = 0$, although of course no physical results depend on this choice.

2.1.2 Casimir energy of a quantum field

We use standard tools to obtain a functional integral expression for the ground state energy of a quantum field in a fixed background described by $\mathbb{V}(\omega, \mathbf{x})$. The overlap between the initial state $|\mathbf{E}_a\rangle$ of a system with the state $|\mathbf{E}_b\rangle$ after time T can be expressed as a functional integral with the fields fixed at the temporal boundaries [86],

$$\langle \mathbf{E}_b | e^{-iHT\hbar} | \mathbf{E}_a \rangle = \int \mathcal{D}\mathbf{A} \, |_{\substack{\mathbf{E}(t=0)=\mathbf{E}_a \\ \mathbf{E}(t=T)=\mathbf{E}_b}} \, e^{\frac{i}{\hbar} S[T]}, \tag{2.1.5}$$

where $S(T)$ is the action of Eq. (2.1.2) with the time integrals taken between zero and T, and H is the corresponding Hamiltonian.

If the initial and final states are set equal and summed over, the resulting functional integration defines the Minkowski space functional integral

$$\mathcal{Z}(T) \equiv \sum_a \langle \mathbf{E}_a | e^{-iHT/\hbar} | \mathbf{E}_a \rangle = \text{tr } e^{-iHT/\hbar} = \int \mathcal{D}\mathbf{A} \, e^{\frac{i}{\hbar} S[T]}, \tag{2.1.6}$$

which depends on the time T and the background potential $\mathbb{V}(\omega, \mathbf{x})$. The partition function that describes this system at temperature $1/\beta$ is defined by

$$Z(\beta) = \mathcal{Z}(-i\hbar\beta) = \text{tr } e^{-\beta H}, \tag{2.1.7}$$

and the free energy F of the field is

$$F(\beta) = -\frac{1}{\beta} \log Z(\beta). \tag{2.1.8}$$

The limit $\beta \to \infty$ projects the ground state energy out of the trace,

$$\mathcal{E}_0 = F(\beta = \infty) = -\lim_{\beta \to \infty} \frac{1}{\beta} \log Z(\beta). \tag{2.1.9}$$

The unrenormalized energy $\mathcal{E}_0$ generally depends on the ultraviolet cutoff, but cutoff-dependent contributions arise from the objects individually and do not depend on their separations or orientations. Such terms can also arise after renormalization if

objects are assumed to constrain electromagnetic waves with arbitrarily high frequencies (for example, if the fields are forced to vanish on a surface). Such boundary conditions should be regarded as artificial idealizations; in reality, when the wavelengths of the electromagnetic waves become shorter than the length scales that characterize the interactions of the material, the influence of the material on the waves vanishes [87]. Accordingly, the potential $\mathbb{V}$ should vanish for real materials in the high-frequency limit. Since we are only interested in energy *differences*, we can remove these divergences by subtracting the ground state energy of the system when the objects are in some reference configuration. In most cases we will take this configuration to have the objects infinitely far apart, but when calculating Casimir energies for one object inside another, some other configuration must be used. We denote the partition function for this reference configuration by $\overline{Z}$. In this way we obtain the Casimir energy,

$$\mathcal{E} = -\lim_{\beta\to\infty} \frac{1}{\beta} \log Z(\beta)/\overline{Z}(\beta). \tag{2.1.10}$$

Throughout our calculation of $\mathcal{E}$, we will thus be able to neglect any overall factors that are independent of the relative positions and orientations of the objects.

2.1.3 Euclidean Electromagnetic Action

By replacing the time T by $-i\hbar\beta$, we transform the Minkowski space functional integral $\mathcal{Z}(T)$ into the partition function $Z(\beta)$. In $A^0 = 0$ gauge, the result is simply to replace the frequencies $\omega_n = \frac{2\pi n}{T}$ in Eq. (2.1.4) by $i\frac{2\pi n}{\hbar\beta} = ic\kappa_n$, where κ_n is the n^{th} Matsubara frequency divided by c. (In other gauges the temporal component A^0 of the vector field must be rotated too.)

The Lagrangian is quadratic, so the modes with different κ_n decouple and the partition function decomposes into a product of partition functions for each mode. Since the electromagnetic field is real, we have $\mathbf{E}^*(\omega) = \mathbf{E}(-\omega)$ on the real axis. We can thus further simplify this decomposition on the imaginary axis by considering $\kappa \geq 0$ only, but allowing $\mathbf{E}$ and $\mathbf{E}^*$ to vary independently in the path integral. Restricting to positive κ is possible because the response functions $\epsilon(ic\kappa, \mathbf{x})$ and $\mu(ic\kappa, \mathbf{x})$ are

invariant under a change of sign in $ic\kappa$, as shown Appendix A. In the limit $\beta \to \infty$, the sum $\sum_{n\geq 0}$ turns into an integral $\frac{\hbar c\beta}{2\pi}\int_0^\infty d\kappa$, and we have

$$\mathcal{E}_0 = -\frac{\hbar c}{2\pi}\int_0^\infty d\kappa \log Z(\kappa), \tag{2.1.11}$$

where

$$Z(\kappa) = \int \mathcal{D}\mathbf{A}\mathcal{D}\mathbf{A}^* \exp\left[-\beta \int d\mathbf{x}\, \mathbf{E}^* \cdot \left(\mathbb{I} + \frac{1}{\kappa^2}\boldsymbol{\nabla}\times\boldsymbol{\nabla}\times\right)\mathbf{E} + \frac{1}{\kappa^2}\mathbf{E}^* \cdot \mathbb{V}(ic\kappa, \mathbf{x})\,\mathbf{E}\right], \tag{2.1.12}$$

$$\mathbb{V}(ic\kappa, \mathbf{x}) = \mathbb{I}\,\kappa^2\left(\epsilon(ic\kappa, \mathbf{x}) - 1\right) + \boldsymbol{\nabla}\times\left(\frac{1}{\mu(ic\kappa, \mathbf{x})} - 1\right)\boldsymbol{\nabla}\times\,. \tag{2.1.13}$$

The potential $\mathbb{V}(ic\kappa, \mathbf{x})$ is real for real κ, even though ϵ and μ can have imaginary parts for real frequencies ω. Our goal is now to manipulate $Z(\kappa)$ in Eq. (2.1.12) so that it is computable from the scattering properties of the objects.

2.2 Green's function expansions and translation formulas

2.2.1 The free Green's function

The free Green's function and its representations in various coordinate systems are crucial to our formalism. The free electromagnetic field ($\mathbb{V} = 0$) obeys equations of motion obtained by extremizing the corresponding action, Eq. (2.1.2),

$$\left(-\mathbb{I}\frac{\omega^2}{c^2} + \boldsymbol{\nabla}\times\boldsymbol{\nabla}\times\right)\mathbf{E}(\omega, \mathbf{x}) = 0. \tag{2.2.1}$$

We will employ the electromagnetic dyadic Green's function $\mathbb{G}_0$, defined by

$$\left(-\mathbb{I}\frac{\omega^2}{c^2} + \boldsymbol{\nabla}\times\boldsymbol{\nabla}\times\right)\mathbb{G}_0(\omega, \mathbf{x}, \mathbf{x}') = \mathbb{I}\delta^{(3)}(\mathbf{x} - \mathbf{x}'), \tag{2.2.2}$$

written here in the position space representation. It is easy to express $\mathbb{G}_0$ as a Fourier transform,

$$\mathbb{G}_0(\omega, \mathbf{x}, \mathbf{x}') = \int \frac{d\mathbf{k}}{(2\pi)^3} \frac{e^{i\mathbf{k}\cdot(\mathbf{x}-\mathbf{x}')}}{k^2 - (\omega/c + i\epsilon)^2} \left(\mathbb{I} - \frac{c^2}{\omega^2} \mathbf{k} \otimes \mathbf{k} \right) \tag{2.2.3}$$

where the displacement of the singularities at $k = \pm\frac{\omega}{c}$ corresponds to outgoing wave boundary conditions at infinity. By replacing the factors of $\mathbf{k}$ by gradients, $\mathbb{G}_0$ may be expressed in terms of elementary functions,

$$\mathbb{G}_0(\omega, \mathbf{x}, \mathbf{x}') = \left(\mathbb{I} - \frac{c^2}{\omega^2} \boldsymbol{\nabla} \otimes \boldsymbol{\nabla}' \right) \frac{e^{i\omega|\mathbf{x}-\mathbf{x}'|/c}}{4\pi|\mathbf{x} - \mathbf{x}'|}. \tag{2.2.4}$$

In this representation it is easy to see that $\mathbb{G}_0$ is transverse, *i.e.* $\boldsymbol{\nabla} \cdot \mathbb{G}_0(\mathbf{x}, \mathbf{x}', \omega) = \mathbb{G}_0(\mathbf{x}, \mathbf{x}', \omega) \cdot \overleftarrow{\boldsymbol{\nabla}}' = 0$, for $\mathbf{x} \neq \mathbf{x}'$. $\mathbb{G}_0$ is not transverse at $\mathbf{x} = \mathbf{x}'$, as can be seen by taking the divergence of Eq. (2.2.2).

We work in coordinate systems in which we can use separation of variables and employ a spectral representation of $\mathbb{G}_0(\mathbf{x}, \mathbf{x}', \omega)$. That is, we represent the Green's function through the complete set of non-singular ("regular"), transverse solutions to the differential equation, Eq. (2.2.1),

$$\mathbf{E}_\alpha^{\text{reg}}(\omega, \mathbf{x}) = \langle \mathbf{x} | \mathbf{E}_\alpha^{\text{reg}}(\omega) \rangle, \tag{2.2.5}$$

represented formally by the eigenstate kets $|\mathbf{E}_\alpha^{\text{reg}}(\omega)\rangle$, where the generalized index α labels the scattering channel, including the polarization. For example, for spherical wave functions it represents the angular momentum quantum numbers (l, m) and the polarization E or M. We will choose to normalize these states in accord with standard conventions in electromagnetic scattering theory; as a result they are not necessarily normalized according to the conventions typically used in quantum mechanics. A list of the eigenfunctions for various common bases is given in Appendix B. The Green's functions can be expressed as the coordinate-space matrix element of the operator

$$\mathbb{G}_0(\omega) = \int_0^\infty d\omega' \sum_\alpha \mathcal{C}_\alpha(\omega') \frac{|\mathbf{E}_\alpha^{\text{reg}}(\omega')\rangle \langle \mathbf{E}_\alpha^{\text{reg}}(\omega')|}{(\omega'/c)^2 - (\omega/c + i\epsilon)^2}, \tag{2.2.6}$$

where the $i\epsilon$ has again been included to implement outgoing wave boundary conditions, so that the Green's function is causal.[1] We use the symbol $\mathbb{G}_0$ to represent both the matrix-valued representation of the Green's function in position space, Eq. (2.2.2), and the abstract Hilbert space operator, Eq. (2.2.6). The coefficients $\mathcal{C}_\alpha(\omega')$ are inserted because of our choice of normalization and ensure that

$$\int_0^\infty d\omega' \sum_\alpha \mathcal{C}_\alpha(\omega') |\mathbf{E}_\alpha^{\rm reg}(\omega')\rangle \langle \mathbf{E}_\alpha^{\rm reg}(\omega')| = \mathbb{I}. \tag{2.2.7}$$

It is also useful to represent the Green's function in a different way, in which one of the separable coordinates is identified as the "radial" variable and treated differently from the remaining coordinates. We let ξ_1 represent this coordinate and denote the remaining coordinates as ξ_2 and ξ_3. We introduce the "outgoing" solution in ξ_1, which is in the same scattering channel as the corresponding regular solution but obeys outgoing wave boundary conditions as $\xi_1 \to \infty$. It is linearly independent of the regular solution. The full outgoing solution is then obtained by multiplying the outgoing solution for ξ_1 by the regular solutions for ξ_2 and ξ_3. We can then express one of the regular wave functions in the position space representation of Eq. (2.2.6) as a sum of the outgoing solution for ω and the outgoing solution for $-\omega$. By specifying explicitly which of the two arguments of the Green's function has a greater value of ξ_1, we can carry out the ω integral for each of these two terms separately by closing the contour in the appropriate half-plane [88], and obtain

$$\mathbb{G}_0(\omega, \mathbf{x}, \mathbf{x}') = \sum_\alpha C_\alpha(\omega) \begin{cases} \mathbf{E}_\alpha^{\rm out}(\omega, \xi_1, \xi_2, \xi_3) \otimes \mathbf{E}_\alpha^{\rm reg*}(\omega, \xi_1', \xi_2', \xi_3') & \text{if } \xi_1(\mathbf{x}) > \xi_1'(\mathbf{x}') \\ \mathbf{E}_\alpha^{\rm reg}(\omega, \xi_1, \xi_2, \xi_3) \otimes \mathbf{E}_\alpha^{\rm in*}(\omega, \xi_1', \xi_2', \xi_3') & \text{if } \xi_1(\mathbf{x}) < \xi_1'(\mathbf{x}') \end{cases}. \tag{2.2.8}$$

In this form, the outgoing wave boundary condition is implemented explicitly. Since the Green's function is written as a linear combination of solutions to the free wave

[1] The coordinate space matrix element of Eq. (2.2.6) is transverse for all $\mathbf{x}$ and $\mathbf{x}'$, and therefore differs from the Green's function defined in Eq. (2.2.4) by terms local at $\mathbf{x} = \mathbf{x}'$. Since we never employ $\mathbb{G}_0$ at coincident points, we ignore this subtlety [88]. The use of the retarded Green's function not only makes sense physically, but is also dictated by the imaginary-frequency formalism, just as is the case for the response functions ϵ and μ. It is the *retarded* response functions that are analytically continued in the frequency domain to positive imaginary frequency, as shown in Appendix A.

equation, it clearly satisfies Eq. (2.2.2) for $\mathbf{x} \neq \mathbf{x}'$. The normalization constant $C_\alpha(\omega)$, which is determined using the Wronskian of the regular and outgoing solutions and the completeness relationship for the regular solutions in ξ_2 and ξ_3, sets the correct "jump condition" for $\mathbf{x} = \mathbf{x}'$.

The outgoing solution is typically singular at $\xi_1 = 0$, but the Green's function with distinct arguments does not encounter that region, because the outgoing function is always evaluated for the larger argument. For example, in a spherical system the outgoing solution could take the form of a spherical Hankel function $h_l^{(1)}(kr) \sim \frac{e^{ikr}}{kr}$ with $k = \omega/c$, which obeys outgoing wave boundary conditions, is singular at the origin, and is independent of the corresponding regular solution $j_l(kr)$.

We will usually work on the imaginary k-axis, in which case we will encounter the corresponding modified special functions. We continue to label these functions as "regular," "outgoing," and "incoming," even though they now increase exponentially for large ξ_1 for incoming and regular waves and decrease exponentially for outgoing waves. We also note that it may be convenient to redefine the wave functions to match the standard form of the corresponding modified functions, and to assign different phases to the two polarizations. The prefactor $C_\alpha(\omega)$ is then correspondingly redefined as $C_\alpha(\kappa)$ to incorporate these changes. A list of Green's function expansions in various common bases is given in Appendix B.

For a Cartesian coordinate system some of the previous statements have to be adapted slightly. We will take one of the Cartesian coordinates, say z, to be the "radial" coordinate, as required by the context. For example, z might be the direction normal to the planar surface of a dielectric. The solutions are then given in terms of plane waves, $e^{ik_x x + ik_y y \pm i\sqrt{(\omega/c)^2 - \mathbf{k}_\perp^2} z}$, where $\mathbf{k}_\perp$ is the momentum perpendicular to the $\hat{\mathbf{z}}$ direction. All are regular and all contribute in the integral representation of Eq. (2.2.6). After analytic continuation to imaginary frequency, the free Green's function in Cartesian coordinates is expressed by the above formula if we identify outgoing solutions with plane wave functions that are exponentially decreasing in the $+\hat{\mathbf{z}}$ direction, $e^{ik_x x + ik_y y - \sqrt{\kappa^2 + \mathbf{k}_\perp^2} z}$, and regular solutions with the exponentially growing solutions $e^{ik_x x + ik_y y + \sqrt{\kappa^2 + \mathbf{k}_\perp^2} z}$.

The wave functions that appear in the series expansion of the free Green's functions in Eq. (2.2.8) satisfy wave equations with frequency ω. The integral representations in Eq. (2.2.6), on the other hand, contain wave functions of all frequencies. As we will see in Sec. 2.3, the ability to express the Casimir energy entirely in terms of an "on-shell" partial wave expansion with fixed ω will greatly simplify our calculations.

2.2.2 Translation matrices

We will use the free Green's function described in the previous subsection to combine the scattering amplitudes for two different objects. In this calculation, the one argument of the Green's function will be located on each object. As a result, if Eq. (2.2.8) is written in the basis appropriate to one object, we will want to "translate" one of the scattering solutions to the basis appropriate to the other object. The configuration of the two objects — either outside of each other, or one inside the other — will determine which object has the larger or smaller value of ξ_1, and therefore which solution needs to be expanded in the other basis.

We will make use of two expansions:

1. The regular solutions form a complete set no matter what origin is used to define the decomposition into partial waves. Let $\{\mathbf{E}_\beta^{\mathrm{reg}}(\kappa, \mathbf{x}_j)\}$ be the regular solutions expressed with respect to the origin of coordinates appropriate to object j, $\mathcal{O}_j$. It must be possible to expand a regular solution $\mathbf{E}_\alpha^{\mathrm{reg}}(\kappa, \mathbf{x}_i)$, defined with respect to the origin $\mathcal{O}_i$ appropriate to object i, in terms of the $\{\mathbf{E}_\beta^{\mathrm{reg}}(\kappa, \mathbf{x}_j)\}$,

$$\mathbf{E}_\alpha^{\mathrm{reg}}(\kappa, \mathbf{x}_i) = \sum_\beta \mathcal{V}_{\beta,\alpha}^{ji}(\kappa, \mathbf{X}_{ji}) \mathbf{E}_\beta^{\mathrm{reg}}(\kappa, \mathbf{x}_j), \tag{2.2.9}$$

   where $\mathbf{X}_{ij} = -\mathbf{X}_{ji} = \mathbf{x}_i - \mathbf{x}_j$ is shown in Fig. 2-1. Note that $\mathbf{x}_i$ and $\mathbf{x}_j$ refer to the same space point $\mathbf{x}$, expressed as the displacement from different origins. This expansion will be applicable to the case of one object inside the other.

2. The same type of expansion must also exist when the original wave obeys outgoing boundary conditions *except in a region that contains the origin* $\mathcal{O}_i$, where

$\mathbf{E}_\alpha^{\text{out}}(\kappa, \mathbf{x}_i)$ is singular. We therefore have the expansion

$$\mathbf{E}_\alpha^{\text{out}}(\kappa, \mathbf{x}_i) = \sum_\beta \mathcal{U}_{\beta,\alpha}^{ji}(\kappa, \mathbf{X}_{ji}) \mathbf{E}_\beta^{\text{reg}}(\kappa, \mathbf{x}_j), \text{ for } \mathbf{x} \notin N(\mathcal{O}_i) \tag{2.2.10}$$

where $N(\mathcal{O}_i)$ is a neighborhood of the origin $\mathcal{O}_i$. This expansion will be applicable to the case where the objects are outside each other.

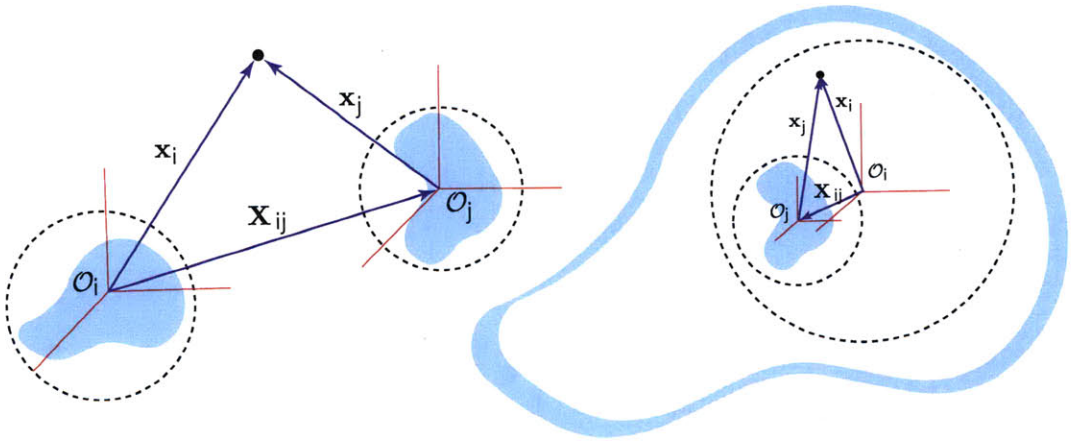

Figure 2-1: Geometry of the outside (left) and inside (right) configurations. The dotted lines show surfaces separating the objects on which the radial variable is constant. The translation vector $\mathbf{X}_{ij} = \mathbf{x}_i - \mathbf{x}_j = -\mathbf{X}_{ji}$ describes the relative positions of the two origins.

To apply these results to a given geometry, we must be able to distinguish between regular and outgoing waves over the whole of each object. That is, we require there to exist an origin and a separable coordinate system so that for all points $\mathbf{x}$ in one object and $\mathbf{x}'$ in another object, $\xi_1(\mathbf{x})$ is always greater than $\xi_1(\mathbf{x}')$, or vice versa. Having $\xi_1(\mathbf{x}) > \xi_1(\mathbf{x}')$ ensures that the Green's function is always evaluated by letting $\mathbf{x}$ be the argument of the outgoing wave function and $\mathbf{x}'$ be the argument of the regular wave function. We therefore require that any two objects be separated by a surface

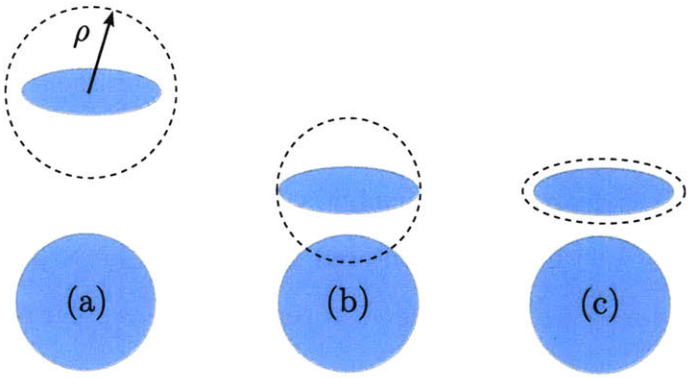

Figure 2-2: An elliptic cylinder approaching another cylinder. When the elliptic cylinder is far (a), every point on the cylinder has smaller radius than any point on the lower cylinder and an expansion using an ordinary cylindrical basis can be used. This expansion breaks down once the elliptic cylinder is close (b), but in that case an expansion using an elliptic cylindrical basis applies (c).

defined by the locations $\mathbf{x}$ where $\xi_1(\mathbf{x})$ is constant, as shown in Fig. 2-1. Depending on the coordinate system, this surface could be a plane, cylinder, sphere, etc.

The case of an elliptic cylinder and a circular cylinder illustrates this requirement. At large distances, the elliptic cylinder object can be separated from the circular cylinder object by a circular cylinder of radius ρ, as shown in Fig. 2-2a. All points on the elliptic cylinder object have values of ρ_1 that are smaller than any point on the circular cylinder object, so in this case we could carry out the calculation in ordinary cylindrical coordinates. However, as shown in Fig. 2-2b, if the separation becomes small enough, points on the circular cylinder object are closer to the center of the elliptic cylinder object (*i.e.* they lie at smaller ρ_1 than points on the elliptic cylinder object), and our method cannot be used in ordinary cylindrical coordinates. However, in *elliptic cylindrical* coordinates (see Appendix B.5), the surface of the elliptic cylinder object is itself a surface of constant elliptical radius μ_1, so all points on the elliptic cylinder object have smaller μ_1 than any point on the the circular cylinder object, and our method applies. This case is shown in Fig. 2-2c.

In a plane wave basis, we would exclude the case of two interlocking combs [68], since each comb has values of z that are both bigger and smaller than points on the

other object, so again a single assignment of regular and outgoing solutions cannot be made.

When object j lies wholly outside of object i, as shown in the left panel of Fig. 2-1, in the basis of object i the point on object j will always have greater ξ_1 than the point on object i. We will therefore need to expand the outgoing wave in the basis for object j. Since the origin $\mathcal{O}_i$ is never encountered when the point $\mathbf{x}$ lies on object j, the outgoing solutions for i can be expanded in terms of the regular solutions for object j using Eq. (2.2.10). Since i is also wholly outside j, we can also proceed the other way around and expand the outgoing wave functions in the basis of object j in terms of regular solutions in the basis of object i. This implies that the translation matrix satisfies $\mathcal{U}^{ij} = \mathcal{U}^{ji,\dagger}$. When one object is inside another, as shown in the right panel of Fig. 2-1, in the basis of object i, the point on object j will always have smaller ξ_1 than the point on object i. We will therefore need to expand the regular wave in the basis for object j using Eq. (2.2.9). In contrast, we cannot use the expansion of the outgoing wave functions, because the origin of the inside object may overlap with the origin of the outside object, in which case the expansion does not converge.

For a Cartesian geometry, the translation matrix is proportional to $e^{-i\mathbf{k}_\perp \cdot \mathbf{X}_{ji,\perp} - \sqrt{\kappa^2+\mathbf{k}_\perp^2} X_{ji,z}}$. It takes this simple form because plane wave functions are eigenfunctions of the translation operator. Then the "regular" wave function is evaluated on the object whose z coordinates are smaller and the outer and inner objects have larger and smaller z values, respectively.

The criterion for the expansion of the outgoing or regular wave functions is not topological. Instead, the proximity of the objects and their origins determines which expansion to use. In practice, it is usually easy to see which expansion is appropriate for any objects.

After expanding wave functions with respect to another origin using translation matrices, we can convert the wave functions from one basis to another, for example from plane wave to spherical or cylindrical wave functions. This transformation is useful when the two objects are best described in different coordinate bases. The needed conversion matrices are supplied in Appendix D. Since it is more convenient

to describe this conversion as a change of basis of the scattering amplitudes, we will not explicitly consider the combination of translation and conversion in this derivation, but instead we will illustrate the change of basis of the scattering amplitude in the examples.

2.2.3 Green's functions and translation matrices

To obtain the Green's function when one argument, say $\mathbf{x}$, lies on object i and the other argument, say $\mathbf{x}'$, lies on object j, we expand $\mathbb{G}_0(ic\kappa, \mathbf{x}, \mathbf{x}')$ in terms of coordinates $\mathbf{x}_i$ and $\mathbf{x}'_j$ that describe each point relative to the origin of the body on which it lies. For the different situations given above we have

$$\mathbb{G}_0(ic\kappa, \mathbf{x}, \mathbf{x}') = \sum_{\alpha,\beta} C_\beta(\kappa) \begin{cases} \mathbf{E}_\alpha^{\mathrm{reg}}(\kappa, \mathbf{x}_i) \otimes \mathcal{U}_{\alpha\beta}^{ji}(\kappa) \mathbf{E}_\beta^{\mathrm{reg}*}(\kappa, \mathbf{x}'_j) & \text{if } i \text{ and } j \text{ are outside each other} \\ \mathbf{E}_\alpha^{\mathrm{reg}}(\kappa, \mathbf{x}_i) \otimes \mathcal{V}_{\alpha\beta}^{ij}(\kappa) \mathbf{E}_\beta^{\mathrm{in}*}(\kappa, \mathbf{x}'_j) & \begin{cases} \text{if } i \text{ is inside } j, \text{ or} \\ \text{if } i \text{ is below } j \text{ (plane wave basis)} \end{cases} \\ \mathbf{E}_\alpha^{\mathrm{out}}(\kappa, \mathbf{x}_i) \otimes \mathcal{W}_{\alpha\beta}^{ji}(\kappa) \mathbf{E}_\beta^{\mathrm{reg}*}(\kappa, \mathbf{x}'_j) & \begin{cases} \text{if } j \text{ is inside } i, \text{ or} \\ \text{if } j \text{ is below } i \text{ (plane wave basis)} \end{cases} \end{cases} \tag{2.2.11}$$

where $\mathcal{W}_{\alpha\beta}^{ji}(\kappa) = \mathcal{V}_{\alpha\beta}^{ji,\dagger}(\kappa) \frac{C_\alpha(\kappa)}{C_\beta(\kappa)}$ and C_α is the normalization constant defined in Eq. (2.2.8). We can express these cases in the consolidated form,

$$\mathbb{G}_0(ic\kappa, \mathbf{x}, \mathbf{x}') = \sum_{\alpha,\beta} C_\beta(\kappa) \begin{pmatrix} \mathbf{E}_\alpha^{\mathrm{reg}}(\kappa, \mathbf{x}_i) & \mathbf{E}_\alpha^{\mathrm{out}}(\kappa, \mathbf{x}_i) \end{pmatrix} \otimes \begin{pmatrix} \mathcal{U}_{\alpha\beta}^{ji}(\kappa) & \mathcal{V}_{\alpha\beta}^{ij}(\kappa) \\ \mathcal{W}_{\alpha\beta}^{ji}(\kappa) & 0 \end{pmatrix} \begin{pmatrix} \mathbf{E}_\beta^{\mathrm{reg}*}(\kappa, \mathbf{x}'_j) \\ \mathbf{E}_\beta^{\mathrm{in}*}(\kappa, \mathbf{x}'_j) \end{pmatrix}, \tag{2.2.12}$$

where only one of the three submatrices is nonzero for any pair of objects i and j as given in Eq. (2.2.11). The expansion can be written more formally as

$$\mathbb{G}_0(ic\kappa) = \sum_{\alpha,\beta} (-C_\beta(\kappa)) \begin{pmatrix} |\mathbf{E}_\alpha^{\mathrm{reg}}(\kappa)\rangle & |\mathbf{E}_\alpha^{\mathrm{out}}(\kappa)\rangle \end{pmatrix} \mathbb{X}_{\alpha\beta}^{ij}(\kappa) \begin{pmatrix} \langle \mathbf{E}_\beta^{\mathrm{reg}}(\kappa)| \\ \langle \mathbf{E}_\beta^{\mathrm{in}}(\kappa)| \end{pmatrix}, \tag{2.2.13}$$

where the bras and kets are to be evaluated in position space in the appropriately restricted domains and the $\mathbb{X}$ matrix is defined, for convenience, as the negative of the matrix containing the translation matrices,

$$\mathbb{X}^{ij}(\kappa) = \begin{pmatrix} -\mathcal{U}^{ji}(\kappa) & -\mathcal{V}^{ij}(\kappa) \\ -\mathcal{W}^{ji}(\kappa) & 0 \end{pmatrix}. \tag{2.2.14}$$

The translation matrices for various geometries are provided in Appendix C.

2.3 A review of aspects of the classical scattering of electromagnetic fields

In this section, we review the key results from scattering theory needed to compute the scattering amplitude of each body individually. Comprehensive derivations can be found in Refs. [89, 90]. The approach we will use was first developed by Waterman [91, 92], albeit not in the operator form that is used here. In the subsequent section we will then combine these results with the translation matrices of the previous section to compute $Z(\kappa)$.

The Fourier-transformed electromagnetic action of Eq. (2.1.2) yields the frequency-dependent Maxwell equations:

$$\boldsymbol{\nabla} \times \mathbf{E}(\omega, \mathbf{x}) = i\frac{\omega}{c}\mathbf{B}(\omega, \mathbf{x}), \qquad \boldsymbol{\nabla} \times \frac{1}{\mu}\mathbf{B}(\omega, \mathbf{x}) = -i\frac{\omega}{c}\epsilon\mathbf{E}(\omega, \mathbf{x}). \tag{2.3.1}$$

Combining these two equations, we obtain

$$(\mathbb{H}_0 + \mathbb{V}(\omega, \mathbf{x}))\mathbf{E}(\omega, \mathbf{x}) = \frac{\omega^2}{c^2}\mathbf{E}(\omega, \mathbf{x}), \tag{2.3.2}$$

where

$$\begin{aligned} \mathbb{H}_0 &= \boldsymbol{\nabla} \times \boldsymbol{\nabla}\times, \\ \mathbb{V}(\omega, \mathbf{x}) &= \mathbb{I}\frac{\omega^2}{c^2}\left(1 - \epsilon(\omega, \mathbf{x})\right) + \boldsymbol{\nabla} \times \left(\frac{1}{\mu(\omega, \mathbf{x})} - 1\right)\boldsymbol{\nabla}\times, \end{aligned} \tag{2.3.3}$$

which is the same potential operator as the one obtained by rearranging the Lagrangian (see Eq. (2.1.4)). Since the electromagnetic potential is a differential operator, care must be taken with operator ordering.

The Lippmann-Schwinger equation [93]

$$|\mathbf{E}\rangle = |\mathbf{E}_0\rangle - \mathbb{G}_0\mathbb{V}|\mathbf{E}\rangle \tag{2.3.4}$$

expresses the general solution to Eq. (2.3.2). Here $\mathbb{G}_0$ is the free electromagnetic tensor Green's function discussed in Sec. 2.2 and the homogeneous solution $|\mathbf{E}_0\rangle$ obeys $\left(-\frac{\omega^2}{c^2}\mathbb{I} + \mathbb{H}_0\right)|\mathbf{E}_0\rangle = 0$, which can be chosen to be either a regular or outgoing wave for a particular frequency ω. We can iteratively substitute for $|\mathbf{E}\rangle$ in Eq. (2.3.4) to obtain the formal expansion

$$\begin{aligned} |\mathbf{E}\rangle &= |\mathbf{E}_0\rangle - \mathbb{G}_0\mathbb{V}|\mathbf{E}_0\rangle + \mathbb{G}_0\mathbb{V}\mathbb{G}_0\mathbb{V}|\mathbf{E}\rangle - \dots \\ &= |\mathbf{E}_0\rangle - \mathbb{G}_0\mathbb{T}|\mathbf{E}_0\rangle, \end{aligned} \tag{2.3.5}$$

where the electromagnetic $\mathbb{T}$-operator is defined as

$$\mathbb{T} = \mathbb{V}\frac{\mathbb{I}}{\mathbb{I} + \mathbb{G}_0\mathbb{V}} = \mathbb{V}\mathbb{G}\mathbb{G}_0^{-1}, \tag{2.3.6}$$

and $\mathbb{G}$ is the Green's function of the full Hamiltonian, $\left(-\frac{\omega^2}{c^2}\mathbb{I} + \mathbb{H}_0 + \mathbb{V}\right)\mathbb{G} = \mathbb{I}$. We note that $\mathbb{T}$, $\mathbb{G}_0$, and $\mathbb{G}$ are all functions of frequency ω and non-local in space. As can be seen from expanding $\mathbb{T}$ in Eq. (2.3.6) in a power series, $\mathbb{T}(\omega, \mathbf{x}, \mathbf{x}') = \langle\mathbf{x}|\mathbb{T}(\omega)|\mathbf{x}'\rangle$ is zero whenever $\mathbf{x}$ or $\mathbf{x}'$ are not located on an object, *i.e.*, where $\mathbb{V}(\omega, \mathbf{x})$ is zero. This result does not, however, apply to

$$\mathbb{T}^{-1} = \mathbb{G}_0 + \mathbb{V}^{-1}, \tag{2.3.7}$$

because the free Green's function is nonlocal.

Next we connect the matrix elements of the $\mathbb{T}$-operator between states with equal ω to the scattering amplitude $\mathcal{F}$. In our formalism, only this restricted subset of

$\mathbb{T}$-operator matrix elements is needed in the computation of the Casimir energy.

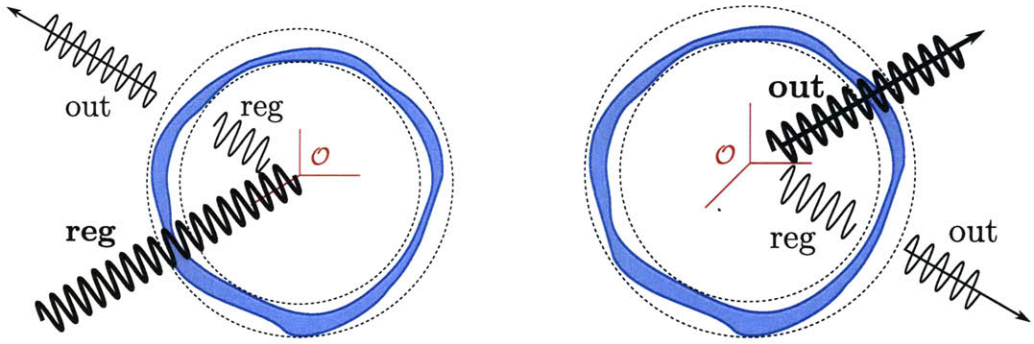

Figure 2-3: The scattering waves for outside scattering (left panel) and inside scattering (right panel). In both cases the homogeneous solution $\mathbf{E}_0(\omega)$ is shown in bold. For outside scattering, the homogeneous solution is a regular wave, which produces a regular wave inside the object and an outgoing wave outside the object. For inside scattering, the homogeneous solution is an outgoing wave, which produces a regular wave inside the object and an outgoing wave outside the object.

Outside scattering

We consider a scattering process in which a regular wave interacts with an object and scatters outward, as depicted in the left panel of Fig. 2-3.[2] For outside scattering the homogeneous solution $|\mathbf{E}_0\rangle$ in Eq. (2.3.5) is taken to be the regular wave function $|\mathbf{E}^{\text{reg}}_\alpha(\omega)\rangle$. We choose a convenient "scattering origin" in the inside region, consistent with any symmetries of the problem if possible.

To find the field $\mathbf{E}$ at a coordinate $\mathbf{x}$ far enough outside the object, we use Eq. (2.3.5) in position space and the expansion in Eq. (2.2.8) for $\mathbb{G}_0$:

$$\mathbf{E}(\omega,\mathbf{x}) = \mathbf{E}^{\text{reg}}_\alpha(\omega,\mathbf{x}) - \sum_\beta \mathbf{E}^{\text{out}}_\beta(\omega,\mathbf{x}) \int C_\beta(\omega)\mathbf{E}^{\text{reg}*}_\beta(\omega,\mathbf{x}')\cdot\mathbb{T}(\omega,\mathbf{x}',\mathbf{x}'')\mathbf{E}^{\text{reg}}_\alpha(\omega,\mathbf{x}'')d\mathbf{x}'d\mathbf{x}''. \tag{2.3.8}$$

Here "far enough outside" means that $\mathbf{x}$ has larger ξ_1 than any point on the object, meaning that we are always taking the same choice in Eq. (2.2.8), as described in

[2]Alternatively, we can set up asymptotically incoming and outgoing waves on the outside and regular waves inside. The amplitudes of the outgoing waves are then given by the $\mathcal{S}$-matrix, which is related to the scattering amplitude $\mathcal{F}$ by $\mathcal{F} = (\mathcal{S} - \mathcal{I})/2$. Although these two matrices carry equivalent information, the scattering amplitude will be more convenient for our calculation.

Sec. 2.2. The equation can be written in Dirac notation, again with the condition that the domain of the functional Hilbert space is chosen appropriately to the type of solution,

$$|\mathbf{E}(\omega)\rangle = |\mathbf{E}_\alpha^{\mathrm{reg}}(\omega)\rangle + \sum_\beta |\mathbf{E}_\beta^{\mathrm{out}}(\omega)\rangle \times \underbrace{(-1)C_\beta(\omega)\langle \mathbf{E}_\beta^{\mathrm{reg}}(\omega)|\mathbb{T}(\omega)|\mathbf{E}_\alpha^{\mathrm{reg}}(\omega)\rangle}_{\mathcal{F}^{ee}_{\beta,\alpha}(\omega)}, \qquad (2.3.9)$$

which defines $\mathcal{F}^{ee}_{\beta,\alpha}$ as the exterior/exterior scattering amplitude (the one evaluated between two regular solutions). We will use analogous notation in the other cases below.

At coordinates $\mathbf{x}$ "far enough inside" a cavity of the object, meaning that $\mathbf{x}$ has smaller ξ_1 than any point on the object, we have the opposite case in Eq. (2.2.8) and the field $\mathbf{E}$ is given by

$$|\mathbf{E}(\omega)\rangle = |\mathbf{E}_\alpha^{\mathrm{reg}}(\omega)\rangle + \sum_\beta |\mathbf{E}_\beta^{\mathrm{reg}}(\omega)\rangle \times \underbrace{(-1)C_\beta(\omega)\langle \mathbf{E}_\beta^{\mathrm{in}}(\omega)|\mathbb{T}(\omega)|\mathbf{E}_\alpha^{\mathrm{reg}}(\omega)\rangle}_{\mathcal{F}^{ie}_{\beta,\alpha}(\omega)}, \qquad (2.3.10)$$

where again the free states are only defined over the appropriate domain in position space, and $\mathcal{F}^{ie}$ indicates the interior/exterior scattering amplitude.

Inside scattering

In the study of Casimir problems with one object inside the other, it is useful to imagine a situation that would be difficult to realize in actual scattering experiments, in which the wave probing the object originates inside the object and is scattered as a regular wave inside the object and as an outgoing wave outside, as depicted in the right panel of Fig. 2-3.

The situation is expressed mathematically by letting the homogeneous solution $|\mathbf{E}_0\rangle$ in Eq. (2.3.5) be an outgoing wave $|\mathbf{E}_\alpha^{\mathrm{out}}(\omega)\rangle$. The equation can be expressed in

condensed form as before. Inside the object we have

$$|\mathbf{E}(\omega)\rangle = |\mathbf{E}_\alpha^{\text{out}}(\omega)\rangle + \sum_\beta |\mathbf{E}_\beta^{\text{reg}}(\omega)\rangle \times \underbrace{(-1)C_\beta(\omega)\langle \mathbf{E}_\beta^{\text{in}}(\omega)|\mathbb{T}(\omega)|\mathbf{E}_\alpha^{\text{out}}(\omega)\rangle}_{\mathcal{F}^{ii}_{\beta,\alpha}(\omega)}, \quad (2.3.11)$$

and outside the object we have

$$|\mathbf{E}(\omega)\rangle = |\mathbf{E}_\alpha^{\text{out}}(\omega)\rangle + \sum_\beta |\mathbf{E}_\beta^{\text{out}}(\omega)\rangle \times \underbrace{(-1)C_\beta(\omega)\langle \mathbf{E}_\beta^{\text{reg}}(\omega)|\mathbb{T}(\omega)|\mathbf{E}_\alpha^{\text{out}}(\omega)\rangle}_{\mathcal{F}^{ei}_{\beta,\alpha}(\omega)}. \quad (2.3.12)$$

Remarks

We have obtained the scattering amplitude in the basis of free solutions with fixed ω. Since one is normally interested in the scattering of waves outside the object, the scattering amplitude usually refers to $\mathcal{F}^{ee}$. We will use a more general definition, which encompasses all possible combinations of inside and outside. The scattering amplitude is always "on-shell," because the frequencies of the bra and ket wave functions are both equal to ω. As a result, it is a special case of the $\mathbb{T}$-operator, which connects wave functions with different ω.

It is usually not practical to calculate the matrix elements by finding the abstract $\mathbb{T}$-operator and taking its inner products with free wave functions. Instead, one typically considers an ansatz for the solutions appropriate for inside or outside scattering in the various regions, with unknown scattering amplitudes, and then solves the wave equation, matching the solutions in different regions at their boundaries.

We will find it convenient to assemble the scattering amplitudes for inside and outside into a single matrix,

$$\begin{aligned}\mathbb{F}(\kappa) &= \begin{pmatrix} \mathcal{F}^{ee}(\kappa) & \mathcal{F}^{ei}(\kappa) \\ \mathcal{F}^{ie}(\kappa) & \mathcal{F}^{ii}(\kappa) \end{pmatrix} \\ &= (-1)C_\alpha(\kappa) \begin{pmatrix} \langle \mathbf{E}_\alpha^{\text{reg}}(\kappa)|\mathbb{T}(ic\kappa)|\mathbf{E}_\beta^{\text{reg}}(\kappa)\rangle & \langle \mathbf{E}_\alpha^{\text{reg}}(\kappa)|\mathbb{T}(ic\kappa)|\mathbf{E}_\beta^{\text{out}}(\kappa)\rangle \\ \langle \mathbf{E}_\alpha^{\text{in}}(\kappa)|\mathbb{T}(ic\kappa)|\mathbf{E}_\beta^{\text{reg}}(\kappa)\rangle & \langle \mathbf{E}_\alpha^{\text{in}}(\kappa)|\mathbb{T}(ic\kappa)|\mathbf{E}_\beta^{\text{out}}(\kappa)\rangle \end{pmatrix}. \end{aligned} \quad (2.3.13)$$

Here we have written this expression in terms of modified wave functions for $\omega = ic\kappa$, with the corresponding normalization constant, since that is the case we will use. The derivations of the scattering amplitudes carry over directly to this case, with κ replaced by ω; for example, Eq. (2.3.9) becomes

$$|\mathbf{E}(\kappa)\rangle = |\mathbf{E}^{\mathrm{reg}}_{\alpha}(\kappa)\rangle + \sum_{\beta} |\mathbf{E}^{\mathrm{out}}_{\alpha}(\kappa)\rangle \times \underbrace{(-1)C_{\beta}(\kappa)\langle \mathbf{E}^{\mathrm{reg}}_{\beta}(\kappa)|\mathbb{T}(ic\kappa)|\mathbf{E}^{\mathrm{reg}}_{\alpha}(\kappa)\rangle}_{\mathcal{F}^{ee}_{\beta,\alpha}(\kappa)} . \quad (2.3.14)$$

2.4 Partition function in terms of the scattering amplitude

With the tools of the previous two sections, we are now able to re-express the Euclidean electromagnetic partition function of Eq. (2.1.12) in terms of the scattering theory results derived in Section 2.3 for imaginary frequency. We will exchange the fluctuating field $\mathbf{A}$, which is subject to the potential $\mathbb{V}(ic\kappa, \mathbf{x})$, for a free field $\mathbf{A}'$, together with fluctuating currents $\mathbf{J}$ and charges $-\frac{i}{\omega}\nabla \cdot \mathbf{J}$ that are confined to the objects. The sequence of two changes of variables that will be performed is often referred to as the Hubbard-Stratonovich transformation in condensed matter physics.

We multiply and divide the partition function Eq. (2.1.12) by

$$W = \int \mathcal{D}\mathbf{J}\mathcal{D}\mathbf{J}^*|_{\mathrm{obj}} \exp\left[-\beta \int d\mathbf{x}\, \mathbf{J}^*(\mathbf{x}) \cdot \mathbb{V}^{-1}(ic\kappa, \mathbf{x})\mathbf{J}(\mathbf{x})\right] = \det \mathbb{V}(ic\kappa, \mathbf{x}, \mathbf{x}') , \quad (2.4.1)$$

where $|_{\mathrm{obj}}$ indicates that the currents are defined only over the objects, *i.e.* the domain where $\mathbb{V}$ is nonzero (and therefore $\mathbb{V}^{-1}$ exists), and we have represented the local potential as a matrix in position space, $\mathbb{V}(ic\kappa, \mathbf{x}, \mathbf{x}') = \mathbb{V}(ic\kappa, \mathbf{x})\delta^{(3)}(\mathbf{x} - \mathbf{x}')$. Our derivation generalizes straightforwardly to the case of a nonlocal potential $\mathbb{V}(ic\kappa, \mathbf{x}, \mathbf{x}')$, assuming it is still confined to each object individually.

We then change variables in the integration, $\mathbf{J}(\mathbf{x}) = \mathbf{J}'(\mathbf{x}) + \frac{i}{\kappa}\mathbb{V}(ic\kappa, \mathbf{x})\mathbf{E}(\mathbf{x})$ and

$\mathbf{J}^*(\mathbf{x}) = \mathbf{J}'^*(\mathbf{x}) + \frac{i}{\kappa}\mathbb{V}(ic\kappa, \mathbf{x})\mathbf{E}^*(\mathbf{x})$, to obtain

$$Z(\kappa) = \frac{1}{W}\int \mathcal{D}\mathbf{A}\mathcal{D}\mathbf{A}^*\, \mathcal{D}\mathbf{J}'\mathcal{D}\mathbf{J}'^*\big|_{\text{obj}} \exp\left[-\beta \int d\mathbf{x}\, \left(\mathcal{H} + \left(\mathbf{J}'^*(\mathbf{x}) + \frac{i}{\kappa}\mathbb{V}(ic\kappa, \mathbf{x})\mathbf{E}^*(\mathbf{x})\right) \cdot \mathbb{V}^{-1}(ic\kappa, \mathbf{x}) \left(\mathbf{J}'(\mathbf{x}) + \frac{i}{\kappa}\mathbb{V}(ic\kappa, \mathbf{x})\mathbf{E}(\mathbf{x})\right)\right)\right], \tag{2.4.2}$$

where

$$\mathcal{H} = \mathbf{E}^*(\mathbf{x}) \cdot \left(\mathbb{I} + \frac{1}{\kappa^2}\boldsymbol{\nabla} \times \boldsymbol{\nabla}\times\right)\mathbf{E}(\mathbf{x}) + \frac{1}{\kappa^2}\mathbf{E}^*(\mathbf{x}) \cdot \mathbb{V}(ic\kappa, \mathbf{x})\mathbf{E}(\mathbf{x}). \tag{2.4.3}$$

Next we use a second change of variables, $\mathbf{E}(ic\kappa, \mathbf{x}) = \mathbf{E}'(ic\kappa, \mathbf{x}) - i\kappa \int d\mathbf{x}'\, \mathbb{G}_0(ic\kappa, \mathbf{x}, \mathbf{x}')\mathbf{J}'(\mathbf{x}')$ and $\mathbf{E}^*(ic\kappa, \mathbf{x}) = \mathbf{E}'^*(ic\kappa, \mathbf{x}) - i\kappa \int d\mathbf{x}'\, \mathbb{G}_0(ic\kappa, \mathbf{x}, \mathbf{x}')\mathbf{J}'^*(\mathbf{x}')$, which simplifies Eq. (2.4.2) to

$$Z(\kappa) = \frac{Z_0}{W}\int \mathcal{D}\mathbf{J}'\mathcal{D}\mathbf{J}'^*\big|_{\text{obj}} \exp\left[-\beta \int d\mathbf{x}d\mathbf{x}'\, \mathbf{J}'^*(\mathbf{x}) \cdot \left(\mathbb{G}_0(ic\kappa, \mathbf{x}, \mathbf{x}') + \mathbb{V}^{-1}(ic\kappa, \mathbf{x}, \mathbf{x}')\right)\mathbf{J}'(\mathbf{x}')\right], \tag{2.4.4}$$

where

$$Z_0 = \int \mathcal{D}\mathbf{A}'\mathcal{D}\mathbf{A}'^* \exp\left[-\beta \int d\mathbf{x}\, \mathbf{E}'^*(\mathbf{x}) \cdot \left(\mathbb{I} + \frac{1}{\kappa^2}\boldsymbol{\nabla} \times \boldsymbol{\nabla}\times\right)\mathbf{E}'(\mathbf{x})\right] \tag{2.4.5}$$

is the partition function of the free field, which is independent of the objects. The new partition function of Eq. (2.4.4) contains a sum over current fluctuations in place of the original field fluctuations in Eq. (2.1.12). The interaction of current fluctuations at different points $\mathbf{x}$ and $\mathbf{x}'$ is described by the free Green's function $\mathbb{G}_0(ic\kappa, \mathbf{x}, \mathbf{x}')$ alone. (If the potential $\mathbb{V}(ic\kappa, \mathbf{x}, \mathbf{x}')$ is nonlocal, this statement still holds for two points $\mathbf{x}$ and $\mathbf{x}'$ on two different objects.) This is the expected interaction term. For example, in the static limit $\kappa = 0$, the free Green's function is just the Coulomb interaction term $\frac{1}{4\pi|\mathbf{x}-\mathbf{x}'|}$. The inverse potential penalizes current fluctuations if the potential is small. In vacuum, the potential vanishes, so current fluctuations are

infinitely costly and thus are not permitted. But of course the current fluctuations are already constrained to the objects.

To put the partition function into a suitable form for practical computations, we will use the results of the previous sections to re-express the microscopic current fluctuations as macroscopic multipole fluctuations, which then can be connected to the individual objects' scattering amplitudes. This transformation comes about naturally once the current fluctuations are decomposed according to the objects on which they occur and the appropriate expansions of the Green's function are introduced. We begin this process by noticing that the operator in the exponent of the integrand in Eq. (2.4.4) is the negative of the inverse of the $\mathbb{T}$-operator (see Eq. (2.3.7)), and hence

$$Z(\kappa) = Z_0 \det \mathbb{V}^{-1}(ic\kappa, \mathbf{x}, \mathbf{x}') \det \mathbb{T}(ic\kappa, \mathbf{x}, \mathbf{x}') \tag{2.4.6}$$

which is in agreement with a more direct calculation: Since $Z_0 = \det \mathbb{G}_0(ic\kappa, \mathbf{x}, \mathbf{x}')$ and $Z(\kappa) = \det \mathbb{G}(ic\kappa, \mathbf{x}, \mathbf{x}')$, we only need to take the determinant of Eq. (2.3.6) to arrive at the result of Eq. (2.4.6).

Both Z_0 and $\det \mathbb{V}^{-1}(ic\kappa, \mathbf{x})$ are independent of the separation of the objects, since the former is simply the free Green's function, while the latter is diagonal in $\mathbf{x}$. Even a nonlocal potential $\mathbb{V}(ic\kappa, \mathbf{x}, \mathbf{x}')$ only connects points within the same object, so its determinant is also independent of the objects' separation. Because these determinants do not depend on separation, they will be canceled by a reference partition function in the final result. We are thus left with the task of computing the determinant of the $\mathbb{T}$-operator.

As has been discussed in Sec. 2.3, the $\mathbb{T}$-operator $\mathbb{T}(ic\kappa, \mathbf{x}, \mathbf{x}')$ is not diagonal in the spatial coordinates. Its determinant needs to be taken over the spatial indices $\mathbf{x}$ and $\mathbf{x}'$, which are restricted to the objects because the fluctuating currents $\mathbf{J}(\mathbf{x})$ in the functional integrals are zero away from the objects. This determinant also runs over the ordinary vector components of the electromagnetic $\mathbb{T}$ operator.

A change of basis to momentum space does not help in computing the determinant of the $\mathbb{T}$-operator, even though it does help in finding the determinant of the free

Green's function. One reason is that the momentum basis is not orthogonal over the domain of the indices $\mathbf{x}$ and $\mathbf{x}'$, which is restricted to the objects. In addition, a complete momentum basis includes not only all directions of the momentum vector, but also all magnitudes of the momenta. So, in the matrix element $\langle \mathbf{E}_{\mathbf{k}} | \mathbb{T}(\omega) | \mathbf{E}_{\mathbf{k}'} \rangle$ the wave numbers k and k' would not have to match, and could also differ from ω/c. That is, the matrix elements could be "off-shell." Therefore, the $\mathbb{T}$-operator could not simply be treated as if it was the scattering amplitude, which is the on-shell representation of the operator in the subbasis of frequency ω (see Sec. 2.3), and is significantly easier to calculate. Nonetheless, we will see that it is possible to express the Casimir energy in terms of the on-shell operator only, by remaining in the position basis.

From Eq. (2.3.6), we know that the inverse of the $\mathbb{T}$-operator equals the sum of the free Green's function and the inverse of the potential. Since the determinant of the inverse operator is the reciprocal of the determinant, it is expedient to start with the inverse $\mathbb{T}$-operator. We then separate the basis involving all the objects into blocks for the n objects. In a schematic notation, we have

$$[\langle \mathbf{x} | \mathbb{T}^{-1} | \mathbf{x}' \rangle] = \left(\begin{array}{c|c|c} [\langle \mathbf{x}_1 | \mathbb{T}_1^{-1} | \mathbf{x}_1' \rangle] & [\langle \mathbf{x}_1 | \mathbb{G}_0 | \mathbf{x}_2' \rangle] & \cdots \\ \hline [\langle \mathbf{x}_2 | \mathbb{G}_0 | \mathbf{x}_1' \rangle] & [\langle \mathbf{x}_2 | \mathbb{T}_2^{-1} | \mathbf{x}_2' \rangle] & \cdots \\ \hline \cdots & \cdots & \cdots \end{array} \right), \tag{2.4.7}$$

where the ij^{th} submatrix refers to $\mathbf{x} \in$ object i and $\mathbf{x}' \in$ object j and $\mathbf{x}_i$ represents a point in object i measured with respect to some fixed coordinate system. Unlike the position vectors in Sec. 2.2, at this point the subscript of $\mathbf{x}_i$ does not indicate the origin with respect to which the vector is measured, but rather the object on which the point lies. Square brackets are used to remind us that we are considering the entire matrix or submatrix and not a single matrix element. We note that the operators $\mathbb{T}$ and $\mathbb{G}_0$ are functions of $ic\kappa$, but for simplicity we suppress this argument throughout this derivation. When the two spatial indices lie on different objects, only the free Green's function remains in the off-diagonal submatrices. Even if the potential $\mathbb{V}(ic\kappa, \mathbf{x}, \mathbf{x}')$ is nonlocal in space, it does not connect points on different

objects. It follows that the inverse of the potential is block diagonal in position space, where each block involves points on the same object, *i.e.*, $\langle \mathbf{x}_i | \mathbb{V}^{-1} | \mathbf{x}'_j \rangle = 0$ for $i \neq j$.

Next, we multiply $\mathbb{T}^{-1}$ by a reference $\mathbb{T}$-operator $\mathbb{T}_\infty$ without off-diagonal submatrices, which can be interpreted as the $\mathbb{T}$-operator at infinite separation,

$$[\langle \mathbf{x} | \mathbb{T}_\infty \mathbb{T}^{-1} | \mathbf{x}'' \rangle] = \left(\begin{array}{c|c|c} [\langle \mathbf{x}_1 | \mathbf{x}''_1 \rangle] & [\int d\mathbf{x}'_1 \, \langle \mathbf{x}_1 | \mathbb{T}_1 | \mathbf{x}'_1 \rangle \langle \mathbf{x}'_1 | \mathbb{G}_0 | \mathbf{x}''_2 \rangle] & \cdots \\ \hline [\int d\mathbf{x}'_2 \, \langle \mathbf{x}_2 | \mathbb{T}_2 | \mathbf{x}'_2 \rangle \langle \mathbf{x}'_2 | \mathbb{G}_0 | \mathbf{x}''_1 \rangle] & [\langle \mathbf{x}_2 | \mathbf{x}''_2 \rangle] & \cdots \\ \hline \cdots & \cdots & \cdots \end{array} \right) . \tag{2.4.8}$$

Each off-diagonal submatrix $[\int d\mathbf{x}'_i \langle \mathbf{x}_i | \mathbb{T}_i | \mathbf{x}'_i \rangle \langle \mathbf{x}'_i | \mathbb{G}_0 | \mathbf{x}''_j \rangle]$ is the product of the $\mathbb{T}$-operator of object i, evaluated at two points $\mathbf{x}_i$ and $\mathbf{x}'_i$ on that object, multiplied by the free Green's function, which connects $\mathbf{x}'_i$ to some point $\mathbf{x}''_j$ on object j.

Now we shift all variables to the coordinate systems of the objects on which they lie. As a result, the index on a position vector $\mathbf{x}_i$ now refers to the object i on which the point lies *and* to the coordinate system with origin $\mathcal{O}_i$ in which the vector is represented, in agreement with the notation of Sec. 2.2. The off-diagonal submatrices in Eq. (2.4.8) can then be rewritten using Eq. (2.2.13) as,

$$\sum_{\alpha,\beta} \left[\left(\langle \mathbf{x}_i | \mathbb{T}_i | \mathbf{E}^{\text{reg}}_\alpha(\kappa) \rangle \;\; \langle \mathbf{x}_i | \mathbb{T}_i | \mathbf{E}^{\text{out}}_\alpha(\kappa) \rangle \right) \mathbb{X}^{ij}_{\alpha\beta} \begin{pmatrix} \langle \mathbf{E}^{\text{reg}}_\beta(\kappa) | \mathbf{x}''_j \rangle \\ \langle \mathbf{E}^{\text{in}}_\beta(\kappa) | \mathbf{x}''_j \rangle \end{pmatrix} (-C_\beta(\kappa)) \right] . \tag{2.4.9}$$

The matrix $[\langle \mathbf{x} | \mathbb{T}_\infty \mathbb{T}^{-1} | \mathbf{x}'' \rangle]$ has the structure $\mathbb{I} + \mathbb{A}\mathbb{B}$, where

$$\mathbb{A} = \sum_\alpha \left(\begin{array}{cc|cc|c} 0 & 0 & [\langle \mathbf{x}_1 | \mathbb{T}_1 | \mathbf{E}^{\text{reg}}_\alpha(\kappa) \rangle \mathbb{X}^{12}_{\alpha\beta}] & [\langle \mathbf{x}_1 | \mathbb{T}_1 | \mathbf{E}^{\text{out}}_\alpha(\kappa) \rangle \mathbb{X}^{12}_{\alpha\beta}] & \cdots \\ \hline [\langle \mathbf{x}_2 | \mathbb{T}_2 | \mathbf{E}^{\text{reg}}_\alpha(\kappa) \rangle \mathbb{X}^{21}_{\alpha\beta}] & [\langle \mathbf{x}_2 | \mathbb{T}_2 | \mathbf{E}^{\text{out}}_\alpha(\kappa) \rangle \mathbb{X}^{21}_{\alpha\beta}] & 0 & 0 & \cdots \\ \hline \cdots & \cdots & \cdots & \cdots & \cdots \end{array} \right) \tag{2.4.10}$$

and

$$\mathbb{B} = \left(\begin{array}{c|c|c} \left[-C_\beta(\kappa)\langle \mathbf{E}^{\rm reg}_\beta(\kappa)|\mathbf{x}_1''\rangle\right] & 0 & \cdots \\ \left[-C_\beta(\kappa)\langle \mathbf{E}^{\rm in}_\beta(\kappa)|\mathbf{x}_1''\rangle\right] & 0 & \cdots \\ \hline 0 & \left[-C_\beta(\kappa)\langle \mathbf{E}^{\rm reg}_\beta(\kappa)|\mathbf{x}_2''\rangle\right] & \cdots \\ 0 & \left[-C_\beta(\kappa)\langle \mathbf{E}^{\rm in}_\beta(\kappa)|\mathbf{x}_2''\rangle\right] & \cdots \\ \hline \cdots & \cdots & \cdots \end{array}\right) \tag{2.4.11}$$

and the matrix multiplication now encompasses both the object index and the partial wave index β. Although the same symbols are used for each wave function, the bases (spherical, planar, etc.) can be chosen differently for each object.

Using Sylvester's determinant formula $\det(\mathbb{I}+\mathbb{A}\mathbb{B}) = \det(\mathbb{I}+\mathbb{B}\mathbb{A})$, we see that the determinant is unchanged if we replace the off-diagonal submatrices in Eq. (2.4.8) by

$$\left[\sum_\beta (-1)C_\alpha(\kappa) \begin{pmatrix} \langle \mathbf{E}^{\rm reg}_\alpha(\kappa)|\mathbb{T}_i|\mathbf{E}^{\rm reg}_\beta(\kappa)\rangle & \langle \mathbf{E}^{\rm reg}_\alpha(\kappa)|\mathbb{T}_i|\mathbf{E}^{\rm out}_\beta(\kappa)\rangle \\ \langle \mathbf{E}^{\rm in}_\alpha(\kappa)|\mathbb{T}_i|\mathbf{E}^{\rm reg}_\beta(\kappa)\rangle & \langle \mathbf{E}^{\rm in}_\alpha(\kappa)|\mathbb{T}_i|\mathbf{E}^{\rm out}_\beta(\kappa)\rangle \end{pmatrix} \mathbb{X}^{ij}_{\beta,\gamma}\right]. \tag{2.4.12}$$

With this change, the diagonal submatrices in Eq. (2.4.8) become diagonal in the partial wave indices rather than in position space. The matrix elements of the $\mathbb{T}$-operator are the scattering amplitudes, which can be obtained from ordinary scattering calculations, as demonstrated in Sec. 2.3. The first matrix in Eq. (2.4.12), including the prefactor $(-1)C_\alpha(\kappa)$, is $\mathbb{F}_i(\kappa)$, the modified scattering amplitude of object i, defined in Eq. (2.3.13).

Putting together Eqs. (2.1.11), (2.1.12), (2.4.6), and (2.4.8), we obtain

$$\mathcal{E} = \frac{\hbar c}{2\pi}\int_0^\infty d\kappa \log\det(\mathbb{M}\mathbb{M}_\infty^{-1}), \tag{2.4.13}$$

where

$$\mathbb{M} = \begin{pmatrix} \mathbb{F}_1^{-1} & \mathbb{X}^{12} & \mathbb{X}^{13} & \cdots \\ \mathbb{X}^{21} & \mathbb{F}_2^{-1} & \mathbb{X}^{23} & \cdots \\ \cdots & \cdots & \cdots & \cdots \end{pmatrix} \tag{2.4.14}$$

and $\mathbb{M}_\infty^{-1}$ is a block diagonal matrix $\mathrm{diag}(\mathbb{F}_1 \;\; \mathbb{F}_2 \;\; \cdots)$.

Using the block determinant identity

$$\det\begin{pmatrix}\mathbb{A} & \mathbb{B}\\ \mathbb{C} & \mathbb{D}\end{pmatrix} = \det(\mathbb{A})\det\left(\mathbb{D}-\mathbb{C}\mathbb{A}^{-1}\mathbb{B}\right) = \det(\mathbb{D})\det\left(\mathbb{A}-\mathbb{B}\mathbb{D}^{-1}\mathbb{C}\right), \quad (2.4.15)$$

we can simplify this expression for the case of the interaction between two objects,

$$\mathcal{E} = \frac{\hbar c}{2\pi}\int_0^\infty d\kappa \log\det\left(\mathbb{I}-\mathbb{F}_a\mathbb{X}^{ab}\mathbb{F}_b\mathbb{X}^{ba}\right). \quad (2.4.16)$$

Usually, not all of the submatrices of $\mathbb{F}$ and $\mathbb{X}$ are actually needed for a computation. For example, if all objects are outside of one another, only the submatrices $\mathcal{F}^{ee}$ of the scattering amplitude that describe outside reflection are needed. If there are only two objects, one inside another, then only the inside reflection submatrix $\mathcal{F}^{ii}$ of the outside object and the outside reflection submatrix $\mathcal{F}^{ee}$ of the inside object are needed.

In order to obtain the free energy at nonzero temperature instead of the ground state energy, we do not take the limit $\beta\to\infty$ in Eq. (2.1.9) [24]. Instead, the integral $\frac{\hbar c}{2\pi}\int_0^\infty d\kappa$ is replaced everywhere by $\frac{1}{\beta}\sum_n'$, where $c\kappa_n = \frac{2\pi n}{\hbar\beta}$ with $n = 0,1,2,3\ldots$ is the nth Matsubara frequency. A careful analysis of the derivation shows that the zero frequency mode is weighted by $1/2$ compared to the rest of the terms in the sum; this modification of the sum is denoted by a prime on the summation symbol. The factor of $1/2$ comes about because the fluctuating charges or currents have to be real for zero frequency. Thus, for κ_0, the expressions on the right hand side of Eq. (2.4.6) should be placed under a square root. (For a complex field, both signs of the integer n would be included separately, and $n=0$ would be included once, with the normal weight.)

If the medium between the objects is not vacuum but instead has permittivity $\epsilon_m(ic\kappa)$ and magnetic permeability $\mu_m(ic\kappa)$ different from unity, then the free Green's function is multiplied by $\mu_m(ic\kappa)$, and its argument κ is replaced by $n_m(ic\kappa)\kappa$, where $n_m(ic\kappa) = \sqrt{\epsilon_m(ic\kappa)\mu_m(ic\kappa)}$ is the medium's index of refraction. Effectively, this change just scales all frequency dependencies in the translation matrices $\mathbb{X}(\kappa)$,

which become $\mathbb{X}(n_m(ic\kappa)\kappa)$. Furthermore, the scattering amplitudes absorb the factor $\mu_m(ic\kappa)$ from the free Green's function and change non-trivially, *i.e.* not just by some overall factor or a scaling of the frequency. They have to be computed with the nonzero electric and magnetic susceptibilities of the medium.

Chapter 3

Results

3.1 Constraints on stable equilibria

Before presenting particular applications of the Casimir energy expression in Eq. (2.4.13), we consider some general properties of electrodynamic Casimir interactions in this section. Explicit calculations for simple geometries indicate that the direction of the force can be predicted based on the relative permittivities, and permeabilities, of the objects and the medium. Separating materials into two groups, with *(i)* permittivity higher than the medium or permeability lower than the medium ($\epsilon > \epsilon_M$ and $\mu \leq \mu_M$), or *(ii)* the other way around ($\epsilon < \epsilon_M$ and $\mu \geq \mu_M$), Casimir forces are usually found to be attractive between members of the same group and repulsive for different types. (While this has been shown in several examples, e.g. in Refs. [27, 22, 23, 94, 95], a theorem regarding the sign of the force only exists for mirror symmetric arrangements of objects [58, 70].) Since ordinary materials have permittivity higher than air and permeability very close to one, this effect causes objects to stick to one another. (The above statements will be made precise shortly.) Particularly for nanomachines this is detrimental as the Casimir force increases rapidly with decreasing separation. This has motivated research into reversing the force; for example, a recent experiment [17] shows that, in accord with the above rules, a dielectric medium can lead to repulsion. But the sign of the force is largely a matter of perspective, since attractive forces can be easily arranged to produce repulsion along a specific direction, e.g., as in Ref. [68].

Instead, we focus on the question of stability, see Fig. 3-1, which is more relevant to the design and development of MEMs and levitating devices. We find that interactions between objects within the same class of material cannot produce stable configurations.

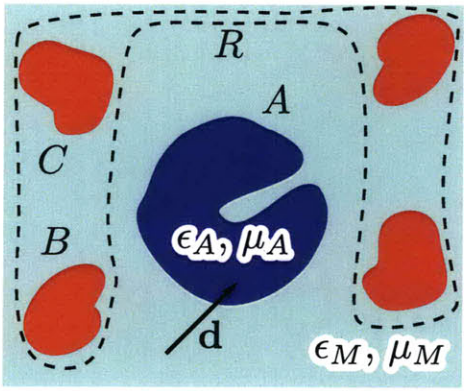

Figure 3-1: The Casimir energy is considered for objects with electric permittivity $\epsilon_i(\omega, \mathbf{x})$ and magnetic permeability $\mu_i(\omega, \mathbf{x})$, embedded in a medium with uniform, isotropic, $\epsilon_M(\omega)$ and $\mu_M(\omega)$. To study the stability of object A, the rest of the objects are grouped in the combined entity R. The stability of the position of object A is probed by displacing it infinitesimally by vector $\mathbf{d}$.

Let us take a step back and consider the question of stability of mechanical equilibria in the realm of electromagnetism. Earnshaw's theorem [96] states that a collection of charges cannot be held in stable equilibrium solely by electrostatic forces. The charges can attract or repel, but cannot be stably levitated. While the stability of matter (due to quantum phenomena) is a vivid reminder of the caveats to this theorem, it remains a powerful indicator of the constraints to stability in electrostatics. An extension of Earnshaw's theorem to polarizable objects by Braunbek [97, 98] establishes that dielectric and paramagnetic ($\epsilon > 1$ and $\mu > 1$) matter cannot be stably levitated by electrostatic forces, while diamagnetic ($\mu < 1$) matter can. This is impressively demonstrated by superconductors and frogs that fly freely above magnets [99]. If the enveloping medium is not vacuum, the criteria for stability are modified by substituting the static electric permittivity ϵ_M and magnetic permeability μ_M of the medium in place of the vacuum value of 1 in the respective inequalities. In fact, if the medium itself has a dielectric constant higher than the objects ($\epsilon < \epsilon_M$),

stable levitation is possible, as demonstrated for bubbles in liquids (see Ref. [100], and references therein). For dynamic fields the restrictions of electrostatics do not apply; for example, lasers can lift and hold dielectric beads with index of refraction $n = \sqrt{\epsilon\mu} > 1$ [101]. In addition to the force which keeps the bead in the center of the laser beam there is radiation pressure which pushes the bead along the direction of the Poynting vector. Ashkin and Gordon have proved that no arrangement of lasers can stably levitate an object just based on radiation pressure [102].

We begin our analysis of equilibria of the electrodynamic Casimir force with the precursor of Eq. (2.4.13), which contains the abstract $\mathbb{T}$ and $\mathbb{G}$-operators,

$$\mathcal{E} = \frac{\hbar c}{2\pi} \int_0^\infty d\kappa \ \mathrm{tr} \ \ln \mathbb{T}^{-1}\mathbb{T}_\infty \,, \tag{3.1.1}$$

where the operator $[\mathbb{T}^{-1}(ic\kappa, \mathbf{x}, \mathbf{x}')]$ equals

$$\begin{pmatrix} \left[\mathbb{T}_A^{-1}(ic\kappa, \mathbf{x}_1, \mathbf{x}_1')\right] & \left[\mathbb{G}(ic\kappa, \mathbf{x}_1, \mathbf{x}_2')\right] & \cdots \\ \left[\mathbb{G}(ic\kappa, \mathbf{x}_2, \mathbf{x}_1')\right] & \left[\mathbb{T}_B^{-1}(ic\kappa, \mathbf{x}_2, \mathbf{x}_2')\right] & \\ \cdots & & \cdots \end{pmatrix}, \tag{3.1.2}$$

and $\mathbb{T}_\infty$ is the inverse of $\mathbb{T}^{-1}$ with $\mathbb{G}$ set to zero. The square brackets "[ ]" denote the entire matrix or submatrix with rows indicated by $\mathbf{x}$ and columns by $\mathbf{x}'$. To obtain the free energy at finite temperature, in place of the ground state energy $\mathcal{E}$, $\int \frac{d\kappa}{2\pi}$ is replaced by the sum $\frac{kT}{\hbar c} \sum'_{\kappa_n \geq 0}$ over Matsubara 'wavenumbers' $\kappa_n = 2\pi nkT/\hbar c$ with the $\kappa_0 = 0$ mode weighted by $1/2$. The operator $[\mathbb{T}^{-1}(ic\kappa, \mathbf{x}, \mathbf{x}')]$ has indices in position space. Each spatial index is limited to lie inside the objects $A, B, \cdots$. For both indices $\mathbf{x}$ and $\mathbf{x}'$ in the same object A the operator is just the inverse $\mathbb{T}$ operator of that object, $[\mathbb{T}_A^{-1}(ic\kappa, \mathbf{x}, \mathbf{x}')]$. For indices on different objects, $\mathbf{x}$ in A and $\mathbf{x}'$ in B, it equals the electromagnetic Green's function operator $[\mathbb{G}(ic\kappa, \mathbf{x}, \mathbf{x}')]$ for an isotropic, homogeneous medium. [1] As shown in section 2.4, after a few manipulations, the

[1] $\mathbb{G}$ satisfies $\left(\boldsymbol{\nabla} \times \mu_M^{-1}(ic\kappa)\boldsymbol{\nabla} \times + \epsilon_M(ic\kappa)\kappa^2\right) \mathbb{G}(ic\kappa, \mathbf{x}, \mathbf{x}') = \delta(\mathbf{x} - \mathbf{x}')\mathbb{I}$, and is related to G_M, the Green's function of the imaginary frequency Helmholtz equation, by $\mathbb{G}(ic\kappa, \mathbf{x}, \mathbf{x}') = \mu_M(ic\kappa)\left(\mathbb{I} + (n_M\kappa)^{-2}\boldsymbol{\nabla} \otimes \boldsymbol{\nabla}'\right) G_M(icn_M\kappa, \mathbf{x}, \mathbf{x}')$. Here, $n_M(ic\kappa) = \sqrt{\epsilon_M(ic\kappa)\mu_M(ic\kappa)}$ is the index of refraction of the medium, whose argument is suppressed to simplify the presentation. Thus $\mathbb{G}$, in contrast to $\mathbb{G}_0$, takes into account the permittivity and permeability of the medium when it is

operators $\mathbb{T}_J$ and $\mathbb{G}$ turn into the on-shell scattering amplitude matrix, $\mathbb{F}_J$, of object J and the translation matrix $\mathbb{X}$, which converts wave functions between the origins of different objects. While practical computations require evaluation of the matrices in a particular wave function basis, the position space operators $\mathbb{T}_J$ and $\mathbb{G}$ are better suited to our general discussion here.

To investigate the stability of object A, we group the 'rest' of the objects into a single entity R. So, $\mathbb{T}$ consists of 2×2 blocks, and the integrand in Eq. (3.1.1) reduces to tr $\ln(\mathbb{I} - \mathbb{T}_A\mathbb{G}\mathbb{T}_R\mathbb{G})$. Merging the components of R poses no conceptual difficulty given that the operators are expressed in a position basis, while an actual computation of the force between A and R would remain a daunting task. If object A is moved infinitesimally by vector $\mathbf{d}$, the Laplacian of the energy is given by

$$\nabla^2_{\mathbf{d}}\,\mathcal{E}\big|_{\mathbf{d}=0} = -\frac{\hbar c}{2\pi}\int_0^\infty d\kappa\ \mathrm{tr}\ \Big[2n_M^2(ic\kappa)\kappa^2\tfrac{\mathbb{T}_A\mathbb{G}\mathbb{T}_R\mathbb{G}}{\mathbb{I}-\mathbb{T}_A\mathbb{G}\mathbb{T}_R\mathbb{G}} \tag{3.1.3}$$

$$+\,2\mathbb{T}_A\boldsymbol{\nabla}\mathbb{G}\mathbb{T}_R\left(\boldsymbol{\nabla}\mathbb{G}\right)^T\tfrac{\mathbb{I}}{\mathbb{I}-\mathbb{T}_A\mathbb{G}\mathbb{T}_R\mathbb{G}} \tag{3.1.4}$$

$$+\,2\mathbb{T}_A\boldsymbol{\nabla}\mathbb{G}\mathbb{T}_R\mathbb{G}\tfrac{\mathbb{I}}{\mathbb{I}-\mathbb{T}_A\mathbb{G}\mathbb{T}_R\mathbb{G}} \tag{3.1.5}$$

$$\cdot\left(\mathbb{T}_A\boldsymbol{\nabla}\mathbb{G}\mathbb{T}_R\mathbb{G}+\mathbb{T}_A\mathbb{G}\mathbb{T}_R\left(\boldsymbol{\nabla}\mathbb{G}\right)^T\right)\tfrac{\mathbb{I}}{\mathbb{I}-\mathbb{T}_A\mathbb{G}\mathbb{T}_R\mathbb{G}}\Big]\,.$$

After displacement of object A, the Green's function multiplied by $\mathbb{T}_A$ on the left and $\mathbb{T}_R$ on the right ($\mathbb{T}_A\mathbb{G}\mathbb{T}_R$) becomes $\mathbb{G}(ic\kappa, \mathbf{x}+\mathbf{d}, \mathbf{x}')$, while that multiplied by $\mathbb{T}_R$ on the left and $\mathbb{T}_A$ on the right ($\mathbb{T}_R\mathbb{G}\mathbb{T}_A$) becomes $\mathbb{G}(ic\kappa, \mathbf{x}, \mathbf{x}'+\mathbf{d})$. The two are related by transposition, and indicated by $\boldsymbol{\nabla}\mathbb{G}(ic\kappa, \mathbf{x}, \mathbf{x}') = \boldsymbol{\nabla}_{\mathbf{d}}\mathbb{G}(ic\kappa, \mathbf{x}+\mathbf{d}, \mathbf{x}')|_{\mathbf{d}=0}$ and $\left(\boldsymbol{\nabla}\mathbb{G}(ic\kappa, \mathbf{x}, \mathbf{x}')\right)^T = \boldsymbol{\nabla}_{\mathbf{d}}\mathbb{G}(ic\kappa, \mathbf{x}, \mathbf{x}'+\mathbf{d})|_{\mathbf{d}=0}$ in the above equation. In the first line we have substituted $n_M^2(ic\kappa)\kappa^2\mathbb{G}$ for $\nabla^2\mathbb{G}$; the two differ only by derivatives of δ–functions which vanish since $\mathbb{G}\left(ic\kappa, \mathbf{x}, \mathbf{x}'\right)$ is evaluated with $\mathbf{x}$ in one object and $\mathbf{x}'$ in another. In expressions not containing inverses of $\mathbb{T}$-operators, we can extend the domain of all operators to the entire space: $\mathbb{T}_J(ic\kappa, \mathbf{x}, \mathbf{x}') = 0$ if $\mathbf{x}$ or $\mathbf{x}'$ are not on object J and thus operator multiplication is unchanged.

To determine the signs of the various terms in $\nabla^2_{\mathbf{d}}\,\mathcal{E}|_{\mathbf{d}=0}$, we perform an analysis similar to Ref. [58]. However, we do not investigate convergence issues and

different from one.

treat the operators like matrices from the start. This means that the necessary criteria (smoothness, boundedness, compact support, etc.) are assumed to be fulfilled in realistic situations, as dealt with in Ref. [58]. The operators $\mathbb{T}_J$ and $\mathbb{G}$ are real and symmetric. An operator is positive (negative) semidefinite if all its eigenvalues are greater than or equal to zero (smaller than or equal to zero). It is easy to verify that $\mathbb{G}$ is a positive semidefinite operator, since it is diagonal in momentum space, with $\mathbb{G}(ic\kappa, \mathbf{k}) = \mu_M(ic\kappa)\left(\mathbb{I} + \frac{\mathbf{k}\otimes\mathbf{k}}{n_M^2(ic\kappa)\kappa^2}\right)/(k^2 + n_M^2(ic\kappa)\kappa^2)$. If $\mathbb{L}$ is a real and symmetric matrix, it is positive semidefinite if and only if there exists a matrix $\mathbb{K}$ such that $\mathbb{L} = \mathbb{K}^T\mathbb{K}$. Let us assume that $\mathbb{T}_A$ and $\mathbb{T}_R$ are each either positive or negative semidefinite, indicated by $s^A = \pm 1$ and $s^R = \pm 1$. (We shall shortly show how the sign of $\mathbb{T}_J$ can be obtained from the object's permittivity and permeability.) The eigenvalues of $\mathbb{I} - \mathbb{T}_A\mathbb{G}\mathbb{T}_R\mathbb{G}$, which equal those of $\mathbb{I} - s^A\sqrt{s^A\mathbb{T}_A}\mathbb{G}\mathbb{T}_R\mathbb{G}\sqrt{s^A\mathbb{T}_A}$, are strictly positive, since the energy is real. (The above expression appears in the integrand of Eq. (3.1.1) if there are only two objects.) Under the trace we always encounter the combination $(\mathbb{I} - \mathbb{T}_A\mathbb{G}\mathbb{T}_R\mathbb{G})^{-1}\mathbb{T}_A$, which, taking advantage of its symmetries and definite sign, can be written as $s^A\mathbb{K}^T\mathbb{K}$, where $\mathbb{K} = \left(\mathbb{I} - s^A\sqrt{s^A\mathbb{T}_A}\mathbb{G}\mathbb{T}_R\mathbb{G}\sqrt{s^A\mathbb{T}_A}\right)^{-1/2}\sqrt{s^A\mathbb{T}_A}$. The first term, line (3.1.3), can now be rearranged as $\mathrm{tr}\ s^A\mathbb{K}^T\mathbb{K}\mathbb{G}\mathbb{T}_R\mathbb{G} = s^As^R\mathrm{tr}\left[(\mathbb{K}\mathbb{G}\mathbb{R})\left(\mathbb{R}^T\mathbb{G}\mathbb{K}^T\right)\right]$ by setting $\mathbb{T}_R = s^R\mathbb{R}\mathbb{R}^T$ and its sign is s^As^R. In the same way line (3.1.4) can be recast as $s^As^R\mathrm{tr}\left[(\mathbb{K}\boldsymbol{\nabla}\mathbb{G}\mathbb{R})\cdot(\mathbb{K}\boldsymbol{\nabla}\mathbb{G}\mathbb{R})^T\right]$, and its sign is thus also set by s^As^R. Lastly, the term in line (3.1.5) can be rewritten as $\left(\mathbb{K}\boldsymbol{\nabla}\mathbb{G}\mathbb{T}_R\mathbb{G}\mathbb{K}^T + \mathbb{K}\mathbb{G}\mathbb{T}_R\left(\boldsymbol{\nabla}\mathbb{G}\right)^T\mathbb{K}^T\right)^2$. Since this is the square of a symmetric matrix, its eigenvalues are greater than or equal to zero, irrespective of the signs of $\mathbb{T}_A$ and $\mathbb{T}_R$. Overall, the Laplacian of the energy is smaller than or equal to zero as long as $s^As^R \geq 0$.

How can we determine the sign of $\mathbb{T}_J$, defined in Eq. (2.3.6)? It is positive or negative semidefinite depending on the sign s^J of $\mathbb{V}_J$, since $\mathbb{T}_J = s^J\sqrt{s^J\mathbb{V}_J}\frac{\mathbb{I}}{\mathbb{I}+s^J\sqrt{s^J\mathbb{V}_J}\mathbb{G}\sqrt{s^J\mathbb{V}_J}}\sqrt{s^J\mathbb{V}_J}$. The denominator $\mathbb{I} + s^J\sqrt{s^J\mathbb{V}_J}\mathbb{G}\sqrt{s^J\mathbb{V}_J}$ is positive semidefinite, even if $s^J = -1$, as its eigenvalues are the same as $\sqrt{\mathbb{G}}(\mathbb{G}^{-1} + \mathbb{V}_J)\sqrt{\mathbb{G}}$; the term in the parantheses is just the (nonnegative) Hamiltonian of the field and the object J, $\mathbb{G}^{-1} + \mathbb{V}_J = \boldsymbol{\nabla}\times\mu^{-1}(ic\kappa, \mathbf{x})\boldsymbol{\nabla}\times + \mathbb{I}\,\kappa^2\epsilon(ic\kappa, \mathbf{x})$. Here, we have used $\mathbb{V}_J$ as given below, and

$\epsilon(ic\kappa, \mathbf{x})$ and $\mu(ic\kappa, \mathbf{x})$ are the reponse functions defined everywhere in space, either of object J or of the medium, depending on the point $\mathbf{x}$.

The analysis so far applies to each imaginary frequency $ic\kappa$. As long as the signs of $\mathbb{T}_A$ and $\mathbb{T}_R$ are the same over all frequencies $\nabla^2_{\mathbf{d}} \mathcal{E}|_{\mathbf{d}=0}$ is proportional to $-s^A s^R$ – (positive term) [2]. We are left to find the sign of the potential $\mathbb{V}_J(ic\kappa, \mathbf{x}) = \mathbb{I}\kappa^2 (\epsilon_J(ic\kappa, \mathbf{x}) - \epsilon_M(ic\kappa)) + \boldsymbol{\nabla} \times \left(\mu_J^{-1}(ic\kappa, \mathbf{x}) - \mu_M^{-1}(ic\kappa)\right) \boldsymbol{\nabla}\times$ of the object A, and the compound object R [3]. The sign is determined by the relative permittivities and permeabilities of the objects and the medium: If $\epsilon_J(ic\kappa, \mathbf{x}) > \epsilon_M(ic\kappa)$ and $\mu_J(ic\kappa, \mathbf{x}) \leq \mu_M(ic\kappa)$ hold for all $\mathbf{x}$ in object J, the potential $\mathbb{V}_J$ is positive. If the opposite inequalities are true, $\mathbb{V}_J$ is negative. The curl operators surrounding the magnetic permeability do not influence the sign, as in computing an inner product with $\mathbb{V}_J$ they act symmetrically on both sides. For vacuum $\epsilon_M = \mu_M = 1$, and material response functions $\epsilon(ic\kappa, \mathbf{x})$ and $\mu(ic\kappa, \mathbf{x})$ are analytical continuations of the permittivity and permeability for real frequencies [103]. While $\epsilon(ic\kappa, \mathbf{x}) > 1$ for positive κ, there are no restrictions other than positivity on $\mu(ic\kappa, \mathbf{x})$. (For non-local and non-isotropic response, various inequalities must be generalized to the tensorial operators $\overleftrightarrow{\boldsymbol{\epsilon}}(ic\kappa, \mathbf{x}, \mathbf{x}')$ and $\overleftrightarrow{\boldsymbol{\mu}}(ic\kappa, \mathbf{x}, \mathbf{x}')$.)

Thus, levitation is not possible for collections of objects characterized by $\epsilon_J(ic\kappa, \mathbf{x})$ and $\mu_J(ic\kappa, \mathbf{x})$ falling into one of the two classes described earlier, i) $\epsilon_J/\epsilon_M > 1$ and $\mu_J/\mu_M \leq 1$ (positive $\mathbb{V}_J$ and $\mathbb{T}_J$), or ii) $\epsilon_J/\epsilon_M < 1$ and $\mu_J/\mu_M \geq 1$ with (negative $\mathbb{V}_J$ and $\mathbb{T}_J$). (Under these conditions parallel slabs attract.) The frequency and space dependence of the functions has been suppressed in these inequalities. In vacuum, $\epsilon_M(ic\kappa) = \mu_M(ic\kappa) = 1$; since $\epsilon(ic\kappa, \mathbf{x}) > 1$ and the magnetic response of ordinary materials is typically negligible [103], one concludes that stable equilibria of the Casimir force do not exist. If objects A and R, however, belong to different categories –under which conditions the parallel plate force is repulsive–, then the terms under the trace in lines (3.1.3) and (3.1.4) are negative. The positive term in

[2] In practice, $\mathbb{T}_A$ and $\mathbb{T}_R$ suffice to have the same sign over the frequencies, which contribute most to the integral (or the sum) in Eq. (3.1.1).

[3] The first curl in the operator $\mathbb{V}_J$ results from an integration by parts. It is understood that it acts on the wave function multiplying $\mathbb{V}_J$ from the left.

line (3.1.5) is typically smaller than the first two, as it involves higher powers of $\mathbb{T}$ and $\mathbb{G}$. In this case stable equilibrium is possible, as demonstrated below for a small inclusion within a dielectric filled cavity [84]. For the remaining two combinations of inequalities involving ϵ_J/ϵ_M and μ_J/μ_M the sign of $\mathbb{V}_J$ cannot be determined a priori. But for realistic distances between objects and the corresponding frequency ranges, the magnetic susceptibility is negligible for ordinary materials, and the inequalities involving μ can be ignored.

It is clear that even very complicated materials cannot avoid the conditions required for the above result. In particular, metamaterials, incorporating arrays of micro-engineered circuity display strong magnetic response at certain frequencies, and have been discussed as candidates for Casimir repulsion across vacuum [104, 105]. In our treatment, in accord with the usual electrodynamics of macroscopic media, the materials are characterized by $\epsilon(ic\kappa, \mathbf{x})$ and $\mu(ic\kappa, \mathbf{x})$ at mesoscopic scales. This may not always be valid, as for example in the case of magnetoelectric materials. Chirality, and large magnetic response, in metamaterials is, however, achieved by patterns made from ordinary metals and dielectrics with well-behaved $\epsilon(ic\kappa, \mathbf{x})$ and $\mu(ic\kappa, \mathbf{x}) \approx 1$ at short scales [106]. Clearly, the coarse-grained response functions, in their region of validity, should produce the same scattering amplitudes as the detailed mesoscopic description. Consequently, as long as the metamaterial can be described by $\epsilon(ic\kappa, \mathbf{x})$ and $\mu(ic\kappa, \mathbf{x}) \approx 1$, the eigenvalues of the $\mathbb{T}$ operators are constrained as described above, and hence subject to the instability theorem. Finally, we note that instability also excludes repulsion between such materials, if one of the objects is an infinite slab with continuous translational symmetry: Repulsion would require that the energy as a function of separation from the slab should have $\partial_d^2 \mathcal{E} > 0$ at some point since the force has to vanish at infinite separation. A metamaterial does not have continuous translational symmetry at short length scales but this symmetry is approximately valid in the limit of large separations (long wavelengths), where the material can be effectively described as a homogeneous medium. In this limit there cannot be repulsion while for short separations the material does not act like a metamaterial, that is, it cannot be described by uniform electromagnetic response functions.

3.2 Applications

Our technique for calculating the Casimir energy applies to a wide range of situations. In this section we demonstrate the method through a variety of examples.

3.2.1 London and Casimir-Polder interaction between two atoms

As a simple example, we re-derive the interaction between two identical neutral atoms in the ground state [20]. The atoms are described in a two-state approximation. Within this approximation, the electric dipole polarizability of the atoms is given by

$$\alpha^E = \frac{e^2}{m}\frac{f_{10}}{\omega_{10}^2 - \omega^2}\,, \tag{3.2.1}$$

where e is the electron charge, m is the mass, f_{10} is the oscillator strength of the $0 \to 1$ transition, and ω_{10} is the frequency of that transition. We perform a Wick rotation $\omega \to ic\kappa$ and set $\kappa = u/d$, where d is the distance between the atoms. By introducing the characteristic length scale $d_{10} = c/\omega_{10}$ and the static electric polarizability

$$\alpha_0 = f_{10} r_0 d_{10}^2\,, \tag{3.2.2}$$

where $r_0 = e^2/(mc^2) \approx 10^{-15}$m is the classical electron radius, the polarizability can be written as

$$\alpha^E(u) = \frac{(d/d_{10})^2 \alpha_0}{(d/d_{10})^2 + u^2}\,. \tag{3.2.3}$$

In the isotropic-dipole approximation, the only nonzero element of the scattering amplitude of the atom is given in terms of the electric dipole polarizability as

$$\mathcal{F}^{ee}_{1mE,1mE} = \frac{2}{3}\,\alpha^E \kappa^3 \tag{3.2.4}$$

for $m = -1,\ 0,\ 1$. The atoms are assumed to have no magnetic polarizability. Using the general expression of Eq. (2.4.16) for the interaction energy between two objects,

we get

$$\mathcal{E} = \frac{\hbar c}{2\pi d}\int_0^\infty du \log\left[\left(1-4(1+u)^2 e^{-2u}\frac{\left(\alpha^E\right)^2}{d^6}\right)\left(1-(1+u+u^2)^2 e^{-2u}\frac{\left(\alpha^E\right)^2}{d^6}\right)\right] \quad (3.2.5)$$

$$= -\frac{\hbar c}{\pi d^7}\int_0^\infty du\,\left(\alpha^E(u)\right)^2\left(3+6u+5u^2+2u^3+u^4\right)e^{-2u}\,, \quad (3.2.6)$$

where we have expanded the logarithm assuming $\alpha^E(u) \ll d^3$, so that the interaction energy is proportional to the product of the polarizabilities of the atoms. It is instructive to consider two limits. First, assume that $d \ll d_{10}$. By the change of variable $u = (d/d_{10})z$, one easily finds that in Eq. (3.2.6), only the leading constant term of the polynomial in u has to be considered, and the exponential factor can be ignored. The integral is convergent at large u due to the behavior of the polarizability $\alpha^E(u)$ at large u. The integral over z yields, to leading order in d/d_{10}, the energy

$$\mathcal{E}_{\rm L} = -\frac{3}{4}\,\hbar\omega_{10}\,\frac{\alpha_0^2}{d^6}\,, \quad (3.2.7)$$

which is the well-known London interaction [107].

In the opposite limit $d \gg d_{10}$ retardation is important. From Eq. (3.2.3) we see that the frequency (u) dependence of the polarizability now can be neglected, so that $\alpha \approx \alpha_0$. In this retarded limit, the polynomial and exponential in u in Eq. (3.2.6) are important, and integration yields the energy

$$\mathcal{E}_{\rm CP} = -\frac{23}{4\pi}\,\hbar c\,\frac{\alpha_0^2}{d^7}\,, \quad (3.2.8)$$

which is known as the Casimir-Polder interaction [20].

For general distances d, the interaction between the atoms can be computed numerically; to quadratic order in the polarizability it is given by the integral of Eq. (3.2.6). The numerical result and the two limiting forms of the interaction are shown in Fig. 3-2.

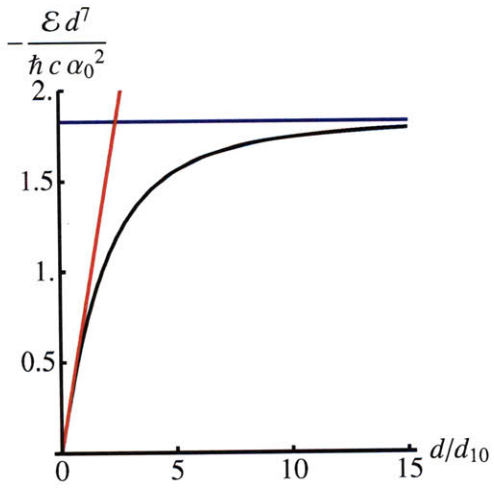

Figure 3-2: Interaction energy $\mathcal{E}$ of two identical atoms, Eq. (3.2.6), as a function of their separation d. The curve shows the crossover between the London interaction ($d \ll d_{10} = c/\omega_{10}$), Eq. (3.2.7), and the Casimir-Polder interaction ($d \gg d_{10}$), Eq. (3.2.8).

3.2.2 Derivation of the Lifshitz formula

Next we consider two semi-infinite half-spaces with uniform electric and magnetic susceptibility, as depicted in Fig. 3-3 [24, 25, 26, 27, 28]. We choose a plane wave basis oriented along the $\hat{\mathbf{z}}$ axis.

We decompose the scattering amplitude into magnetic (transverse electric) modes $\mathbf{M}$ and electric (transverse magnetic) modes $\mathbf{N}$.

For the upper object a the scattering solution is [108]

$$\begin{aligned}
\mathbf{E}(\kappa,\mathbf{x}) &= \mathbf{M}^{\text{out}}_{\mathbf{k}_\perp}(\kappa,\mathbf{x}) + \int \frac{L^2 d\mathbf{k}'_\perp}{(2\pi)^2}\left[\mathbf{M}^{\text{reg}}_{\mathbf{k}'_\perp}(\kappa,\mathbf{x})\mathcal{F}^{ii}_{a,\mathbf{k}'_\perp M,\mathbf{k}_\perp M} + \mathbf{N}^{\text{reg}}_{\mathbf{k}'_\perp}(\kappa,\mathbf{x})\mathcal{F}^{ii}_{a,\mathbf{k}'_\perp E,\mathbf{k}_\perp M}\right], \\
\mathbf{E}(\kappa,\mathbf{x}) &= \mathbf{N}^{\text{out}}_{\mathbf{k}_\perp}(\kappa,\mathbf{x}) + \int \frac{L^2 d^2\mathbf{k}'_\perp}{(2\pi)^2}\left[\mathbf{M}^{\text{reg}}_{\mathbf{k}'_\perp}(\kappa,\mathbf{x})\mathcal{F}^{ii}_{a,\mathbf{k}'_\perp M,\mathbf{k}_\perp E} + \mathbf{N}^{\text{reg}}_{\mathbf{k}'_\perp}(\kappa,\mathbf{x})\mathcal{F}^{ii}_{a,\mathbf{k}'_\perp E,\mathbf{k}_\perp E}\right],
\end{aligned} \tag{3.2.9}$$

Here L is the length of each side of the plates, $\mathbf{k}_\perp$ is the momentum perpendicular to the $\hat{\mathbf{z}}$ direction, and the subscripts M and E on the scattering amplitudes denote the magnetic and electric polarizations respectively. We consider the limit $L \to \infty$. The

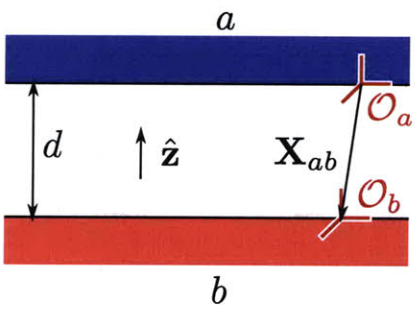

Figure 3-3: The upper infinite half space a is located a distance d above the half space b. This is the original configuration considered by Lifshitz. Each half space has its own uniform electric permittivity $\epsilon_i(ic\kappa)$ and magnetic permeability $\mu_i(ic\kappa)$. We note that our calculation holds even if the two origins $\mathcal{O}_a$ and $\mathcal{O}_b$ are displaced horizontally from one another, as shown here.

scattering amplitudes are given by

$$\begin{aligned}
\mathcal{F}^{ii}_{a,\mathbf{k}'_\perp E,\mathbf{k}_\perp M} &= \mathcal{F}^{ii}_{a,\mathbf{k}'_\perp M,\mathbf{k}_\perp E} = 0\,, \\
\mathcal{F}^{ii}_{a,\mathbf{k}'_\perp M,\mathbf{k}_\perp M} &= \tfrac{(2\pi)^2}{L^2}\delta^{(2)}(\mathbf{k}_\perp - \mathbf{k}'_\perp)\, r_a^M\left(ic\kappa, \sqrt{1+\mathbf{k}_\perp^2/\kappa^2}^{-1}\right), \\
\mathcal{F}^{ii}_{a,\mathbf{k}'_\perp E,\mathbf{k}_\perp E} &= \tfrac{(2\pi)^2}{L^2}\delta^{(2)}(\mathbf{k}_\perp - \mathbf{k}'_\perp)\, r_a^E\left(ic\kappa, \sqrt{1+\mathbf{k}_\perp^2/\kappa^2}^{-1}\right),
\end{aligned} \tag{3.2.10}$$

in terms of the Fresnel coefficients

$$\begin{aligned}
r_a^M(ic\kappa, x) &= \frac{\mu_a(ic\kappa) - \sqrt{1+(n_a^2(ic\kappa)-1)x^2}}{\mu_a(ic\kappa) + \sqrt{1+(n_a^2(ic\kappa)-1)x^2}}, \\
r_a^E(ic\kappa, x) &= \frac{\epsilon_a(ic\kappa) - \sqrt{1+(n_a^2(ic\kappa)-1)x^2}}{\epsilon_a(ic\kappa) + \sqrt{1+(n_a^2(ic\kappa)-1)x^2}}.
\end{aligned} \tag{3.2.11}$$

Here, n_a is the index of refraction, $n_a(ic\kappa) = \sqrt{\epsilon_a(ic\kappa)\mu_a(ic\kappa)}$. In the literature the Fresnel coefficients are also sometimes labeled with s instead of M and p in place of E.

The lower object b has the same scattering properties. The relevant scattering equation is the same as in Eq. (3.2.9), with "reg" and "out" exchanged and $\mathcal{F}_a^{ii}$ replaced by $\mathcal{F}_b^{ee}$, which is obtained from $\mathcal{F}_a^{ii}$ simply by substituting the permittivity $\epsilon_b(ic\kappa)$ and permeability $\mu_b(ic\kappa)$ in place of those of object a.

Using the appropriate $\mathbb{X}$ submatrices as specified in Eq. (2.2.11) and the cor-

responding submatrices of $\mathbb{F}$, the energy (2.4.16) for two objects can be expressed as

$$\mathcal{E} = \frac{\hbar c}{2\pi} \int_0^\infty d\kappa \log\det\left(\mathcal{I} - \mathcal{F}_a^{ii}\mathcal{W}^{ba}\mathcal{F}_b^{ee}\mathcal{V}^{ba}\right). \tag{3.2.12}$$

Since the matrix in the determinant is diagonal in $\mathbf{k}_\perp$, the determinant factors into a product of determinants, each with fixed $\mathbf{k}_\perp$. The logarithm of the product is then given by an integral over the two-dimensional space of $\mathbf{k}_\perp$. Since the integrand is invariant under rotations in $\mathbf{k}_\perp$, we can write this integral in polar coordinates as

$$\mathcal{E} = \frac{\hbar c}{2\pi} \int_0^\infty d\kappa \int_0^\infty \frac{L^2}{2\pi} k_\perp dk_\perp \log \prod_{i=E,M} \left(1 - r_a^i r_b^i e^{-2\kappa d\sqrt{1+\mathbf{k}_\perp^2/\kappa^2}}\right), \tag{3.2.13}$$

where $k_\perp = |\mathbf{k}_\perp|$.

After a change of variable $p = \sqrt{1+\mathbf{k}_\perp^2/\kappa^2}$ we obtain the Lifshitz formula for the energy,

$$\mathcal{E} = \frac{\hbar c L^2}{(2\pi)^2} \int_0^\infty \kappa^2 d\kappa \int_1^\infty p dp \log\left[\left(1 - r_a^M r_b^M e^{-2\kappa p d}\right)\left(1 - r_a^E r_b^E e^{-2\kappa p d}\right)\right]. \tag{3.2.14}$$

3.2.3 Two cylinders

We now rederive the Casimir energy for two perfectly conducting, infinitely long cylinders, depicted in Fig. 3-4. The result for one cylinder inside the other has been presented in Ref. [81] and the result for both outside each other was presented in Refs. [82, 109].

For scattering from outside cylinder a, we have the scattering solutions

$$\begin{aligned}
\mathbf{E}(\kappa,\mathbf{x}) &= \mathbf{M}^{\text{reg}}_{k_z,n}(\kappa,\mathbf{x}) + \int \frac{L dk_z'}{2\pi} \sum_{n'} \left[\mathbf{M}^{\text{out}}_{k_z',n'}(\kappa,\mathbf{x})\mathcal{F}^{ee}_{a,k_z'n'M,k_znM} + \mathbf{N}^{\text{out}}_{k_z',n'}(\kappa,\mathbf{x})\mathcal{F}^{ee}_{a,k_z'n'E,k_znM}\right], \\
\mathbf{E}(\kappa,\mathbf{x}) &= \mathbf{N}^{\text{reg}}_{k_z,n}(\kappa,\mathbf{x}) + \int \frac{L dk_z'}{2\pi} \sum_{n'} \left[\mathbf{M}^{\text{out}}_{k_z',n'}(\kappa,\mathbf{x})\mathcal{F}^{ee}_{a,k_z'n'M,k_znE} + \mathbf{N}^{\text{out}}_{k_z',n'}(\kappa,\mathbf{x})\mathcal{F}^{ee}_{a,k_z'n'E,k_znE}\right],
\end{aligned} \tag{3.2.15}$$

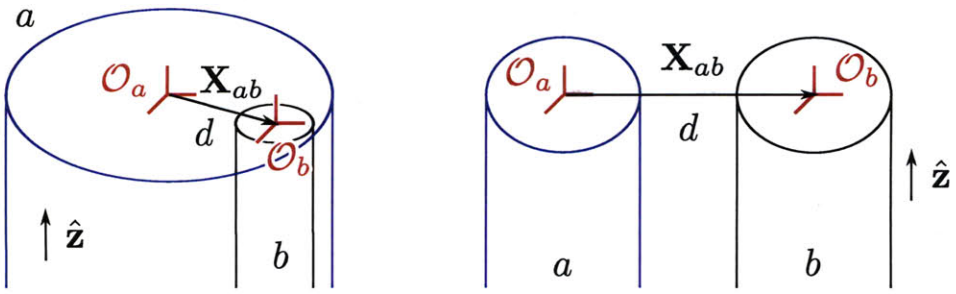

Figure 3-4: Two perfectly conducting infinite cylinders with radii R_a and R_b are separated by a center-to-center distance d. They can be outside one another, or one may be inside the other.

with boundary conditions $\mathbf{E}^{\parallel} = 0$ and $\mathbf{B}^{\perp} = 0$ on the cylinder surface. L is the length of the cylinders, and we are considering the limit $L \to \infty$. We have

$$\begin{aligned}
\mathcal{F}^{ee}_{a,k_z'n'E,k_znM} &= \mathcal{F}^{ee}_{a,k_z'n'M,k_znE} = 0, \\
\mathcal{F}^{ee}_{a,k_z'n'M,k_znM} &= -\tfrac{2\pi}{L}\delta(k_z - k_z')\delta_{n,n'}\frac{I_n'(R_a p)}{K_n'(R_a p)}, \\
\mathcal{F}^{ee}_{a,k_z'n'E,k_znE} &= -\tfrac{2\pi}{L}\delta(k_z - k_z')\delta_{n,n'}\frac{I_n(R_a p)}{K_n(R_a p)},
\end{aligned} \tag{3.2.16}$$

and analogous equations hold for scattering from cylinder b. The energy in Eq. (2.4.16) is given in terms of exterior scattering amplitudes only,

$$\mathcal{E} = \frac{\hbar c}{2\pi}\int_0^\infty d\kappa \log\det\left(\mathcal{I} - \mathcal{F}_a^{ee}\mathcal{U}^{ba}\mathcal{F}_b^{ee}\mathcal{U}^{ab}\right). \tag{3.2.17}$$

The matrix inside the determinant is diagonal in k_z, so the log-determinant over this index turns into an overall integral. A change of variable to polar coordinates converts the integrals over κ and k_z to a single integral over $p = \sqrt{k_z^2 + \kappa^2}$, yielding

$$\mathcal{E} = \frac{\hbar c L}{4\pi}\int_0^\infty p dp \left(\log\det\mathcal{N}^M + \log\det\mathcal{N}^E\right), \tag{3.2.18}$$

where

$$\mathcal{N}^M_{n,n''} = \delta_{n,n''} - \sum_{n'} \frac{I'_n(pR_a)}{K'_n(pR_a)} K_{n+n'}(pd) \frac{I'_{n'}(pR_b)}{K'_{n'}(pR_b)} K_{n'+n''}(pd)$$
$$\mathcal{N}^E_{n,n''} = \delta_{n,n''} - \sum_{n'} \frac{I_n(pR_a)}{K_n(pR_a)} K_{n+n'}(pd) \frac{I_{n'}(pR_b)}{K_{n'}(pR_b)} K_{n'+n''}(pd). \tag{3.2.19}$$

For scattering from inside cylinder a we have the scattering solutions

$$\mathbf{E}(\kappa,\mathbf{x}) = \mathbf{M}^{\text{out}}_{k_z,n}(\kappa,\mathbf{x}) + \int \frac{L dk'_z}{2\pi} \sum_{n'} \left[\mathbf{M}^{\text{reg}}_{k'_z,n'}(\kappa,\mathbf{x}) \mathcal{F}^{ii}_{a,k'_z n' M,k_z n M} + \mathbf{N}^{\text{reg}}_{k'_z,n'}(\kappa,\mathbf{x}) \mathcal{F}^{ii}_{a,k'_z n' E,k_z n M} \right],$$
$$\mathbf{E}(\kappa,\mathbf{x}) = \mathbf{N}^{\text{out}}_{k_z,n}(\kappa,\mathbf{x}) + \int \frac{L dk'_z}{2\pi} \sum_{n'} \left[\mathbf{M}^{\text{reg}}_{k'_z,n'}(\kappa,\mathbf{x}) \mathcal{F}^{ii}_{a,k'_z n' M,k_z n E} + \mathbf{N}^{\text{reg}}_{k'_z,n'}(\kappa,\mathbf{x}) \mathcal{F}^{ii}_{a,k'_z n' E,k_z n E} \right], \tag{3.2.20}$$

yielding

$$\begin{aligned} \mathcal{F}^{ii}_{a,k'_z n' E,k_z n M} &= \mathcal{F}^{ii}_{a,k'_z n' M,k_z n E} = 0\,, \\ \mathcal{F}^{ii}_{a,k'_z n' M,k_z n M} &= -\tfrac{2\pi}{L} \delta(k_z - k'_z) \delta_{n,n'} \frac{K'_n(R_a p)}{I'_n(R_a p)}\,, \\ \mathcal{F}^{ii}_{a,k'_z n' E,k_z n E} &= -\tfrac{2\pi}{L} \delta(k_z - k'_z) \delta_{n,n'} \frac{K_n(R_a p)}{I_n(R_a p)}. \end{aligned} \tag{3.2.21}$$

We note that the inside scattering amplitude matrix is the the inverse of the corresponding outside result. The energy, expressed in Eq. (2.4.16), now becomes

$$\mathcal{E} = \frac{\hbar c}{2\pi} \int_0^\infty d\kappa \log\det\left(\mathcal{I} - \mathcal{F}^{ii}_a \mathcal{W}^{ba} \mathcal{F}^{ee}_b \mathcal{V}^{ba}\right), \tag{3.2.22}$$

which contains the appropriate scattering amplitudes for the inside problem, $\mathcal{F}^{ii}_a$ for interior scattering of object a and $\mathcal{F}^{ee}_b$ for exterior scattering of object b. Using the same simplifications as in the outside case, we have

$$\mathcal{E} = \frac{\hbar c L}{4\pi} \int_0^\infty p dp \left(\log\det\mathcal{N}^M + \log\det\mathcal{N}^E\right), \tag{3.2.23}$$

where

$$\begin{aligned}\mathcal{N}^M_{n,n''} &= \delta_{n,n''} - \sum_{n'} \frac{K'_n(pR_a)}{I'_n(pR_a)} I_{n+n'}(pd) \frac{I'_{n'}(pR_b)}{K'_{n'}(pR_b)} I_{n'+n''}(pd)\,, \\ \mathcal{N}^E_{n,n''} &= \delta_{n,n''} - \sum_{n'} \frac{K_n(pR_a)}{I_n(pR_a)} I_{n+n'}(pd) \frac{I_{n'}(pR_b)}{K_{n'}(pR_b)} I_{n'+n''}(pd).\end{aligned} \tag{3.2.24}$$

3.2.4 Sphere and plate

In this subsection we investigate the Casimir interaction of an infinitely thick plate a opposite a sphere b, each with frequency-dependent permittivity and permeability. The geometry is depicted in Fig. 3-5.

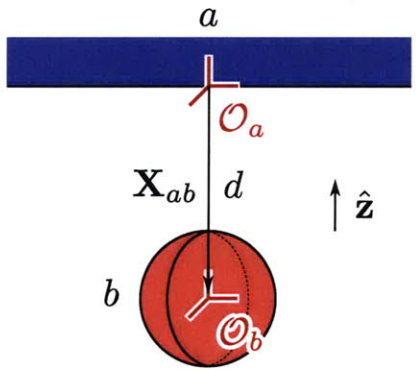

Figure 3-5: A sphere b of radius R is located opposite a plate a, separated by a center-to-surface distance d.

The scattering amplitude for the plate is easy to express in the plane wave basis using Eq. (3.2.10). We can apply our result from the plane geometry, Eq. (3.2.12), changing only $\mathcal{F}^{ee}_b$, which now becomes the scattering amplitude for vector plane wave functions outside a sphere. To express the scattering amplitude of the sphere in the spherical vector wave basis, we use Eqs. (D.1.1) and (D.1.2) and obtain

$$\begin{aligned}\mathcal{F}^{ee}_{b,\mathbf{k}_\perp P,\mathbf{k}'_\perp P'} &= (-1) C_{\mathbf{k}_\perp P}(\kappa) \langle \mathbf{E}^{\mathrm{reg}}_{\mathbf{k}_\perp P}(\kappa) | \mathbb{T}_b | \mathbf{E}^{\mathrm{reg}}_{\mathbf{k}'_\perp P'}(\kappa) \rangle \\ &= \sum_{lmQ,l'm'Q'} (-1) \frac{C_{\mathbf{k}_\perp P}(\kappa)}{C_Q(\kappa)} D^\dagger_{\mathbf{k}_\perp P,lmQ} C_Q(\kappa) \langle \mathbf{E}^{\mathrm{reg}}_{lmQ}(\kappa) | \mathbb{T}_b | \mathbf{E}^{\mathrm{reg}}_{l'm'Q'}(\kappa) \rangle D_{l'm'Q',\mathbf{k}'_\perp P'} \\ &= \sum_{lmQ,l'm'Q'} \frac{C_{\mathbf{k}_\perp P}(\kappa)}{C_Q(\kappa)} D^\dagger_{\mathbf{k}_\perp P,lmQ} \mathcal{F}^{ee}_{b,lmQ,l'm'Q'} D_{l'm'Q',\mathbf{k}'_\perp P'},\end{aligned} \tag{3.2.25}$$

where P and P' label the polarizations in the planar basis and Q and Q' label the polarizations in the spherical basis. The normalization factors $C_{\mathbf{k}_\perp P}(\kappa)$ and $C_Q(\kappa)$, defined below Eq. (B.1.1) and Eq. (B.3.1), arise from the definition of the scattering amplitude (see, for example, Eq. (2.3.9)). For a sphere with uniform permittivity and permeability, we compute the scattering amplitude by solving Eq. (2.3.9) in the spherical vector wave basis, which yields

$$\begin{aligned}
\mathcal{F}^{ee}_{b,lmE,l'm'M} &= \mathcal{F}^{ee}_{b,lmM,l'm'E} = 0\,, \\
\mathcal{F}^{ee}_{b,lmM,l'm'M} &= -\delta_{l,l'}\delta_{m,m'}\frac{i_l(\kappa R)\partial_R(Ri_l(n_b\kappa R)) - \mu_b\partial_R(Ri_l(\kappa R))i_l(n_b\kappa R)}{k_l(\kappa R)\partial_R(Ri_l(n_b\kappa R)) - \mu_b\partial_R(Rk_l(\kappa R))i_l(n_b\kappa R)}\,, \\
\mathcal{F}^{ee}_{b,lmE,l'm'E} &= -\delta_{l,l'}\delta_{m,m'}\frac{i_l(\kappa R)\partial_R(Ri_l(n_b\kappa R)) - \epsilon_b\partial_R(Ri_l(\kappa R))i_l(n_b\kappa R)}{k_l(\kappa R)\partial_R(Ri_l(n_b\kappa R)) - \epsilon_b\partial_R(Rk_l(\kappa R))i_l(n_b\kappa R)},
\end{aligned} \tag{3.2.26}$$

where n_b is the index of refraction, $n_b(ic\kappa) = \sqrt{\epsilon_b(ic\kappa)\mu_b(ic\kappa)}$. The modified spherical Bessel functions i_l and k_l are defined in Appendix B.

Plugging into Eq. (3.2.12) and using $\det(\mathbb{I} + \mathbb{A}\mathbb{B}) = \det(\mathbb{I} + \mathbb{B}\mathbb{A})$, the energy simplifies to

$$\mathcal{E} = \frac{\hbar c}{2\pi}\int_0^\infty d\kappa \log\det\left(\mathcal{I} - \mathcal{N}\right), \tag{3.2.27}$$

where

$$\begin{aligned}
\mathcal{N}_{lmP,l'm'P'} &= \delta_{m,m'}\,\mathcal{F}^{ee}_{b,lmP,lmP} \\
&\times \int_0^\infty \frac{k_\perp dk_\perp}{2\pi}\frac{e^{-2d\sqrt{\mathbf{k}_\perp^2+\kappa^2}}}{2\kappa\sqrt{\mathbf{k}_\perp^2+\kappa^2}} \\
&\times \sum_Q D_{lmP,\mathbf{k}_\perp Q}\, r_a^Q\left(ic\kappa, \sqrt{1+\mathbf{k}_\perp^2/\kappa^2}^{-1}\right) D^\dagger_{\mathbf{k}_\perp Q,l'mP'}(2\delta_{Q,P'} - 1).
\end{aligned} \tag{3.2.28}$$

Here $k_\perp = |\mathbf{k}_\perp|$ and r_a^Q, defined in Eq. (3.2.11), is the Fresnel coefficient for reflection of a wave with polarization Q. The ratio of $C_{\mathbf{k}_\perp P}(\kappa)$ to $C_Q(\kappa)$ in Eq. (3.2.25) has opposite signs depending on whether P and Q represent the same polarization or the opposite polarization, which we have implemented through the term $(2\delta_{P,Q} - 1)$. The integration over all angles of $\mathbf{k}_\perp$ has already been carried out, which makes $\mathcal{N}$ diagonal in m and m'. (Although $D_{lmp,\mathbf{k}_\perp Q}$ seems to depend on the angle of $\mathbf{k}_\perp$, the

multiplication with its Hermitian conjugate cancels this dependence.)

To leading order for large d/R, the $l = 1$ components of the sphere's scattering amplitude and the $\kappa \to 0$ limit of the permittivities and permeabilities contribute. The scattering amplitude can be expanded to lowest order in terms of the sphere's electric and magnetic polarizabilities, $\mathcal{F}^{ee}_{b,1mM,1mM} \to \frac{2}{3}\alpha^M \kappa^3$ and $\mathcal{F}^{ee}_{b,1mE,1mE} \to \frac{2}{3}\alpha^E \kappa^3$, where the polarizabilities $\alpha^M = \frac{\mu_{b0}-1}{\mu_{b0}+2}R^3$ and $\alpha^E = \frac{\epsilon_{b0}-1}{\epsilon_{b0}+2}R^3$ are given in terms of the zero frequency permittivity $\epsilon_{b0} = \epsilon_b(0)$ and permeability $\mu_{b0} = \mu_b(0)$. To leading order the energy is given by

$$\mathcal{E} = -\frac{3\hbar c}{8\pi d^4}(\alpha^M \phi^M + \alpha^E \phi^E), \tag{3.2.29}$$

where

$$\begin{aligned} \phi^M &= \int_0^1 dx \left[\left(1 - \frac{x^2}{2}\right) r_a^M(0,x) - \frac{x^2}{2} r_a^E(0,x)\right], \\ \phi^E &= \int_0^1 dx \left[\left(1 - \frac{x^2}{2}\right) r_a^E(0,x) - \frac{x^2}{2} r_a^M(0,x)\right] \end{aligned} \tag{3.2.30}$$

can be expressed in terms of elementary functions, but the expressions are too complicated to be worth reproducing here. The two functions are plotted in Fig. 3-6.

The expression for the energy in Eq. (3.2.29) agrees with the results in Ref. [75] for a perfect metal plate $\epsilon_a \to \infty$ and a sphere with general ϵ_b. It also agrees with the results in Ref. [110] for a perfect metal plate and a perfect metal sphere, $\epsilon_a \to \infty$, and $\epsilon_b \to \infty$. Both of these works arrive at similar general expressions for the energy to what we have found here; Ref. [75] combines scattering theory techniques we have used here with the method of images, while Ref. [110] uses Wigner rotation matrices.

In the calculations of Refs. [75] and [110], when $\epsilon \to \infty$ the corresponding μ is set to zero to reproduce perfect metal boundary conditions within a low-frequency expansion. (Ref. [27] contains the asymptotic Casimir energy formula Eq. (3.2.29) in the case where the magnetic permeabilities are set equal to one.) As the plots in Fig. 3-6 show, however, the perfect reflectivity limit of the plate is approached slowly with increasing ϵ_a. To compare with experiments it is thus important to compute the energy (3.2.27) using the actual permittivities and permeabilities of the material

instead of perfect metal limits.

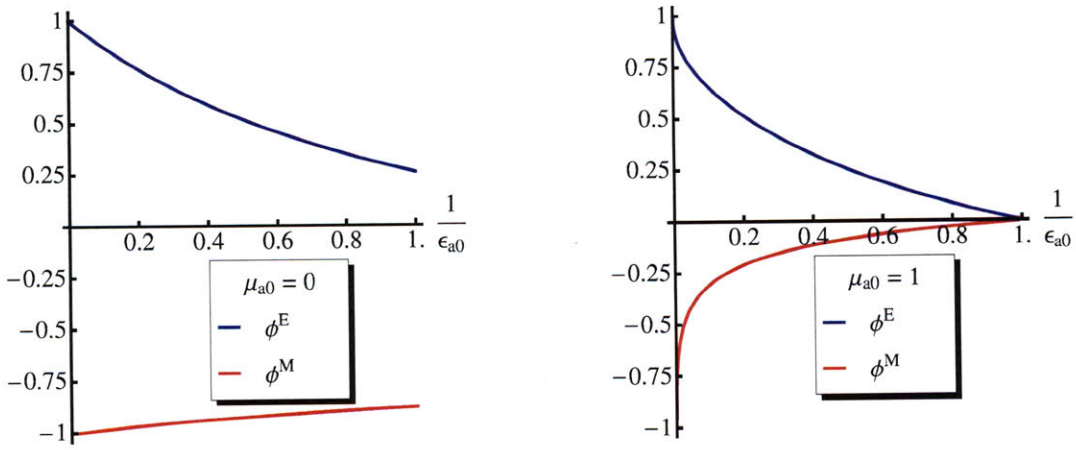

Figure 3-6: Plots of ϕ^E (blue, positive) and ϕ^M (red, negative) as functions of $1/\epsilon_{a0}$ for fixed $\mu_{a0} = 0$ (left) or fixed $\mu_{a0} = 1$ (right). For $\mu_{a0} = 1$ the two functions ϕ^E and ϕ^M approach 1 rather slowly from the right (perfect metal limit). So, for comparison with experiments, it may not be justified to use the perfect metal limit $\epsilon_a \to \infty$ of the plate to compute the Casimir energy.

3.2.5 Object inside a sphere or spheroid

Typically, it is found that the Casimir force is attractive, as long as the space between the objects is empty, and the magnetic susceptibility of the objects is negligible compared to their electric susceptibilities. But when space is filled with a medium with electric permittivity ϵ_M intermediate between that of two objects, $\epsilon_1 < \epsilon_M < \epsilon_2$, the force between the two becomes repulsive [27]. This effect has recently been verified experimentally in the large separation (retarded) regime [17]. But while repulsive forces are nothing new, they become interesting for applications when they produce stable equilibria, which, for example, the Coulomb force cannot.

For an infinite cylinder enclosed in another, the Casimir force has recently been shown to have a stable equilibrium in the two directions perpendicular to the cylinder axes, when the material properties are chosen so that the force between two slabs of the same materials would be repulsive [111]. If the inner and outer cylinders have

square cross sections, the direction of the torque exerted by one cylinder on the other is found to agree qualitatively with the predictions of the pairwise summation or proximity force approximations (PSA or PFA). Orientation dependence has also been studied recently for a small spheroid interacting via quantum electrodynamic fluctuations with another spheroid or an infinite plate [112] and for an ellipsoid near a wall subject to the *critical* Casimir effect, which arises from thermal fluctuations in a liquid near a critical point [113]. (The smallness of the spheroid refers to keeping only the first term in the series expansion of the Casimir energy in the largest length scale of the spheroid.)

Here, we present the following cases, studied in Refs. [83, 84]: a finite sphere or a small spheroid inside a spherical cavity, and a small spheroid inside a slightly deformed spherical cavity, depicted in Fig. 3-7. The spring constant for displacements from the center of the cavity and the dependence of the energy on the relative orientations of the inner object and the cavity walls are computed. We find that the stability of the force equilibrium can be predicted based on the sign of the force between two parallel plates of the same material, but the direction of the torque cannot be.

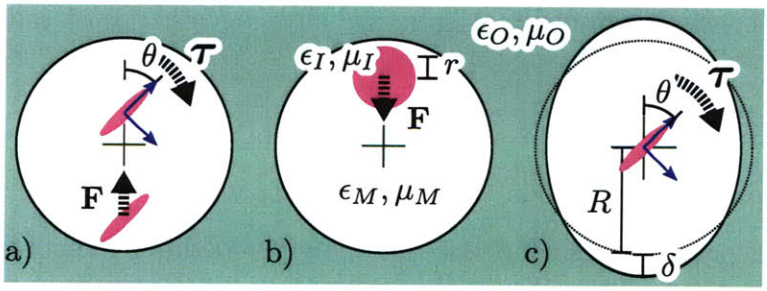

Figure 3-7: Summary of the configurations we consider and of the results. We have assumed that the small spheroid's zero frequency permittivity satisfies $\epsilon_{I,0} > \epsilon_{M,0}$ and that it is larger in the body-fixed $\hat{\mathbf{z}}$ direction, so $\alpha^E_{zz} > \alpha^E_{\perp\perp}$. Furthermore, the magnetic permeabilities are all set to one. a) Direction of the force $\mathbf{F}$ on such a spheroid in a spherical cavity if $\epsilon_{M,0} > \epsilon_{O,0}$, and the direction of the torque $\boldsymbol{\tau}$ when either $\epsilon_{M,0} > \epsilon_{O,0}$ or $\epsilon_{M,0} \ll \epsilon_{O,0}$. b) A finite size sphere experiences a restoring force $\mathbf{F}$ for the various combinations of materials listed in Table 3.1. c) Direction of the torque $\boldsymbol{\tau}$ in the center of a slightly spheroidal cavity if either $\epsilon_{M,0} < \epsilon_{O,0}$ or $\epsilon_{M,0} \gg \epsilon_{O,0}$.

The Casimir energy

$$\mathcal{E} = \mathcal{E}_0 + \frac{1}{2}k\frac{a^2}{R^2} + \frac{1}{3!}k_3\frac{a^3}{R^3} + \frac{1}{4!}k_4\frac{a^4}{R^4} + \cdots \tag{3.2.31}$$

is characterized by the spring constant k and the coefficients k_n in a series expansion in a/R, where a is the magnitude of the displacement from the center of the cavity and R the radius of the (undeformed) spherical cavity. (k has units of energy here.) Unlike the case of infinite cylinders, where one object can be displaced along the cylinder axes without changing the energy, our case exhibits, for appropriately chosen materials, true stability in all directions and applies to realistic situations. For example, we compute the force on a metal sphere in a spherical drop of liquid surrounded by air. By determining the mean square deviation from the center, $\langle a^2 \rangle = 3k_BTR^2/k$, the spring constant k can be measured experimentally. We can estimate that the size of the droplet R has to be smaller than $\approx 3\mu\text{m}\frac{r^3}{R^3}$, where r is the typical dimension of the inner object, for the thermal motion to be confined near the center of the cavity. (This length scale is obtained by balancing $3k_BT$ for room temperature with a rough estimate of the spring constant, $k \sim \frac{\hbar c}{R}\frac{r^3}{R^3}$.) To keep the two objects nearly concentric against the gravitational force, R has to be smaller than $\approx 1\mu$m for the typical metal or liquid densities considered here. Our calculations show that, for example, a sphere of gold of radius $r = \frac{3}{4}R$ inside a spherical drop of ethanol of radius $R = .1\mu$m has an rms deviation $\sqrt{\langle a^2 \rangle} = 0.04R$ from the center due to thermal motion and a displacement from the center by $a \approx 10^{-6}R$ due to gravity. A variety of applications may benefit from our analysis; in cancer therapy new treatments utilize nanocarriers that trap drug particles inside $R \approx .1\mu$m polymer or lipid membrane shells [114], and molecular cages are proposed as containers for the storage of explosive chemicals [115]. Our results may guide the search for better materials and sizes of the enclosing cell.

Whether the center of the cavity is a point of stable or unstable equilibrium turns out to be correlated with whether the Casimir force is repulsive or attractive for two parallel plates under those conditions. The direction of the torque, on the other

hand, depends on the dielectric properties of the medium and the cavity walls in an unintuitive way, which cannot be predicted by the PSA or PFA, see Fig. 3-7. In particular, this behavior is not due to dispersion effects, which explain similar phenomena reported in Ref. [111]. We calculate the torque on a small spheroid that is displaced from the center of a spherical cavity (Fig. 3-7 a)) or concentric with a slightly spheroidal cavity (Fig. 3-7 c)). In the former case, the orientation dependence manifests itself in k, which captures both the torque and the orientation dependence of the total force. In the latter case, $\mathcal{E}_0$ depends on the relative orientation of the spheroid inside the deformed cavity. (If the cavity is spherical, $\mathcal{E}_0$ is a finite constant that can be ignored.) By choosing appropriate materials, the inside object, e.g., a nanorod, can be made to align in different ways with the cavity shape, a situation which is reminiscent of a compass needle aligning with the magnetic field of the earth.

The Casimir energy for one object inside another,

$$\mathcal{E} = \frac{\hbar c}{2\pi} \int_0^\infty d\kappa \ln \det(\mathcal{I} - \mathcal{F}_O^{ii} \mathcal{W}^{io} \mathcal{F}_I^{ee} \mathcal{V}^{io}) \tag{3.2.32}$$

is expressed in terms of the inner object's exterior scattering amplitude matrix, $\mathcal{F}_I^{ee}$, and the outer object's interior scattering amplitude matrix, $\mathcal{F}_O^{ii}$, like in the case of one cylinder inside another, Eq. (3.2.22). The exterior scattering amplitudes describe the scattering of regular wave functions to outgoing waves when the source lies at infinity. The interior scattering amplitudes express the opposite, the amplitudes of the regular wave functions, which result from scattering outgoing waves from a source inside the object. The translation matrices $\mathcal{W}^{io}$ and $\mathcal{V}^{io}$ convert regular wave functions between the origins of the outer and the inner objects; they are related by complex transpose up to multiplication by (-1) of some matrix elements.

With uniform, isotropic, and frequency-dependent permittivity $\epsilon_x(ic\kappa)$ and permeability $\mu_x(ic\kappa)$ functions ($x = I$: inner object; $x = O$: outer object; $x = M$:

medium) the scattering amplitude matrix of the sphere is diagonal. It is given by

$$\mathcal{F}^{ee}_{I,lmE,lmE}(ic\kappa) = \mathcal{F}^{ee}_{I,lE}(\xi) = \\ -\frac{i_l(\xi)\partial_r(ri_l(z_I\xi)) - \frac{\epsilon_I}{\epsilon_M} i_l(z_I\xi)\partial_r(ri_l(\xi))}{k_l(\xi)\partial_r(ri_l(z_I\xi)) - \frac{\epsilon_I}{\epsilon_M} i_l(z_I\xi)\partial_r(rk_l(\xi))} \tag{3.2.33}$$

for E (electric) polarization and by the same expression with $\frac{\epsilon_I}{\epsilon_M}$ replaced by $\frac{\mu_I}{\mu_M}$ for M (magnetic) polarization (not to be confused with subscript M indicating the medium's response functions). The expression is the same as Eq. (3.2.26), except that it accounts for the surrounding medium, which has non-unit permittivity and permeability. In Eq. (3.2.33) the frequency dependence of the response functions has been suppressed. The indices of refraction $n_x(ic\kappa) = \sqrt{\epsilon_x(ic\kappa)\mu_x(ic\kappa)}$ of the sphere and the medium appear in the ratio $z_I(ic\kappa) = n_I(ic\kappa)/n_M(ic\kappa)$ and the argument $\xi = n_M(ic\kappa)\kappa r$. The first equality in Eq. (3.2.33) defines an abbreviation for the scattering amplitude matrix, in which the superfluous polarization and angular momentum (l, m) indices are suppressed. The interior scattering amplitude matrix of the spherical cavity is obtained from the exterior scattering amplitude matrix of the sphere by inserting the outside object's radius and response functions in place of those of the inside object and exchanging the modified spherical Bessel functions i_l and k_l everywhere.

However, the scattering approach is not limited to simple geometries. An array of techniques is available for calculating the scattering amplitudes of other shapes. We employ the perturbation approach to find the scattering amplitudes of a deformed spherical cavity [116, 117] of radius $R + \delta(1 - 3/2\sin^2\theta)$. The deformation, indicated in Fig. 3-7 c), is chosen so that the volume is unchanged to first order in δ. We find the $O(\delta)$ correction, $\mathcal{F}^{(1)}$, to the scattering amplitude matrix in a perturbation series expansion, $\mathcal{F} = \mathcal{F}^{(0)} + \mathcal{F}^{(1)} + \cdots$, by matching the regular and outgoing fields according to the Maxwell boundary conditions along the deformed object's surface [118]. On the other hand, for a small object (compared to the wavelength of the radiation), we can approximate the scattering amplitudes to lowest order in κ using the static polarizability tensor, $\mathcal{F}^{ee}_{I,1mP,1m'P} = 2/3(n_{M,0}\kappa)^3\alpha^P_{mm'} + O(\kappa^5)$, where the

subscript 0 indicates the static ($ic\kappa = 0$) limit and P is the polarization label. The scattering amplitudes involving higher angular momenta $l > 1$ are higher order in κ. For a small ellipsoid, in particular, the electric polarizability tensor $\boldsymbol{\alpha}^E$ is diagonal in a coordinate system aligned with the ellipsoid's body axes,

$$\alpha_{ii}^E = \frac{V}{4\pi} \frac{\epsilon_{I,0} - \epsilon_{M,0}}{\epsilon_{M,0} + (\epsilon_{I,0} - \epsilon_{M,0})n_i}, \tag{3.2.34}$$

where $i \in \{x, y, z\}$ [103]. The larger the semi-axis in direction i, the smaller the depolarization factor n_i (not to be confused with the index of refraction). The entries of the magnetic polarizability tensor $\boldsymbol{\alpha}^M$ are obtained by exchanging $\mu_{x,0}$ for $\epsilon_{x,0}$ in Eq. (3.2.34). In the small size limit the polarizability tensor of a perfect metal ellipsoid is obtained by taking both $\epsilon_{I,0}$ to infinity and $\mu_{I,0}$ to zero.

For simplicity we specialize to a spheroid, which has two equal semiaxes. We choose the semiaxes along $\hat{\mathbf{x}}$ and $\hat{\mathbf{y}}$ to be equal, therefore, $\alpha_{xx}^P = \alpha_{yy}^P = \alpha_{\perp\perp}^P$. We fix the $\hat{\mathbf{z}}$ axis of the lab frame to be along the direction of displacement of the spheroid from the center of the cavity. θ denotes the angle between the spheroid's and the lab's $\hat{\mathbf{z}}$ axes. For such a small spheroid inside a spherical cavity of radius R (Fig. 3-7 a)), the spring constant is obtained by expanding the log-determinant in Eq. (3.2.32) to first order,

$$\begin{aligned} k_{R\to\infty} = \frac{\hbar c}{R^4 n_{M,0}} \big[&\operatorname{Tr} \boldsymbol{\alpha}^E f_1^E \\ &+ \left(\alpha_{zz}^E - \alpha_{\perp\perp}^E\right) \tfrac{3\cos^2\theta - 1}{2} f_2^E + E \to M \big], \end{aligned} \tag{3.2.35}$$

where the material dependent functions

$$\begin{aligned} f_1^E &= \int_0^\infty \frac{\xi^5 d\xi}{9\pi} \left[\mathcal{F}_{O,1M}^{ii} - 2\mathcal{F}_{O,1E}^{ii} - \mathcal{F}_{O,2E}^{ii}\right], \\ f_2^E &= \int_0^\infty \frac{\xi^5 d\xi}{9\pi} \left[\tfrac{4}{5}\mathcal{F}_{O,1E}^{ii} - \tfrac{1}{5}\mathcal{F}_{O,2E}^{ii} - \mathcal{F}_{O,1M}^{ii}\right] \end{aligned} \tag{3.2.36}$$

express the rotation invariant and the orientation dependent parts of the energy, respectively. f_1^M and f_2^M are obtained from f_1^E and f_2^E by exchanging E and M

everywhere. This result is valid for asymptotically large R; it involves only the zero frequency ($ic\kappa = 0$) response functions since R is greater than any material dependent length scales as well as the size of the inner object. Notice that only the $l = 1, 2$ scattering amplitudes of the cavity walls appear in Eqs. (3.2.35) and (3.2.36).

The behavior of the functions f_1^P, depicted in Fig. 3-8 for $\mu_{M,0} = \mu_{O,0}$, is as expected: f_1^E is monotonic, positive when $\epsilon_{M,0} > \epsilon_{O,0}$, negative when $\epsilon_{M,0} < \epsilon_{O,0}$, and f_1^M always has the opposite sign of f_1^E. When f_1^E is positive, a small object with $\epsilon_{I,0} > \epsilon_{M,0}$ is levitated stably, when f_1^E is negative, $\epsilon_{M,0} > \epsilon_{I,0}$ has to hold. Thus, stability occurs under the same conditions as repulsion for two objects outside of one another. The opposite sign of f_1^M is expected from equivalent expressions for the two-infinite-slab geometry [95]. When the dielectric contrast between the medium and the outer sphere is taken to small or large limits, stability or instability is maximized. To verify whether stability is observable for realistic materials and object sizes, we

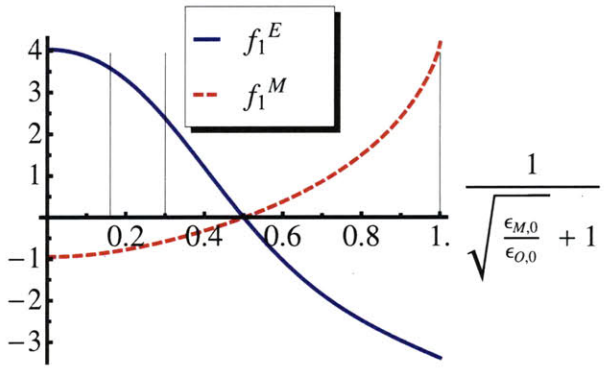

Figure 3-8: f_1^E and f_1^M describe the part of the spring constant $k_{R\to\infty}$, which is invariant under a rotation of the inside object. The vertical lines indicate the values pertaining to the configurations presented in Table 3.1, ethanol-vacuum (0.16), bromobenzene-vacuum (0.30), and gold cavity walls (1). In this plot, $\mu_{M,0} = \mu_{O,0}$.

evaluate Eq. (3.2.32) numerically for a sphere of radius r inside a spherical cavity of radius R filled with various liquids (Fig. 3-7 b)). [4] The coefficients k, k_4, and

[4]For the permittivity function of gold we use $\epsilon(ic\kappa) = 1 + \frac{\omega_p^2}{c\kappa(c\kappa+\gamma)}$, where $\omega_p = 1.14 \cdot 10^{16}$Hz and $\gamma = 9.27 \cdot 10^{13}$Hz [119] as used in Ref. [17]. For the other materials we use an oscillator model, $\epsilon(ic\kappa) = 1 + \sum_{n=1}^{N} \frac{C_n}{1+(c\kappa/\omega_n)^2}$, with $[\omega_n]_{n=1,2} = [6.6, 114] \cdot 10^{14}$Hz and $[C_n]_{n=1,2} = [23.84, 0.852]$ for ethanol [120] as used in Ref. [111], with $[\omega_n]_{n=1,2} = [5.47, 128.6] \cdot 10^{14}$Hz and

k_6 in the series expansion in Eq. (3.2.31) are listed in Table 3.1. For comparison, the asymptotic result $k_{R\to\infty}$ is also included. If both inside and outside object are spherically symmetric, the series in Eq. (3.2.31) does not contain terms $\sim \frac{a^n}{R^n}$ with n odd.

Table 3.1: k, $k_{R\to\infty}$, k_4, and k_6 are listed for various combinations of materials for the case of a spherical inner object inside a spherical cavity, depicted in Fig. 3-7 b). The dimensionless numbers in the table have to be multiplied by $\frac{\hbar c}{R}$. R is given in microns [μm]. $k_{R\to\infty}$ depends on R only through the ratios $\frac{\hbar c}{R}$ and $\frac{r}{R}$, so its numerical prefactor is the same for all R. The highest cutoff used was $l_{\max} = 30$. (The asymptotic result $k_{R\to\infty}$ only requires $l = 1, 2$.)

Inside-Medium-Outside	R	r/R	k	$k_{R\to\infty}$	k_4	k_6
Gold-Bromobenzene-	0.1	1/4	4.0e-2	5.4e-2	1.2	8.2e1
Vacuum		3/4	2.2e1	1.4	4.2e3	1.8e6
	1.0	1/4	6.9e-2	5.4e-2	2.6	2.0e2
		3/4	7.0e1	1.4	1.8e4	1.0e7
Gold-Ethanol-	0.1	1/4	5.0e-2	3.7e-2	1.6	1.0e2
Vacuum		3/4	2.7e1	9.9e-1	5.2e3	2.2e6
	1.0	1/4	4.5e-2	3.7e-2	1.7	1.4e2
		3/4	6.0e1	9.9e-1	1.8e4	1.2e7
Silica-Bromobenzene-	0.1	1/4	6.1e-3	7.1e-3	1.9e-1	1.3e1
Gold		3/4	4.2	1.9e-1	8.6e2	4.0e5
	1.0	1/4	1.8e-2	7.1e-3	7.3e-1	6.0e1
		3/4	2.3e1	1.9e-1	5.7e3	3.1e6
Silica-Ethanol-	0.1	1/4	1.5e-2	1.2e-2	4.6e-1	3.1e1
Gold		3/4	1.0e1	3.3e-1	1.9e3	8.4e5
	1.0	1/4	1.9e-2	1.2e-2	8.2e-1	7.2e1
		3/4	4.1e1	3.3e-1	1.2e4	7.6e6

The three materials were chosen so that the sequence of permittivities ϵ_I, ϵ_M, ϵ_O either increases or decreases for the imaginary frequencies that dominate in Eq. (3.2.32). Contrary to the prediction of the PSA and PFA the force is not symmetric with respect to exchange of the inner and outer permittivities. In the same medium, a high dielectric sphere is held more stably in the center of a cavity with low dielectric walls than a low dielectric sphere inside a cavity with high dielectric walls.

The asymptotic result $k_{R\to\infty}$ yields a good approximation of k for $\frac{r}{R} = \frac{1}{4}$. But from Eq. (3.2.35) one would expect $k_{R\to\infty}$ to grow linearly with the volume of the

$[C_n]_{n=1,2} = [2.967, 1.335]$ for bromobenzene [120] as used in Ref. [17], and with $[\omega_n]_{n=1-4} = [0.867, 1.508, 2.026, 203.4] \cdot 10^{14}$Hz and $[C_n]_{n=1-4} = [0.829, 0.095, 0.798, 1.098]$ for silica (SiO_2) [121].

inner sphere, since polarizability is proportional to the volume, see Eq. (3.2.34). In fact, k for $\frac{r}{R} = \frac{3}{4}$ is about 1000 times larger than for $\frac{r}{R} = \frac{1}{4}$, instead of just 27 times. This means that for a gold sphere in a liquid drop with $\frac{r}{R} = \frac{3}{4}$ and $R = 1\mu$m at room temperature, indeed, the Casimir spring holds the particle near the center effectively, $\sqrt{\langle a^2 \rangle}/R < 0.1$.

Although k, k_4, and k_6 increase by three orders of magnitude in some cases, the prefactor $\frac{1}{n!}$ ensures that the coefficients in the Taylor expansion in Eq. (3.2.31) increase only by one order of magnitude. Thus, for small excursions from the center, e.g., $a/R < 0.1$, the higher corrections $n \geq 4$ can be neglected.

Compared to the stability conditions studied thus far, the orientation dependence of the energy is more varied. f_2^E and f_2^M, plotted in Fig. 3-9, have the same sign for most ratios of medium to outside permittivities, unlike f_1^E and f_1^M, which always have opposite signs. In these ranges of values, the contributions to the torque from electric and magnetic polarizability are opposite for a small perfect metal spheroid, for which $\epsilon_{I,0} > \epsilon_{M,0}$ and $\mu_{I,0} < \mu_{M,0}$. Unlike f_1^E and f_1^M, also, f_2^E and f_2^M change sign again at $\frac{\epsilon_{O,0}}{\epsilon_{M,0}} \approx 80$ and at $\frac{\epsilon_{O,0}}{\epsilon_{M,0}} \approx 2000$, respectively. So, while the direction of the total force and the stability of the equilibrium can be determined based on the relative magnitudes of the permittivities, the torque cannot be. The PSA and PFA predict the orientation with the lowest energy in the vicinity of $\frac{\epsilon_{O,0}}{\epsilon_{M,0}} = 1$ correctly but not when $\frac{\epsilon_{O,0}}{\epsilon_{M,0}} \gg 1$. Furthermore, the second sign change of f_2^E and f_2^M raises the question whether calculations of the Casimir torque for infinite conductivity metals are 'universal' in the sense that they produce the correct qualitative results for real materials.

The orientation dependent part of the energy for the configurations discussed thus far vanishes, of course, when the small spheroid is in the center of the spherical cavity. If the cavity is slightly deformed, however, the energy, $\mathcal{E}_0$, depends on the relative orientation of the spheroid and the cavity (Fig. 3-7 c)). We deform the spherical

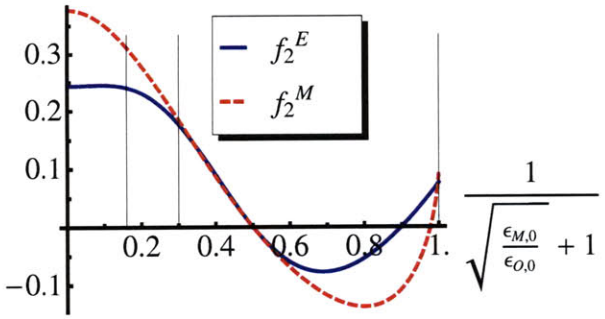

Figure 3-9: f_2^E and f_2^M describe the part of the spring constant $k_{R\to\infty}$, which changes with the orientation of the inside spheroid. In this plot, $\mu_{M,0} = \mu_{O,0}$.

cavity as described earlier and obtain to first order in δ/R,

$$\mathcal{E}_0 = \frac{\hbar c \cos^2\theta}{R^4 n_{M,0}} \frac{\delta}{R} \left[\left(\alpha_{zz}^E - \alpha_{\perp\perp}^E \right) g^E + E \to M \right], \tag{3.2.37}$$

where the orientation-independent part of the energy has been dropped. For $\mu_{O,0} = \mu_{M,0}$, g^E and g^M are given by

$$\begin{aligned} g^E &= \int_0^\infty \frac{\xi^4 d\xi}{10\pi} \frac{i_1 k_0 + i_0 k_1}{\left(\tilde{k}_0 i_1 + \tilde{k}_1 i_0 z_O + i_1 \tilde{k}_1/(z_O\xi)(1-z_O^2)\right)^2} \\ &\quad \times (z_O^2 - 1)\left(4\tilde{k}_1^2/\xi^2 - (\tilde{k}_0 + \tilde{k}_1/(z_O\xi))^2\right), \\ g^M &= \int_0^\infty \frac{\xi^4 d\xi}{10\pi} \frac{i_1 k_0 + i_0 k_1}{\left(\tilde{k}_1 i_0 + \tilde{k}_0 i_1 z_O\right)^2} (z_O^2 - 1)\tilde{k}_1^2, \end{aligned} \tag{3.2.38}$$

where the arguments of the modified spherical Bessel functions and of $z_O(0)$ are suppressed. i_l and k_l are functions of ξ, and $\tilde{k}_l$ stands for $k_l(z_O(0)\xi)$, where $z_O(ic\kappa) = n_O(ic\kappa)/n_M(ic\kappa)$ is the ratio of the permittivities of the cavity walls and the medium. The material dependent functions g^E and g^M are plotted in Fig. 3-10.

Again, g^E has the same sign for $\frac{\epsilon_{O,0}}{\epsilon_{M,0}} \to 0$ (left in Fig. 3-10) and $\frac{\epsilon_{O,0}}{\epsilon_{M,0}} \to \infty$ (right). In addition to the root at $\frac{\epsilon_{O,0}}{\epsilon_{M,0}} = 1$, g^E also vanishes at $\frac{\epsilon_{O,0}}{\epsilon_{M,0}} \approx 0.46$.

The rich orientation dependence of the energy is expected to collapse as the size of the inside object grows to fill the cavity and the PFA becomes applicable. Based on the stability analysis for finite inside spheres, though, we expect the asymptotic results, f_2^P and g^P, to predict the orientation dependence for reasonably small inside

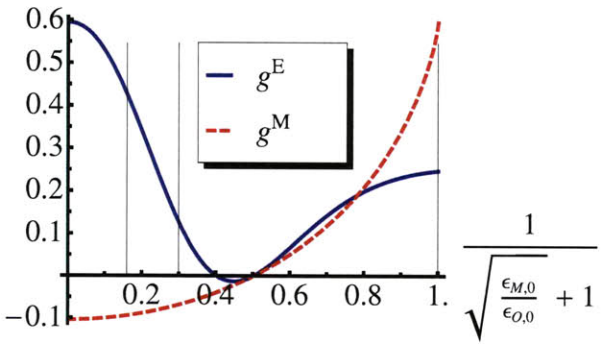

Figure 3-10: g^E and g^M describe the dependence of the energy $\mathcal{E}_0$ on the relative orientation of the inside spheroid and the deformed cavity walls.

spheroids.

In reality, various corrections to the idealized shapes have to be taken into account. A drop of liquid, which is placed on a surface, is influenced by gravity and interactions with the substrate. An asymmetric inner object, or one that is displaced from the center, deforms the shape of the droplet additionally by causing uneven Casimir stresses.

How does the Casimir torque on a small spheroid inside a cavity relate to the torque on a spheroid that is adjacent to a plate or another compact object? To facilitate the discussion, let us assume the spheroid has permittivity greater than one, permeability equal unity, and the medium is vacuum. Then, in the limit where the spheroid is small compared to the separation, the torque vanishes if the second object is a perfect metal plate [37, 38, 112]. The torque aligns the largest semiaxis of the spheroid towards the second object if that object is a dielectric sphere or small spheroid [112, 83]. This is in contrast to the inside configuration, where the spheroid's longest semiaxis is preferred to point away from the closest point on the metallic spherical cavity. Thus, the preferred orientation of the small spheroid flips when it is moved between the inside and the outside of a spherical shell so that there is no torque if the spheroid faces an infinite metal plate, which is the limit of an infinitely large shell. The smooth continuation of the low energy orientation in the inside configuration to the high energy orientation in the outside case is discussed in greater detail in Ref. [83].

Now, let us investigate the opposite limit. We compute the interaction energy of a finite-size perfect metal sphere of radius r with the perfect metal walls of a spherical cavity when the separation, $d = R - r - a$, between their surfaces tends to zero. The leading term in d/r is known to be given by the PFA. By evaluating our closed-form expressions numerically, we find the next to leading term in an expansion in d/r. An understanding of the corrections to the PFA has been sought for some time [122, 123, 10, 124, 125, 76]. Our work extends beyond previous attempts, many of which have treated hypothetical scalar fields, by considering electromagnetic fields for two objects with different curvature and relative position. In Ref. [126] an analytical approach to PFA corrections for the electrodynamic case is sought. For the sphere-plane geometry [75, 110] and two spheres of *equal* radii facing each other [30] the corrections have recently been computed numerically. We repeat these computations for other ratios of radii of two spheres outside one another and find that the inside and outside results connect smoothly. This is of direct experimental significance because Casimir force measurements are usually performed with spherical rather than perfectly planar surfaces.

In the limit where when the interior object is nearly touching the cavity wall, the Casimir force F between two conducting spheres, which is attractive, is proportional in magnitude to d^{-3}, where d is the separation of surfaces. The coefficient of d^{-3} is given by the PFA,

$$\lim_{d\to 0} d^3\, F = -\frac{\pi^3 \hbar c}{360}\frac{rR}{r+R}\,. \tag{3.2.39}$$

This result holds for both the interior and the exterior configuration of two spheres. For fixed r we formally distinguish the cases: $R > 0$ for the exterior, $R \to \infty$ for the plate-sphere, and $R < 0$ for the interior configuration (see Fig. 3-11 for reference). All possible configurations are taken into account by considering $-1 \leq r/R \leq 1$.

Our numerical studies of the interior configuration for perfectly conducting spheres enable us to study the limit $d/r \to 0$. This is a difficult limit because no simplifying approximations can be applied to Eq. (3.2.32). All powers of $\mathcal{F}_O^{ii}\mathcal{W}^{io}\mathcal{F}_I^{ee}\mathcal{V}^{io}$ contribute,

and the number of partial waves (l, l') necessary to obtain convergence grows as $d/r \to 0$. Although we know of no derivation of the functional form of the Casimir force beyond the leading term in the PFA, our numerical data are well fit by a power series in d/r,

$$F = -\frac{\pi^3 \hbar c}{360 d^3} \frac{rR}{r+R} \left(1 + \theta_1(r/R)\frac{d}{2r} - \theta_2(r/R)\frac{d^2}{2r^2} + ...\right)$$

We have used this functional form to extract the coefficient $\theta_1(r/R)$.

It is useful to have an estimate, however crude, of $\theta_1(r/R)$ over the whole range of r/R with which to compare our results. Although the PFA is accurate only in the limit $d/r \to 0$, it can be extended in various ways to the whole range of d, r, and R. The PFA is obtained by considering both surfaces as made up of infinitesimal parallel mirrors. From each point (ξ_1, ξ_2) on the surface of object O one computes the distance $L(\xi_1, \xi_2)$ to the other object's surface along the surface normal $\hat{\mathbf{n}}(\xi_1, \xi_2)$. By integrating the Casimir energy per unit area for two parallel plates separated by $L(\xi_1, \xi_2)$ over the surface of object O one obtains the "O-based" PFA energy. Clearly, the result depends on which object one chooses as O, but the various results do agree to leading order in d/r. We can choose either of the two spheres to arrive at the "r-based PFA" or the "R-based PFA", see Fig. 3-11. Either one yields a 'correction' to the leading order PFA,

$$\theta_{1,r}^{\mathrm{PFA}}(x) = -\left(x + \frac{x}{1+x} + 3\right), \theta_{1,R}^{\mathrm{PFA}} = -\left(3x + \frac{x}{1+x} + 1\right),$$

where $x = r/R$. Again, $\theta_{1,r}^{\mathrm{PFA}}$ and $\theta_{1,R}^{\mathrm{PFA}}$ are only used for comparison with the actual correction θ_1. Note that the PFA predicts a smooth continuation from the interior to the exterior problem.

In Fig. 3-11 we plot the values of θ_1 extracted from a numerical evaluation of the force from Eq. (3.2.32) for various values of $r/R < 0$, along with the values for $r/R = 0$ and $r/R = 1$ from Refs. [30] and [75]. We have also repeated the exterior analysis of Ref. [30] for other values of $r/R > 0$. For reference, the two PFA estimates are also shown.

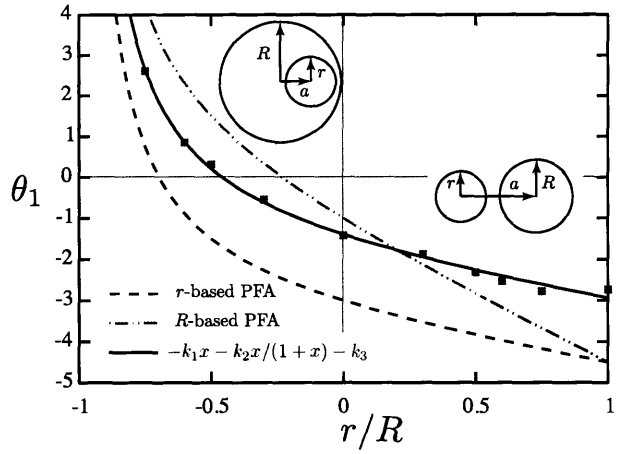

Figure 3-11: PFA correction coefficients for spheres. r/R ranges from -1 (interior concentric), to zero (sphere-plane), to +1 (exterior, equal radii). The data points correspond to the exact values of θ_1 calculated numerically, while the solid black curve is a fit (see text). Inset: "interior" and "exterior" geometrical configurations.

Eq. (3.2.32) is numerically evaluated by truncating the matrix $\mathcal{F}_O^{ii}\mathcal{W}^{io}\mathcal{F}_I^{ee}\mathcal{V}^{io}$ at finite multipole order l, and extrapolating to obtain the $l \to \infty$ limit. For the data in Fig. 3-11, the matrix was truncated at $l = l' \leq 60$ for the interior and at $l = l' \leq 35$ for the exterior configuration.

The numerical data in Fig. 3-11 show a smooth transition from the interior to the exterior configuration. Although the PFA estimates do not describe the data, the r-based PFA has a similar functional form and divergence as $x \to -1$. Therefore, we fit the data in Fig. 3-11 to a function, $\theta_1(x) = -(k_1x + k_2x/(1+x) + k_3)$ and find, $k_1 = 1.05 \pm 0.14, k_2 = 1.08 \pm 0.08, k_3 = 1.38 \pm 0.06$. This provides a simple form for the leading PFA correction for metallic spheres, one inside the other and both outside, which is relevant for many experiments. Notice, however, that the actual function $\theta_1(x)$ is not known analytically and that our fit represents a reasonable choice which may not be unique. Our results show that the correction to the PFA has a significant dependence on ratio of curvatures of the two surfaces. The correction is a factor of two larger for two spheres of equal radii than for the sphere-plane setup; it vanishes near $r/R = -0.5$; and it becomes large positive as $r/R \to -1$. These effects should be taken into account in future experimental searches for PFA corrections.

3.2.6 Cylinder and plate

As another example, we investigate the Casimir interaction energy between an infinitely thick plate a opposite a cylinder b, each with frequency-dependent permittivity and permeability (Fig. 3-12). We will focus on presenting asymptotic ($d/R \to \infty$) results here, but the derivation is straightforward to extend to intermediate separations, for which the evaluation of the final expression can be performed easily on a computer. We choose the $\hat{\mathbf{z}}$ axis as the axis of symmetry of the cylinder and let $\mathbf{k}_\perp$ denote the vector (k_y, k_z).

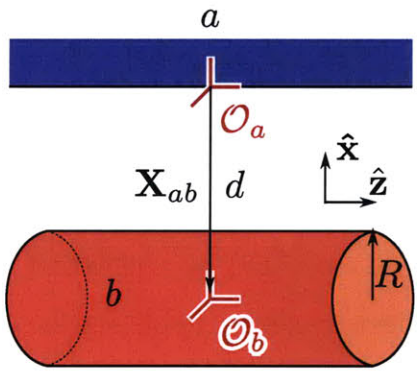

Figure 3-12: A cylinder b of radius R is located opposite a plate a, separated by a center-to-surface distance d.

Just as in the sphere-plate case, it is most convenient to express the scattering amplitude of the cylinder b in a plane wave basis by

$$\begin{aligned}
\mathcal{F}^{ee}_{b,\mathbf{k}_\perp P,\mathbf{k}'_\perp P'} &= (-1)C_{\mathbf{k}_\perp P}(\kappa)\langle \mathbf{E}^{\mathrm{reg}}_{\mathbf{k}_\perp P}(\kappa)|\mathbb{T}_b|\mathbf{E}^{\mathrm{reg}}_{\mathbf{k}'_\perp P'}(\kappa)\rangle \\
&= \sum_{nQ,n'Q'} (-1)\frac{C_{\mathbf{k}_\perp P}(\kappa)}{C_Q} D^\dagger_{\mathbf{k}_\perp P,k_z nQ} C_Q \langle \mathbf{E}^{\mathrm{reg}}_{k_z nQ}(\kappa)|\mathbb{T}_b|\mathbf{E}^{\mathrm{reg}}_{k'_z n'Q'}(\kappa)\rangle D_{k'_z n'Q',\mathbf{k}'_\perp P'} \\
&= \sum_{nQ,n'Q'} \frac{C_{\mathbf{k}_\perp P}(\kappa)}{C_Q} D^\dagger_{\mathbf{k}_\perp P,k'_z nQ} \mathcal{F}^{ee}_{b,k_z nQ,k'_z n'Q'} D_{k'_z n'Q',\mathbf{k}'_\perp P'},
\end{aligned} \tag{3.2.40}$$

where $C_{\mathbf{k}_\perp P}(\kappa)$ and C_Q are defined below Eq. (B.1.1) and Eq. (B.2.1), respectively.

By solving Eq. (2.3.9) in a cylindrical wave basis, it is straightforward to find the scattering amplitude of the cylinder, $\mathcal{F}^{ee}_{b,k_z nQ,k'_z n'Q'}$. For uniform permittivity and

permeability, the matrix elements are diagonal in k_z and the cylindrical wave index n, but not in TE and TM polarization. The expressions are somewhat complicated; since we are presenting asymptotic results here, we only need the small-radius expansion,

$$\begin{aligned}
\mathcal{F}^{ee}_{b,k_z nP,k'_z n'P'} &= \tfrac{2\pi}{L}\delta(k_z - k'_z)\delta_{n,n'} f_{k_z nPP'} + O(R^4)\,, \\
f_{k_z 0MM} &= \tfrac{1}{2}(\kappa^2 + k_z^2)R^2\,(1-\mu_b)\,, \qquad f_{k_z 0EE} = \tfrac{1}{2}(\kappa^2 + k_z^2)R^2\,(1-\epsilon_b)\,, \\
f_{k_z \pm 1MM} &= \tfrac{k_z^2(1+\epsilon_b)(1-\mu_b)-\kappa^2(1-\epsilon_b)(1+\mu_b)}{2(1+\epsilon_b)(1+\mu_b)}R^2\,, \qquad f_{k_z \pm 1EE} = \tfrac{k_z^2(1-\epsilon_b)(1+\mu_b)-\kappa^2(1+\epsilon_b)(1-\mu_b)}{2(1+\epsilon_b)(1+\mu_b)}R^2\,, \\
f_{k_z 1ME} &= f_{k_z -1EM} = \tfrac{\kappa k_z(\epsilon_b\mu_b - 1)}{(1+\epsilon_b)(1+\mu_b)}R^2\,, \qquad f_{k_z 1EM} = f_{k_z -1ME} = -f_{k_z 1ME}.
\end{aligned} \tag{3.2.41}$$

All other matrix elements ($|n| > 1$) contribute at higher order in R. It is assumed here that $\epsilon_b(ic\kappa)$ is finite. In the infinite conductivity limit ($\epsilon_b \to \infty$) only one of these scattering amplitudes contributes; this case is discussed below.

We next plug into Eq. (3.2.12). As in the case of two cylinders, the matrix inside the determinant is diagonal in k_z, so the log-determinant over this index turns into an integral. We obtain for the Casimir energy

$$\mathcal{E} = \frac{\hbar c L}{4\pi^2}\int_0^\infty d\kappa \int_{-\infty}^{\infty} dk_z\, \log\det\left(\mathcal{I} - \mathcal{N}\right), \tag{3.2.42}$$

where

$$\begin{aligned}
\mathcal{N}_{k_z nP,n'P'} = \sum_{P'',Q} f_{k_z nPP''} \int_{-\infty}^{\infty} dk_y \frac{e^{-2d\sqrt{\mathbf{k}_\perp^2+\kappa^2}}}{2\sqrt{\mathbf{k}_\perp^2+\kappa^2}} \\
\times D_{nk_zP'',\mathbf{k}_\perp Q}\, r_a^Q\left(ic\kappa, \sqrt{1+\mathbf{k}_\perp^2/\kappa^2}^{-1}\right) D^\dagger_{\mathbf{k}_\perp Q,n'k_zP'}(1-2\delta_{Q,P'}).
\end{aligned} \tag{3.2.43}$$

To find the interaction energy at separations outside of the asymptotic limit, $f_{k_z nPP'}$ must be replaced by the appropriate scattering amplitude expressions for all n, valid to all orders in R. Expanding the log det in Eq. (3.2.42) to first order in $\mathcal{N}$,

we obtain for the interaction in the large distance limit $d/R \to \infty$,

$$\mathcal{E} = -\frac{3\hbar c L R^2}{128\pi d^4} \int_0^1 dx \frac{\epsilon_{b0} - 1}{\epsilon_{b0} + 1} \left[(7 + \epsilon_{b0} - 4x^2) r^E(0,x) - (3 + \epsilon_{b0}) x^2 r^M(0,x) \right], \tag{3.2.44}$$

if the zero-frequency magnetic permeability μ_{b0} of the cylinder is set to one. If we do not set μ_{b0} equal to one, but instead take the perfect reflectivity limit for the plate, we obtain

$$\mathcal{E} = -\frac{\hbar c L R^2}{32\pi d^4} \frac{(\epsilon_{b0} - \mu_{b0})(9 + \epsilon_{b0} + \mu_{b0} + \epsilon_{b0}\mu_{b0})}{(1 + \epsilon_{b0})(1 + \mu_{b0})}. \tag{3.2.45}$$

Finally, if we let ϵ_b be infinite from the beginning (the perfect metal limit for the cylinder), only the $n = 0$ TM mode of the scattering amplitude, $\mathcal{F}^{ee}_{b,k_z 0E,k'_z 0E} = \frac{2\pi}{L}\delta(k_z - k'_z)\frac{1}{\log R/d} + O(\log^{-2}(R/d))$, contributes at lowest order; the previous expansions of the cylinder's scattering amplitude in Eq. (3.2.41) are not valid. For a plate with zero-frequency permittivity ϵ_{a0} and permeability μ_{a0}, we obtain for the Casimir energy

$$\mathcal{E} = \frac{\hbar c L}{16\pi d^2 \log(R/d)} \phi^E, \tag{3.2.46}$$

where

$$\phi^E = \int_0^1 \frac{dx}{1+x} \left[r_a^E(0,x) - x r_a^M(0,x) \right]. \tag{3.2.47}$$

In Fig. 3-13, ϕ^E is plotted as a function of the zero-frequency permittivity of the plate, ϵ_{a0}, for various zero-frequency permeability values, μ_{a0}.

3.2.7 Parabolic cylinder and plate

As a final example, we present the Casimir interaction energy between a perfect metal plate b opposite a parabolic cylinder a [80], depicted in Fig. 3-14. Although taking into account realistic material properties for the plate would be easy, the scattering amplitude of the parabolic cylinder is difficult to obtain unless perfect metal boundary conditions are applied. Here, we confine ourselves to such boundary conditions for both objects.

The surface of a parabolic cylinder in Cartesian coordinates is described by $y =$

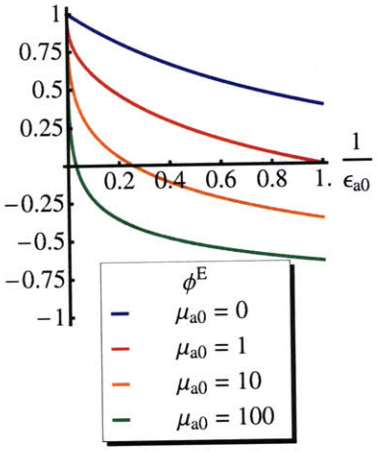

Figure 3-13: Plots of ϕ^E versus $1/\epsilon_{a0}$ for fixed values of μ_{a0}. ϕ^E decreases both with increasing $1/\epsilon_{a0}$ and increasing μ_{a0}. The perfect metal limit ($\phi^E = 1$) is approached slowly for large μ_{a0}, as in the case of a sphere opposite a plate. For large μ_{a0} the interaction becomes repulsive, which is expected given similar results for two infinite plates [95].

$(x^2 - R^2)/2R$ for all z, and R is the radius of curvature at the tip. The distance d to the plate is measured from $x = y = 0$. In parabolic cylinder coordinates [88], defined through $x = \mu\lambda$, $y = (\lambda^2 - \mu^2)/2$, $z = z$, the surface is simply $\mu = \mu_0 = \sqrt{R}$ for $-\infty < \lambda, z < \infty$. One advantage of the latter coordinate system is that the Helmholtz equation

$$\nabla^2\Phi = \frac{1}{\lambda^2 + \mu^2}\left(\frac{d^2\Phi}{d\lambda^2} + \frac{d^2\Phi}{d\mu^2}\right) + \frac{d^2\Phi}{dz^2} = \kappa^2\Phi\,, \tag{3.2.48}$$

which we consider for imaginary wavenumber $k = i\kappa$, admits separable solutions. Since sending $\lambda \to -\lambda$ and $\mu \to -\mu$ returns us to the same point, we restrict our attention to $\mu \geq 0$ while considering all values of λ. Then μ plays the role of the "radial" coordinate in scattering theory and we have regular and outgoing wave solutions

$$\begin{aligned} \phi^{\rm reg}_{k_z\nu}(\kappa, \mathbf{x}) &= (-i)^\nu D_\nu(\tilde{\lambda}) D_\nu(i\tilde{\mu}) e^{ik_z z}\,, \\ \phi^{\rm out}_{k_z\nu}(\kappa, \mathbf{x}) &= D_\nu(\tilde{\lambda}) D_{-\nu-1}(\tilde{\mu}) e^{ik_z z}\,, \end{aligned} \tag{3.2.49}$$

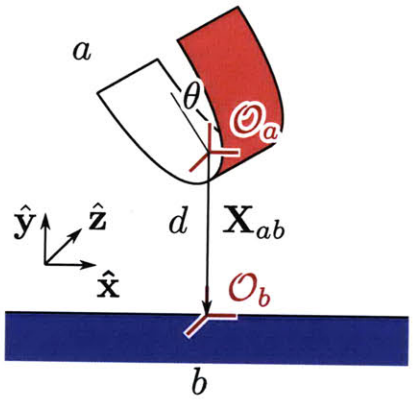

Figure 3-14: A parabolic cylinder a with radius of curvature $R = \mu_0^2$ at the tip is located opposite a plate b. The two are separated by a distance d, which is defined in the main text.

where $D_\nu(u)$ is the parabolic cylinder function, and $\tilde{\lambda} = \lambda\sqrt{2\sqrt{k_z^2+\kappa^2}}$ and similarly for μ. Enforcing the reflection symmetry $\lambda \to -\lambda$ and $\mu \to -\mu$ for the regular solutions restricts the separation constant ν to integer values. The corresponding outgoing solutions do not obey this restriction and thus can only be used away from $\mu = 0$; as is typical for outgoing solutions, they are irregular at $\mu = 0$. For imaginary wavenumber, the regular (outgoing) solutions grow (decay) exponentially in μ and both $(-i)^\nu D_\nu(i\tilde{\mu})$ and $D_\nu(\tilde{\lambda})$ are real. With these solutions to the scalar Helmholtz equation we can construct vector wave functions, the appropriate dyadic Green's function, and conversion matrices to vector plane wave functions. These are listed in the Appendix.

We choose the $\hat{\mathbf{z}}$ axis as the axis of translational symmetry of the cylinder and let $\mathbf{k}_\perp = (k_x, k_z)$. Analogously to the previous cases, we express the scattering amplitude of the parabolic cylinder a in a plane wave basis by

$$\begin{aligned}
\mathcal{F}^{ii}_{a,\mathbf{k}_\perp P,\mathbf{k}'_\perp P'} &= (-1)C_{\mathbf{k}_\perp P}(\kappa)\langle \mathbf{E}^{\text{out}}_{\mathbf{k}_\perp P}(\kappa)|\mathbb{T}_a|\mathbf{E}^{\text{out}}_{\mathbf{k}'_\perp P'}(\kappa)\rangle \\
&= \sum_{\nu Q,\nu' Q'} (-1)\frac{C_{\mathbf{k}_\perp P}(\kappa)}{C_{\nu Q}} D^\dagger_{\mathbf{k}_\perp P,k_z\nu Q} C_{\nu Q}\langle \mathbf{E}^{\text{reg}}_{k_z\nu Q}(\kappa)|\mathbb{T}_a|\mathbf{E}^{\text{reg}}_{k'_z\nu' Q'}(\kappa)\rangle D_{k'_z\nu' Q',\mathbf{k}'_\perp P'} \\
&= \sum_{\nu Q,\nu' Q'} \frac{C_{\mathbf{k}_\perp P}(\kappa)}{C_{\nu Q}} D^\dagger_{\mathbf{k}_\perp P,k_z\nu Q}\mathcal{F}^{ee}_{a,k_z\nu Q,k'_z\nu' Q'} D_{k'_z\nu' Q',\mathbf{k}'_\perp P'},
\end{aligned} \tag{3.2.50}$$

where $C_{\mathbf{k}_\perp P}(\kappa)$ and $C_{\nu Q}$ are defined below Eq. (B.1.1) and Eq. (B.4.1), respectively.

By solving Eq. (2.3.9) in a parabolic cylinder wave basis, it is straightforward to find the scattering amplitude of the perfect metal parabolic cylinder,

$$\begin{aligned}
\mathcal{F}^{ee}_{a,k_z\nu Q,k_z'\nu'Q'} &= \tfrac{2\pi}{L}\delta(k_z-k_z')\delta_{\nu,\nu'}\delta_{Q,Q'}\mathcal{F}^{ee}_{a,\nu Q}\,,\\
\mathcal{F}^{ee}_{a,\nu M} &= (-i)^{\nu+1}\frac{D_\nu'(i\tilde{\mu}_0)}{D_{-\nu-1}'(\tilde{\mu}_0)}\,,\\
\mathcal{F}^{ee}_{a,\nu E} &= -(-i)^{\nu}\frac{D_\nu(i\tilde{\mu}_0)}{D_{-\nu-1}(\tilde{\mu}_0)}\,.
\end{aligned} \tag{3.2.51}$$

Next, we plug into Eq. (3.2.12). As in the case of two cylinders, the matrix inside the determinant is diagonal in k_z, so the log-determinant over this index turns into an integral. We obtain for the Casimir energy

$$\mathcal{E} = \frac{\hbar c L}{4\pi^2}\int_0^\infty d\kappa \int_{-\infty}^\infty dk_z\, \log\det\left(\mathcal{I}-\mathcal{N}\right), \tag{3.2.52}$$

where

$$\begin{aligned}
\mathcal{N}_{k_z\nu P,\nu' P'} = \sum_Q \mathcal{F}^{ee}_{a,\nu P}\int_{-\infty}^\infty \frac{dk_x}{\sqrt{2\pi}}\nu!\frac{e^{-2d\sqrt{\mathbf{k}_\perp^2+\kappa^2}}}{2\sqrt{\mathbf{k}_\perp^2+\kappa^2}}\\
\times D_{k_z\nu P,\mathbf{k}_\perp Q}\, r_b^Q\left(ic\kappa,\sqrt{1+\mathbf{k}_\perp^2/\kappa^2}^{-1}\right) D^\dagger_{\mathbf{k}_\perp Q,k_z\nu' P'}(1-2\delta_{Q,P'}).
\end{aligned} \tag{3.2.53}$$

In the perfect metal limit for the plate, $\mathcal{N}$ becomes diagonal in P and P'. Numerical computations are performed by truncating the determinant at index $\nu_{\max}$. For the numbers quoted below, we have computed for $\nu_{\max}$ up to 200 and then extrapolated the result for $\nu_{\max}\to\infty$, and in the figures we have generally used $\nu_{\max}=100$. We note that the integrals over κ and k_z can be expressed as a single integral in polar coordinates, and for $\theta=0$ the k_x integral is symmetric and the translation matrix elements vanish for $\nu+\nu'$ odd. Since the plane we are considering is a perfect mirror, its scattering amplitude is independent of k_x and we can further simplify the calculation

for $\theta = 0$ using the integral

$$\int_{-\infty}^{\infty} dk_x \frac{1}{\sqrt{\kappa^2 + k_x^2 + k_z^2}} \frac{\left(\tan\frac{\phi}{2}\right)^{2n}}{\cos^2\frac{\phi}{2}} e^{-\sqrt{\kappa^2+k_x^2+k_z^2}2d} = 2\pi \mathrm{k}_{-2n-1}(2d\sqrt{\kappa^2 + k_z^2}), \quad (3.2.54)$$

where $\tan\phi = -ik_x/\sqrt{k_x^2 + k_z^2 + \kappa^2}$ and $\mathrm{k}_\ell(u) = \frac{e^{-u}}{\Gamma(\frac{\ell}{2}+1)} U(-\frac{\ell}{2}, 0, 2u)$ is the Bateman k-function [127], which is zero if ℓ is a negative even integer. Here $U(a, b, u)$ is the confluent hypergeometric function of the second kind.

As a first demonstration, we report on the dependence of the energy on the separation $H = d - R/2$ for $\theta = 0$. At small separations ($H/R \ll 1$) the PFA, given by

$$\frac{\mathcal{E}_{\rm pfa}}{\hbar c L} = -\frac{\pi^2}{720} \int_{-\infty}^{\infty} \frac{dx}{[H + x^2/(2R)]^3} = -\frac{\pi^3}{960\sqrt{2}} \sqrt{\frac{R}{H^5}}, \quad (3.2.55)$$

should be valid. The numerical results in Fig. 3-15 confirm this expectation with a ratio of actual to PFA energy of 0.9961 at $H/R = 0.25$ (for $R = 1$). We note that since the main contribution to PFA is from the proximal parts of the two surfaces, the PFA result in Eq. (3.2.55) also applies to a circular cylinder with the same radius R.

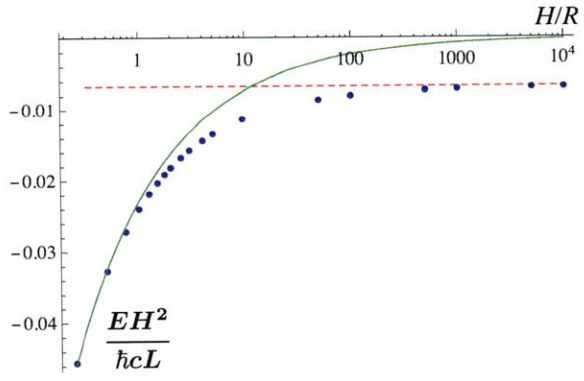

Figure 3-15: The energy per unit length times H^2, $EH^2/(\hbar cL)$, plotted versus H/R for $\theta = 0$ and $R = 1$ on a log-linear scale. The dashed line gives the $R = 0$ limit and the solid curve gives the PFA result.

A more interesting limit is obtained when $R/H \to 0$, corresponding to a semi-infinite plate. Then the PFA result is zero, as are results based on perturbative approximation for the dilute limit [61]. The scattering amplitudes in Eq. (3.2.51)

simplify and can be combined together as $\mathcal{F}_{a,\nu} = (-1)^{\nu+1}\nu!\sqrt{2/\pi}$, where even ν corresponds to Dirichlet and odd ν corresponds to Neumann. Using this result, our expression for the energy for $R = 0$ and $\theta = 0$ simplifies to

$$\frac{\mathcal{E}}{\hbar c L} = \int_0^\infty \frac{qdq}{4\pi} \log\det\left(\mathbb{1}_{\nu\nu'} - \mathrm{k}_{-\nu-\nu'-1}(2qH)\right) = \frac{-C_\perp}{H^2}, \tag{3.2.56}$$

where $C_\perp = 0.0067415$ is obtained by numerical integration. This geometry was studied using the world-line method for a scalar field with *Dirichlet* boundary conditions in Ref. [128, 129]. The world-line approach requires a large-scale numerical computation, and it is not known how to extend this method to Neumann boundary conditions (or any case other than a scalar with Dirichlet boundary conditions). In our calculation, the Dirichlet component of the electromagnetic field makes a contribution $C_\perp^D = 0.0060485$ to our result, in reasonable agreement with the value of $C_\perp^D = 0.00600(2)$ in Ref. [128].

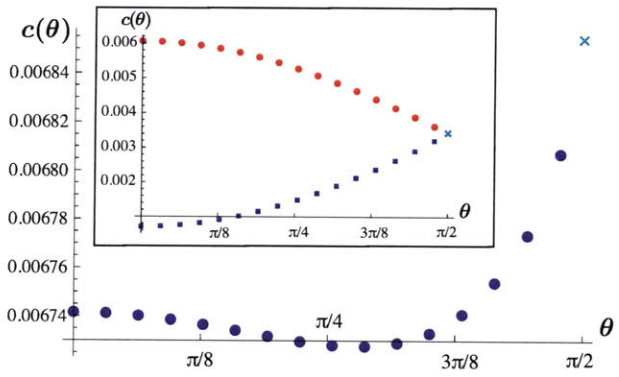

Figure 3-16: The coefficient $c(\theta)$ as a function of angle for $R = 0$. The exact result at $\theta = \pi/2$ is marked with a cross. Inset: Dirichlet (circles) and Neumann (squares) contributions to the full electromagnetic result.

Reference [129] also considers a tilted semi-infinite plate, which corresponds to the $R \to 0$ limit of our formula for general θ. From dimensional analysis, the Casimir energy at $R = 0$ again takes the now θ-dependent form

$$\frac{\mathcal{E}}{\hbar c L} = -\frac{C(\theta)}{H^2}\,. \tag{3.2.57}$$

Following Ref. [129], we plot $c(\theta) = \cos(\theta)C(\theta)$ in Fig. 3-16. A particularly interesting

limit is $\theta \to \pi/2$, when the two plates are parallel. In this case, the leading contribution to the Casimir energy should be proportional to the area of the half-plane according to the parallel plate formula, $E_{\|}/(\hbar c A) = -c_{\|}/H^3$ with $c_{\|} = \pi^2/720$, plus a subleading correction due to the edge. Multiplying by $\cos\theta$ removes the divergence in $C(\theta)$ as $\theta \to \pi/2$. As in Ref. [129], we assume $c(\theta \to \pi/2) = c_{\|}/2 + (\theta - \pi/2)\, c_{\rm edge}$, although we cannot rule out the possibility of additional non-analytic forms, such as logarithmic or other singularities. With this assumption, we can estimate the edge correction $c_{\rm edge} = 0.0009$ from the data in Fig. 3-16. From the inset in Fig. 3-16, we estimate the Dirichlet and Neumann contributions to this result to be $c^D_{\rm edge} = -0.0025$ (in agreement with [129] within our error estimates) and $c^N_{\rm edge} = 0.0034$ respectively. Because higher partial waves become more important as $\theta \to \pi/2$, reflecting the divergence in $C(\theta)$ in this limit, we have used larger values of $\nu_{\rm max}$ for θ near $\pi/2$.

It is straightforward to extend these results to nonzero temperature T. We simply replace the integral $\int_0^\infty \frac{d\kappa}{2\pi}$ by the sum $\frac{T}{\hbar c}{\sum_{n=0}^{\infty}}'$ over Matsubara frequencies $\kappa_n = 2\pi n T/(\hbar c)$, where the prime indicates that the $n = 0$ mode is counted with a weight of $1/2$, as discussed in Section 2.4. In the limit of infinite temperature, only the $n = 0$ mode contributes and we obtain for $R = 0$ the energy $\mathcal{E}/L = -TC_{T=\infty}/H$, with $C_{T=\infty} = 0.0472$. The Dirichlet contribution to our result is $C^D_{T=\infty} = 0.0394$, again in agreement with [129].

The reduction of the parabolic cylinder to a semi-infinite plate enables us to consider a variety of edge geometries. A thin metal disk perpendicular to a nearby metal surface would experience a Casimir force described by an extension of Eq. (3.2.56). Figure 3-15 shows that the PFA breaks down for a thin plate perpendicular to a plane; the PFA approximation to the energy vanishes as the thickness goes to zero, while the correct result instead has a different power law dependence on the separation. Based on the full result for perpendicular planes, however, we can formulate an "edge PFA" that yields the energy by integrating $d\mathcal{E}/dL$ from Eq. (3.2.56) along the edge of the disk. Letting r be the disk radius, in this approximation we have $\mathcal{E}_{\rm Epfa} = -\hbar c C_\perp \int_{-r}^{r} (H + r - \sqrt{r^2 - x^2})^{-2} dx \xrightarrow{H/r \to 0} -\hbar c C_\perp \pi \sqrt{r/(2H^3)}$, which is valid if the thickness of the disk is small compared to its separation from the plane. (For

comparison, note that the ordinary PFA for a metal sphere of radius r and a plate is proportional to r/H^2.)

A disk may be more experimentally tractable than a plane, since its edge does not need to be maintained parallel to the plate. One possibility would be a metal film, evaporated onto a substrate that either has low permittivity or can be etched away beneath the edge of the deposited film. Micromechanical torsion oscillators, which have already been used for Casimir experiments [11], seem readily adaptable for testing Eq. (3.2.57). Because the overall strength of the Casimir effect is weaker for a disk than for a sphere, observing Casimir forces in this geometry will require greater sensitivities or shorter separation distances than the sphere-plane case. As the separation gets smaller, however, the dominant contributions arise from higher-frequency fluctuations, and deviations from the perfect conductor limit can become important. While the effects of finite conductivity could be captured by an extension of our method, the calculation becomes significantly more difficult in this case because the matrix of scattering amplitudes is no longer diagonal.

To estimate the range of important fluctuation frequencies, we consider $R \ll H$ and $\theta = 0$. In this case, the integrand in Eq. (3.2.56) is strongly peaked around $q \approx 0.3/H$. As a result, by including only values of q up to $2/H$, we still capture 95% of the full result (and by going up to $3/H$ we include 99%). This truncation corresponds to a minimum fluctuation wavelength $\lambda_{\text{min}} = \pi H$. For the perfect conductor approximation to hold, λ_{min} must be large compared to the metal's plasma wavelength λ_p, so that these fluctuations are well described by assuming perfect reflectivity. We also need the thickness of the disk to be small enough compared to H that the deviation from the proximity force calculation is evident (see Fig. 3-15), but large enough compared to the metal's skin depth δ that the perfect conductor approximation is valid. For a typical metal film, $\lambda_p \approx 130$ nm and $\delta \approx 25$ nm at the relevant wavelengths. For a disk of radius $r = 100$ μm, the present experimental frontier of 0.1 pN sensitivity corresponds to a separation distance $H \approx 350$ nm, which then falls within the expected range of validity of our calculation according to these criteria. The force could also be enhanced by connecting several identical but well-separated

disks. In that case, the same force could be measured at a larger separation distance, where our calculation is more accurate.

Chapter 4

Concluding Remarks

4.1 Outlook

To flip the direction of the Casimir force, which tends to stick objects together, various ideas have been put forth. Some involve unrealistic materials or a dielectric liquid medium. One promising proposal is to heat bodies to different temperatures [130, 131]. While the prospect of tuning the Casimir force drives the main interest here, much need for fundamental research exists at the level of basic statistical mechanics. Out-of-equilibrium systems, e.g., systems where different parts have different temperatures or whose parts are moving, lie at the frontier of statistical physics. Advances in understanding one example are sure to benefit other areas of physics, for example, biophysics. The advantages of studying out-of-equilibrium Casimir forces, in particular, are that the electrodynamic interactions are well understood and precision measurements have been refined by many research groups over the past years. While some progress has been made, fundamental questions about the validity of the underlying assumptions [130] and the influence of geometry, for example, remain unanswered. Another out-of-equilibrium configuration, where the objects are moving, has also received much attention, not for practical reasons as for its possible connections to, for example, the Hawking effect (radiation from a black hole). In these situations the moving objects emit real photons; the loss of energy and momentum amounts to "vacuum friction". While interest in geometrical considerations is

abundant, see for example, Ref. [132], where a rack driving a pinion at a distance is attempted with crude but unavoidable approximations, tools for studying them have been very limited. With our scattering techniques these *dynamical* Casimir problems may also become tractable. Since our derivation requires a static configuration and thermal equilibrium, however, it is unclear whether and through what steps a scattering formalism can be recovered from an out-of-equilibrium starting point.

Appendix A

Derivation of the macroscopic field theory

In this appendix we justify the starting point of our derivation, the effective or "macroscopic" field theory in Eq. (2.1.1), in order to clarify the causality properties of the permittivity ϵ and permeability μ and incorporate the dissipative properties of the materials naturally into our formalism. We also show that both non-local and non-isotropic permittivity and permeability *tensors* can be used.

In place of Eq. (2.1.1), we begin with the Lagrangian density of the free electromagnetic field plus a coupled system of particles. To be concrete, we imagine that the electromagnetic field couples, say, to electrons of charge $-e$ described by the Lagrangian density operator

$$\hat{\mathcal{L}} = \tfrac{1}{2}\left(\hat{\mathbf{E}}^2 - \hat{\mathbf{B}}^2\right) + i\hbar\hat{\psi}^\dagger\dot{\hat{\psi}} - \frac{\hbar^2}{2m}\left[\left(\nabla - \frac{ie}{\hbar}\hat{\mathbf{A}}\right)\hat{\psi}^\dagger\right]\left[\left(\nabla + \frac{ie}{\hbar}\hat{\mathbf{A}}\right)\hat{\psi}\right], \qquad \text{(A.0.1)}$$

where $\hat{\psi}$ and $\hat{\psi}^\dagger$ are the fermion field annihilation and creation operators, which are spinor functions of space $\mathbf{x}$ and time t. We implicitly sum over spins and suppress the spin index and we continue to work in $A^0 = 0$ gauge. The electrons' coupling to the lattice, their coupling to each other, and their spin-magnetic field interaction can

be explicitly taken into account by adding, for example,

$$\begin{aligned}\hat{\mathcal{L}}_{\text{lattice}} &= -\hat{\psi}^\dagger(t,\mathbf{x})u(\mathbf{x})\hat{\psi}(t,\mathbf{x}) \\ \hat{\mathcal{L}}_{\text{int}} &= -\tfrac{1}{2}\int d\mathbf{x}'\,\hat{\psi}^\dagger(t,\mathbf{x})\hat{\psi}^\dagger(t,\mathbf{x}')v(\mathbf{x}-\mathbf{x}')\hat{\psi}(t,\mathbf{x}')\hat{\psi}(t,\mathbf{x}) \\ \hat{\mathcal{L}}_{\text{spin}} &= \frac{e\hbar g_e}{2mc}\hat{\mathbf{B}}(\mathbf{x})\cdot\hat{\psi}^\dagger(t,\mathbf{x})\boldsymbol{\sigma}\hat{\psi}(t,\mathbf{x}).\end{aligned} \tag{A.0.2}$$

We imagine that such systems, confined to the various regions of space, represent the objects whose Casimir interactions we are calculating. Since the following procedure is quite general, we are not limited to systems described by these particular Lagrangians, but modifications to our approach may be needed in some situations.

The electron-lattice and electron-electron interactions are mediated via the quantum electrodynamic field, but the relevant wavelengths are substantially shorter than the ones dominating the Casimir interaction of different objects, so we can safely approximate the short wavelength interactions by effective potentials $u(\mathbf{x})$ and $v(\mathbf{x}-\mathbf{x}')$.

To compute the total partition function, we exponentiate the time integral of the Lagrangian and analytically continue the time coordinate t to $-i\tau$, yielding

$$Z(\beta) = \int \mathcal{D}\mathbf{A}\, e^{-\frac{1}{\hbar}S_{\text{EM}}} Z_{\text{elec}}[\mathbf{A}], \tag{A.0.3}$$

where

$$S_{\text{EM}} = \tfrac{1}{2}\int_0^{\hbar\beta} d\tau \int d\mathbf{x}\,\left(\mathbf{E}^2+\mathbf{B}^2\right), \tag{A.0.4}$$

is the free electromagnetic action and

$$Z_{\text{elec}}[\mathbf{A}] = \int \mathcal{D}\bar{\psi}\mathcal{D}\psi\, e^{-\frac{1}{\hbar}S_{\text{elec}}} \tag{A.0.5}$$

is the electronic partition function. The Euclidean electronic action is

$$S_{\text{elec}} = \int_0^{\hbar\beta} d\tau \int d\mathbf{x}\,\left(\hbar\bar{\psi}\partial_\tau\psi + \frac{\hbar^2}{2m}\left[\left(\nabla - \frac{ie}{\hbar}\mathbf{A}\right)\bar{\psi}\right]\left[\left(\nabla + \frac{ie}{\hbar}\mathbf{A}\right)\psi\right] + \text{interactions}\right), \tag{A.0.6}$$

where the interaction terms are taken from Eq. (A.0.2), including at least $\hat{\mathcal{L}}_{\text{lattice}}$ to

keep the electrons confined to the various objects. Here the creation and annihilation operators $\hat{\psi}^\dagger$ and $\hat{\psi}$ go over to Grassman path integral variables $\bar{\psi}$ and ψ.

Next, we expand the partition function of the electronic system,

$$Z_{\text{elec}}[\mathbf{A}] \approx Z_{\text{elec}}[0]\left(1+\tfrac{1}{2}\sum_{i,j}\int_0^{\hbar\beta} d\tau d\tau' \int d\mathbf{x}d\mathbf{x}' K_{ij}(\tau-\tau',\mathbf{x},\mathbf{x}')A^i(\tau,\mathbf{x})A^j(\tau',\mathbf{x}')\right), \tag{A.0.7}$$

where the second derivative of Z_{elec},

$$K_{ij}(\tau-\tau',\mathbf{x},\mathbf{x}') = \frac{1}{Z_{\text{elec}}[0]}\frac{\delta^2 Z_{\text{elec}}[\mathbf{A}]}{\delta A^i(\tau,\mathbf{x})\delta A^j(\tau',\mathbf{x}')}\bigg|_{\mathbf{A}=0}, \tag{A.0.8}$$

only depends on the difference in imaginary time $\tau-\tau'$. The linear term has been omitted in this expansion because it vanishes for systems with no mean currents. We then obtain the well-known Kubo formula for electrical conductivity, [133]

$$\sigma_{ij}^T(ic\kappa_n,\mathbf{x},\mathbf{x}') = -\frac{1}{c\kappa_n}\int_0^{\hbar\beta} d\tau\, K_{ij}(\tau,\mathbf{x},\mathbf{x}')e^{ic\kappa_n\tau}. \tag{A.0.9}$$

Conductivity, here, differs from conductivity in classical electrodynamics where it is proportional to only the imaginary part of the permittivity at real frequencies. The T superscript indicates that this is the imaginary-time ordered response function. The retarded response function can be obtained by the substitution $ic\kappa_n \to \omega + i0^+$. The conductivity is related to the permittivity by

$$\sigma_{ij}^T(ic\kappa_n,\mathbf{x},\mathbf{x}') = c\kappa_n\left(\epsilon_{ij}^T(ic\kappa_n,\mathbf{x},\mathbf{x}') - \delta_{ij}\delta(\mathbf{x}-\mathbf{x}')\right). \tag{A.0.10}$$

After substituting into Eq. (A.0.7), we obtain

$$Z_{\text{elec}} \approx Z_{\text{elec}}[0]\left(1+\frac{\beta}{2}\sum_{n=-\infty}^{\infty}\int d\mathbf{x}d\mathbf{x}'\mathbf{E}^*(ic\kappa_n,\mathbf{x})\cdot\left(\mathbb{I}\delta(\mathbf{x}-\mathbf{x}') - \boldsymbol{\epsilon}^T(ic\kappa_n,\mathbf{x},\mathbf{x}')\right)\mathbf{E}(ic\kappa_n,\mathbf{x}')\right) \tag{A.0.11}$$

and, finally, after reexponentiating and plugging into Eq. (A.0.3) we obtain

$$Z(\beta) \approx Z_{\text{elec}}[0] \int \mathcal{D}\mathbf{A} \exp\left[-\frac{\beta}{2} \sum_{n=-\infty}^{\infty} \left(\int d\mathbf{x} d\mathbf{x}' \, \mathbf{E}^*(ic\kappa_n, \mathbf{x}) \cdot \boldsymbol{\epsilon}^T(ic\kappa_n, \mathbf{x}, \mathbf{x}') \mathbf{E}(ic\kappa_n, \mathbf{x}') + \int d\mathbf{x} \, \mathbf{B}^*(ic\kappa_n, \mathbf{x}) \cdot \mathbf{B}(ic\kappa_n, \mathbf{x}) \right) \right]. \tag{A.0.12}$$

The imaginary-time ordered response function can be obtained from the retarded real time response function, which is experimentally accessible, by analytic continuation to imaginary frequencies. The relationship $\epsilon_{ij}^T(ic\kappa_n, \mathbf{x}, \mathbf{x}') = \epsilon_{ij}^R(ic|\kappa_n|, \mathbf{x}, \mathbf{x}')$ between the two response functions and the symmetry of the retarded response function in the indices $(i, \mathbf{x})$ and $(j, \mathbf{x}')$ is discussed in Refs. [134, 135].

To be able to consider two objects as separate and distinct, we assume that $\epsilon^T(ic\kappa_n, \mathbf{x}, \mathbf{x}')$ is zero when $\mathbf{x}$ and $\mathbf{x}'$ are on different objects, separated by the vacuum or a medium. This is justified even for small gaps between the objects, since tunneling probabilities decay exponentially in the gap distance.

Although the dissipative part of the electric response (the conductivity) appears in the above equations, there is not actual dissipation at zero temperature. Rather, Eqs. (A.0.7)–(A.0.9) merely show that the conductivity σ^R, which can be measured in an experiment, can be related to the fluctuations that exist in a system in the absence of an external perturbation. The size of these fluctuations is represented by the second derivative of the partition function, Eq. (A.0.8).

Although the magnetic susceptibility is usually negligible compared to the electric susceptibility at visible and infrared frequencies, we have kept the permeability function μ in our derivations of Casimir interactions. If the spin-magnetic field coupling term $\hat{\mathcal{L}}_{\text{spin}}$ replaces or dominates the standard coupling between charge and electromagnetic field in Eq. (A.0.1), an analogous procedure introduces the magnetic permeability function into the action. In that case, the partition function of the matter field, the analogue of Eq. (A.0.7), has to be expanded in $\mathbf{B}^i = (\boldsymbol{\nabla} \times \mathbf{A})^i$ instead of $\mathbf{A}^i$.

Appendix B

Green's function expansions and modified eigenfunctions

In this appendix we supply the Green's function expansions for imaginary frequency $ic\kappa$ and the associated modified eigenfunctions in various bases. After analytically continuing the wave functions in Eq. (2.2.8), it is convenient to redefine them by multiplication by an overall factor in order to obtain the conventional definitions of the modified wave functions. Since $\mathbf{E}^{\text{in}*}(\kappa, \mathbf{x}) = \mathbf{E}^{\text{out}}(\kappa, \mathbf{x})$, it suffices to supply the modified regular and outgoing wave functions.

Electromagnetic vector waves are typically divided into TE and TM modes, e.g., in media with high symmetry such as homogeneous media. It is customary to name the TE wave functions $\mathbf{M}(\omega, \mathbf{x})$ and the TM waves $\mathbf{N}(\omega, \mathbf{x})$. Often TE modes are referred to as magnetic modes, labeled by M, and TM modes are referred to as electric modes, labeled by E.

B.1 Green's function and eigenfunctions – plane wave basis

We choose the $\hat{\mathbf{z}}$ axis as a convenient symmetry axis and let $\mathbf{k}_\perp$ denote momentum perpendicular to this axis. The free dyadic Green's function is

$$\mathbb{G}_0(ic\kappa, \mathbf{x}, \mathbf{x}') = \int \frac{L^2 d\mathbf{k}_\perp}{(2\pi)^2} \begin{cases} C_{\mathbf{k}_\perp M}(\kappa)\mathbf{M}^{\text{out}}_{\mathbf{k}_\perp}(\kappa, \mathbf{x}) \otimes \mathbf{M}^{\text{reg}*}_{\mathbf{k}_\perp}(\kappa, \mathbf{x}') + C_{\mathbf{k}_\perp E}(\kappa)\mathbf{N}^{\text{out}}_{\mathbf{k}_\perp}(\kappa, \mathbf{x}) \otimes \mathbf{N}^{\text{reg}*}_{\mathbf{k}_\perp}(\kappa, \mathbf{x}') & \text{if } z > z' \\ C_{\mathbf{k}_\perp M}(\kappa)\mathbf{M}^{\text{reg}}_{\mathbf{k}_\perp}(\kappa, \mathbf{x}) \otimes \mathbf{M}^{\text{in}*}_{\mathbf{k}_\perp}(\kappa, \mathbf{x}') + C_{\mathbf{k}_\perp E}(\kappa)\mathbf{N}^{\text{reg}}_{\mathbf{k}_\perp}(\kappa, \mathbf{x}) \otimes \mathbf{N}^{\text{in}*}_{\mathbf{k}_\perp}(\kappa, \mathbf{x}') & \text{if } z < z' \end{cases} \tag{B.1.1}$$

Here, $C_{\mathbf{k}_\perp M}(\kappa) = \frac{1}{2L^2\sqrt{\mathbf{k}_\perp^2+\kappa^2}} = (-1)C_{\mathbf{k}_\perp E}(\kappa)$. Often, it is necessary to discretize the integral expression in (B.1.1) by replacing $\int \frac{L^2 d\mathbf{k}_\perp}{(2\pi)^2}$ by $\sum_{\mathbf{k}_\perp}$. For simplicity, therefore, factors of L denoting the extent of the total system in the directions perpendicular to $\hat{\mathbf{z}}$ have been introduced here, although in the integral expression they cancel in numerator and denominator. The modified vector plane wave functions are given by

$$\begin{aligned} \mathbf{M}^{\text{reg}}_{\mathbf{k}_\perp}(\kappa, \mathbf{x}) &= \frac{1}{|\mathbf{k}_\perp|}\boldsymbol{\nabla} \times \phi^{\text{reg}}_{\mathbf{k}_\perp}(\kappa, \mathbf{x})\hat{\mathbf{z}}, \qquad \mathbf{M}^{\text{out}}_{\mathbf{k}_\perp}(\kappa, \mathbf{x}) = \frac{1}{|\mathbf{k}_\perp|}\boldsymbol{\nabla} \times \phi^{\text{out}}_{\mathbf{k}_\perp}(\kappa, \mathbf{x})\hat{\mathbf{z}}, \\ \mathbf{N}^{\text{reg}}_{\mathbf{k}_\perp}(\kappa, \mathbf{x}) &= \frac{1}{\kappa|\mathbf{k}_\perp|}\boldsymbol{\nabla} \times \boldsymbol{\nabla} \times \phi^{\text{reg}}_{\mathbf{k}_\perp}(\kappa, \mathbf{x})\hat{\mathbf{z}}, \qquad \mathbf{N}^{\text{out}}_{\mathbf{k}_\perp}(\kappa, \mathbf{x}) = \frac{1}{\kappa|\mathbf{k}_\perp|}\boldsymbol{\nabla} \times \boldsymbol{\nabla} \times \phi^{\text{out}}_{\mathbf{k}_\perp}(\kappa, \mathbf{x})\hat{\mathbf{z}}, \end{aligned} \tag{B.1.2}$$

in terms of the modified scalar plane wave functions,

$$\phi^{\text{reg}}_{\mathbf{k}_\perp}(\kappa, \mathbf{x}) = e^{i\mathbf{k}_\perp \cdot \mathbf{x}_\perp + \sqrt{\mathbf{k}_\perp^2+\kappa^2}z}, \qquad \phi^{\text{out}}_{\mathbf{k}_\perp}(\kappa, \mathbf{x}) = e^{i\mathbf{k}_\perp \cdot \mathbf{x}_\perp - \sqrt{\mathbf{k}_\perp^2+\kappa^2}z}. \tag{B.1.3}$$

As discussed in the text, the labels "reg," "out," and "in" are not really appropriate for plane wave functions, but the mathematical results all carry over.

B.2 Green's function and eigenfunctions – cylindrical wave basis

Again, let us take the $\hat{\mathbf{z}}$ axis as a convenient symmetry axis and let $\rho = \sqrt{x^2+y^2}$ be the distance to the $\hat{\mathbf{z}}$ axis. The free dyadic Green's function is given by

$$\mathbb{G}_0(ic\kappa, \mathbf{x}, \mathbf{x}') = \int \frac{L dk_z}{2\pi} \sum_n \begin{cases} C_M \mathbf{M}^{\text{out}}_{k_z n}(\kappa, \mathbf{x}) \otimes \mathbf{M}^{\text{reg}*}_{k_z n}(\kappa, \mathbf{x}') + C_E \mathbf{N}^{\text{out}}_{k_z n}(\kappa, \mathbf{x}) \otimes \mathbf{N}^{\text{reg}*}_{k_z n}(\kappa, \mathbf{x}') & \text{if } \rho > \rho' \\ C_M \mathbf{M}^{\text{reg}}_{k_z n}(\kappa, \mathbf{x}) \otimes \mathbf{M}^{\text{in}*}_{k_z n}(\kappa, \mathbf{x}') + C_E \mathbf{N}^{\text{reg}}_{k_z n}(\kappa, \mathbf{x}) \otimes \mathbf{N}^{\text{in}*}_{k_z n}(\kappa, \mathbf{x}') & \text{if } \rho < \rho' \end{cases} \tag{B.2.1}$$

Here $C_E = \frac{1}{2\pi L} = (-1)C_M$, the vector cylindrical wave functions are given by

$$\begin{aligned} \mathbf{M}^{\text{reg}}_{k_z n}(\kappa, \mathbf{x}) &= \frac{1}{\sqrt{k_z^2+\kappa^2}} \boldsymbol{\nabla} \times \phi^{\text{reg}}_{k_z n}(\kappa, \mathbf{x}) \hat{\mathbf{z}}, \\ \mathbf{M}^{\text{out}}_{k_z n}(\kappa, \mathbf{x}) &= \frac{1}{\sqrt{k_z^2+\kappa^2}} \boldsymbol{\nabla} \times \phi^{\text{out}}_{k_z n}(\kappa, \mathbf{x}) \hat{\mathbf{z}}, \\ \mathbf{N}^{\text{reg}}_{k_z n}(\kappa, \mathbf{x}) &= \frac{1}{\kappa\sqrt{k_z^2+\kappa^2}} \boldsymbol{\nabla} \times \boldsymbol{\nabla} \times \phi^{\text{reg}}_{k_z n}(\kappa, \mathbf{x}) \hat{\mathbf{z}}, \\ \mathbf{N}^{\text{out}}_{k_z n}(\kappa, \mathbf{x}) &= \frac{1}{\kappa\sqrt{k_z^2+\kappa^2}} \boldsymbol{\nabla} \times \boldsymbol{\nabla} \times \phi^{\text{out}}_{k_z n}(\kappa, \mathbf{x}) \hat{\mathbf{z}}, \end{aligned} \tag{B.2.2}$$

and the modified cylindrical wave functions are

$$\phi^{\text{reg}}_{k_z n}(\kappa, \mathbf{x}) = I_n\left(\rho\sqrt{k_z^2+\kappa^2}\right) e^{ik_z z + in\theta}, \qquad \phi^{\text{out}}_{k_z n}(\kappa, \mathbf{x}) = K_n\left(\rho\sqrt{k_z^2+\kappa^2}\right) e^{ik_z z + in\theta}, \tag{B.2.3}$$

where I_n is the modified Bessel function of the first kind and K_n is the modified Bessel function of the third kind.

B.3 Green's function and eigenfunctions – spherical wave basis

In spherical coordinates the free dyadic Green's function is given by

$$\mathbb{G}_0(ic\kappa, \mathbf{x}, \mathbf{x}') = \sum_{lm} \begin{cases} C_M(\kappa)\mathbf{M}^{\text{out}}_{lm}(\kappa, \mathbf{x}) \otimes \mathbf{M}^{\text{reg}*}_{lm}(\kappa, \mathbf{x}') + C_E(\kappa)\mathbf{N}^{\text{out}}_{lm}(\kappa, \mathbf{x}) \otimes \mathbf{N}^{\text{reg}*}_{lm}(\kappa, \mathbf{x}') & \text{if } |\mathbf{x}| > |\mathbf{x}'| \\ C_M(\kappa)\mathbf{M}^{\text{reg}}_{lm}(\kappa, \mathbf{x}) \otimes \mathbf{M}^{\text{in}*}_{lm}(\kappa, \mathbf{x}') + C_E(\kappa)\mathbf{N}^{\text{reg}}_{lm}(\kappa, \mathbf{x}) \otimes \mathbf{N}^{\text{in}*}_{lm}(\kappa, \mathbf{x}') & \text{if } |\mathbf{x}| < |\mathbf{x}'| \end{cases} \tag{B.3.1}$$

Here $C_M(\kappa) = \kappa = (-1)C_E(\kappa)$, the vector spherical wave functions are

$$\mathbf{M}^{\text{reg}}_{lm}(\kappa, \mathbf{x}) = \tfrac{1}{\sqrt{l(l+1)}}\boldsymbol{\nabla} \times \phi^{\text{reg}}_{lm}(\kappa, \mathbf{x})\mathbf{x}, \qquad \mathbf{M}^{\text{out}}_{lm}(\kappa, \mathbf{x}) = \tfrac{1}{\sqrt{l(l+1)}}\boldsymbol{\nabla} \times \phi^{\text{out}}_{lm}(\kappa, \mathbf{x})\mathbf{x},$$
$$\mathbf{N}^{\text{reg}}_{lm}(\kappa, \mathbf{x}) = \tfrac{1}{\kappa\sqrt{l(l+1)}}\boldsymbol{\nabla} \times \boldsymbol{\nabla} \times \phi^{\text{reg}}_{lm}(\kappa, \mathbf{x})\mathbf{x}, \qquad \mathbf{N}^{\text{out}}_{lm}(\kappa, \mathbf{x}) = \tfrac{1}{\kappa\sqrt{l(l+1)}}\boldsymbol{\nabla} \times \boldsymbol{\nabla} \times \phi^{\text{out}}_{lm}(\kappa, \mathbf{x})\mathbf{x}, \tag{B.3.2}$$

and the modified spherical wave functions are

$$\phi^{\text{reg}}_{lm}(\kappa, \mathbf{x}) = i_l(\kappa|\mathbf{x}|)Y_{lm}(\hat{\mathbf{x}}), \qquad \phi^{\text{out}}_{lm}(\kappa, \mathbf{x}) = k_l(\kappa|\mathbf{x}|)Y_{lm}(\hat{\mathbf{x}}), \tag{B.3.3}$$

where $i_l(z) = \sqrt{\frac{\pi}{2z}}I_{l+1/2}(z)$ is the modified spherical Bessel function of the first kind, and $k_l(z) = \sqrt{\frac{2}{\pi z}}K_{l+1/2}(z)$ is the modified spherical Bessel function of the third kind.

B.4 Green's function and eigenfunctions – parabolic cylinder wave basis

Let us take the $\hat{\mathbf{z}}$ axis as a convenient symmetry axis. The parabolic cylinder coordinates are defined through $x = \mu\lambda$, $y = (\lambda^2 - \mu^2)/2$, $z = z$. We assume $\mu \geq 0$ since $\lambda \to -\lambda$ and $\mu \to -\mu$ returns us to the same point. The free dyadic Green's function

is given by

$$\mathbb{G}_0(ic\kappa,\mathbf{x},\mathbf{x}') = \int \frac{L dk_z}{2\pi} \sum_\nu \begin{cases} C_M \mathbf{M}^{\text{out}}_{k_z\nu}(\kappa,\mathbf{x}) \otimes \mathbf{M}^{\text{reg}*}_{k_z\nu}(\kappa,\mathbf{x}') + C_E \mathbf{N}^{\text{out}}_{k_z\nu}(\kappa,\mathbf{x}) \otimes \mathbf{N}^{\text{reg}*}_{k_z\nu}(\kappa,\mathbf{x}') & \text{if } \mu > \mu' \\ C_M \mathbf{M}^{\text{reg}}_{k_z\nu}(\kappa,\mathbf{x}) \otimes \mathbf{M}^{\text{in}*}_{k_z\nu}(\kappa,\mathbf{x}') + C_E \mathbf{N}^{\text{reg}}_{k_z\nu}(\kappa,\mathbf{x}) \otimes \mathbf{N}^{\text{in}*}_{k_z\nu}(\kappa,\mathbf{x}') & \text{if } \mu < \mu' \end{cases} \tag{B.4.1}$$

Here $C_E = \frac{1}{\sqrt{2\pi\nu!L}} = (-1)C_M$. The vector parabolic cylinder wave functions are given by

$$\begin{aligned} \mathbf{M}^{\text{reg}}_{k_z\nu}(\kappa,\mathbf{x}) &= \frac{1}{\sqrt{k_z^2+\kappa^2}} \boldsymbol{\nabla} \times \phi^{\text{reg}}_{k_z\nu}(\kappa,\mathbf{x})\hat{\mathbf{z}}, \\ \mathbf{M}^{\text{out}}_{k_z\nu}(\kappa,\mathbf{x}) &= \frac{1}{\sqrt{k_z^2+\kappa^2}} \boldsymbol{\nabla} \times \phi^{\text{out}}_{k_z\nu}(\kappa,\mathbf{x})\hat{\mathbf{z}}, \\ \mathbf{N}^{\text{reg}}_{k_z\nu}(\kappa,\mathbf{x}) &= \frac{1}{\kappa\sqrt{k_z^2+\kappa^2}} \boldsymbol{\nabla} \times \boldsymbol{\nabla} \times \phi^{\text{reg}}_{k_z\nu}(\kappa,\mathbf{x})\hat{\mathbf{z}}, \\ \mathbf{N}^{\text{out}}_{k_z\nu}(\kappa,\mathbf{x}) &= \frac{1}{\kappa\sqrt{k_z^2+\kappa^2}} \boldsymbol{\nabla} \times \boldsymbol{\nabla} \times \phi^{\text{out}}_{k_z\nu}(\kappa,\mathbf{x})\hat{\mathbf{z}}, \end{aligned} \tag{B.4.2}$$

and the parabolic cylinder wave functions are

$$\phi^{\text{reg}}_{k_z\nu}(\kappa,\mathbf{x}) = (-i)^\nu D_\nu\big(\tilde{\lambda}\big) D_\nu\left(i\tilde{\mu}\right) e^{ik_z z}, \qquad \phi^{\text{out}}_{k_z\nu}(\kappa,\mathbf{x}) = D_\nu\big(\tilde{\lambda}\big) D_{-\nu-1}\left(\tilde{\mu}\right) e^{ik_z z}, \tag{B.4.3}$$

where $D_\nu(x)$ is the parabolic cylinder function, and $\tilde{\lambda} = \lambda\sqrt{2\sqrt{k_z^2+\kappa^2}}$, $\tilde{\mu} = \mu\sqrt{2\sqrt{k_z^2+\kappa^2}}$.

B.5 Green's function – elliptic cylindrical basis

In order to study geometry and orientation dependence of Casimir interactions, it is helpful to be able to study objects with reduced symmetry. In Ref. [112], this formalism was applied to spheroids in scalar field theory. Unfortunately, the vector Helmholtz equation is not separable in spheroidal coordinates as it is in spherical coordinates. While the analogous vector spheroidal harmonics can still be constructed, the scattering matrix for a perfectly conducting spheroid is not diagonal, although it

can be obtained from a more elaborate calculation [136]. For a perfectly conducting elliptic cylinder, however, the vector scattering problem is separable, so we describe that case here. Throughout this appendix, we use the same normalization and conventions as in Ref. [137], in which all functions in elliptic cylindrical coordinates have the same normalization as their circular analogs. As a result, all the functions inherit the usual completeness and orthonormality relations and approach their circular analogs in the limit of long wavelength.

In elliptic cylindrical coordinates, the z coordinate is unchanged, while the components of $\mathbf{x}_\perp$ become $x = a\cosh\mu\cos\theta$ and $y = a\sinh\mu\sin\theta$, where the interfocal separation of the ellipse is $2a$. Far away, θ approaches the ordinary angle in cylindrical coordinates and $|\mathbf{x}_\perp| \approx \frac{a}{2}e^{\mu}$. Separation of variables in these coordinates yields angular and radial Mathieu functions for θ and μ, respectively. The even and odd angular Mathieu functions are $ce_n(\theta,\gamma)$ with $n \geq 0$ and $se_n(\theta,\gamma)$ with $n > 0$, which are the analogs of $\cos n\theta$ and $\sin n\theta$ in the circular case. (We used a complex exponential basis for the circular case, but it could equally well be represented in terms of sines and cosines.) The angular functions now depend on the wave number through the combination $\gamma = -(k_z^2 + \kappa^2)a^2/2$. The corresponding radial functions are now different for the even and odd cases and depend on γ and μ separately rather than through a single product of the two. The even and odd modified radial Mathieu functions of the first kind are denoted $Ie_m(\mu,\gamma)$ and $Io_m(\mu,\gamma)$ respectively, and the even and odd modified radial Mathieu functions of the third kind are denoted $Ke_m(\mu,\gamma)$ and $Ko_m(\mu,\gamma)$, respectively.

We then obtain the same results as in cylindrical coordinates, but now with

$$\begin{aligned}
\phi^{\text{reg}}_{k_z ne}(\kappa,\mathbf{x}) &= Ie_n(\mu,\gamma)ce_n(\theta,\gamma)e^{ik_z z}, \qquad & \phi^{\text{out}}_{k_z ne}(\kappa,\mathbf{x}) &= Ke_n(\mu,\gamma)ce_n(\theta,\gamma)e^{ik_z z},\\
\phi^{\text{reg}}_{k_z no}(\kappa,\mathbf{x}) &= Io_n(\mu,\gamma)se_n(\theta,\gamma)e^{ik_z z}, \qquad & \phi^{\text{out}}_{k_z no}(\kappa,\mathbf{x}) &= Ko_n(\mu,\gamma)se_n(\theta,\gamma)e^{ik_z z}.
\end{aligned} \tag{B.5.1}$$

For numerical calculation the required Mathieu functions can be efficiently computed using the C++ package of Alhargan [138, 139]. Analogous replacements convert the

translation matrices and wave conversion matrices described below into this basis.

Appendix C

Translation matrices

In the following, we list the translation matrices that make up $\mathbb{X}^{ij}$, defined in Eq. (2.2.14). The definition of the vector $\mathbf{X}_{ij}$, which points from the origin of object i to the origin of object j, is illustrated in Fig. 2-1.

C.1 Plane wave basis

Plane waves are eigenfunctions of the translation operator, which does not mix TE and TM vector plane wave functions.

If the z coordinates of object i are smaller than those of object j, then $-\mathcal{V}^{ij}$ is the only nonzero entry in $\mathbb{X}^{ij}$. Taking $\mathbf{X}_{ij}$ to point from the origin of object i, $\mathcal{O}_i$, to the origin of object j, $\mathcal{O}_j$ (that is, upward), we obtain

$$\mathcal{V}^{ij}_{\mathbf{k}_\perp P,\mathbf{k}'_\perp P'} = e^{-i\mathbf{k}_\perp\cdot\mathbf{X}_{ij,\perp}-\sqrt{\mathbf{k}_\perp^2+\kappa^2}X_{ij,z}}\frac{(2\pi)^2}{L^2}\delta^{(2)}(\mathbf{k}_\perp-\mathbf{k}'_\perp)\delta_{P,P'}. \tag{C.1.1}$$

If i is located above j, then $-\mathcal{W}^{ji}$ is the only nonzero entry in $\mathbb{X}^{ij}$. The vector $\mathbf{X}_{ji}$ points upward from $\mathcal{O}_j$ to $\mathcal{O}_i$, and we have

$$\begin{aligned}\mathcal{W}^{ji}_{\mathbf{k}_\perp P,\mathbf{k}'_\perp P'} &= \mathcal{V}^{ji*}_{\mathbf{k}'_\perp P',\mathbf{k}_\perp P}\frac{C_{\mathbf{k}_\perp P}(\kappa)}{C_{\mathbf{k}'_\perp P'}(\kappa)}\\ &= e^{i\mathbf{k}_\perp\cdot\mathbf{X}_{ji,\perp}-\sqrt{\mathbf{k}_\perp^2+\kappa^2}X_{ji,z}}\frac{(2\pi)^2}{L^2}\delta^{(2)}(\mathbf{k}_\perp-\mathbf{k}'_\perp)\delta_{P,P'}.\end{aligned} \tag{C.1.2}$$

Since the matrix is diagonal in $\mathbf{k}_\perp$ and P, the factor $\frac{C_{\mathbf{k}_\perp P}(\kappa)}{C_{\mathbf{k}'_\perp P'}(\kappa)}$ cancels.

C.2 Cylindrical wave basis

Translations do not mix the TE and TM modes of vector cylindrical wave functions. They are constructed by taking the scalar cylindrical wave function, multiplying by the unit vector $\hat{\mathbf{z}}$, and performing one or two curl operations. A TE vector cylindrical wave function is perpendicular to $\hat{\mathbf{z}}$, while the curl of a TM vector cylindrical wave function is perpendicular to $\hat{\mathbf{z}}$. Expanding any of the two vector wave functions around any other point in space must preserve its orthogonality property with respect to the constant vector $\hat{\mathbf{z}}$. So, the two are not mixed by the translation matrix.

If two objects i and j are outside of one another, $-\mathcal{U}^{ji}$ is the only nonzero submatrix of $\mathbb{X}^{ij}$. Again, let $\mathbf{X}_{ji}$ point from $\mathcal{O}_j$ to $\mathcal{O}_i$. We have

$$\mathcal{U}^{ji}_{k_z nP,k'_z n'P'} = K_{n-n'}\left(|\mathbf{X}_{ji,\perp}|\sqrt{k_z^2+\kappa^2}\right) e^{-ik_z X_{ji,z}-i(n-n')\theta_{ji}}(-1)^{n'}\delta_{P,P'}\frac{2\pi}{L}\delta(k_z-k'_z), \tag{C.2.1}$$

where $|\mathbf{X}_{ji,\perp}|$ is the distance of $\mathbf{X}_{ji}$ to the $\hat{\mathbf{z}}$ axis, *i.e.* the length of the projection onto the x-y plane, and θ_{ji} is the angle of $\mathbf{X}_{ji}$ in the x-y plane.

When object i is enclosed inside the surface of an infinite cylinder, inside object j, submatrix $-\mathcal{V}^{ij}$ is the only nonzero entry in $\mathbb{X}^{ij}$. We have

$$\mathcal{V}^{ij}_{k_z nP,k'_z n'P'} = I_{n-n'}\left(|\mathbf{X}_{ij,\perp}|\sqrt{k_z^2+\kappa^2}\right) e^{-ik_z X_{ij,z}-i(n-n')\theta_{ij}}(-1)^{n+n'}\delta_{P,P'}\frac{2\pi}{L}\delta(k_z-k'_z), \tag{C.2.2}$$

where $\mathbf{X}_{ij}$ points from $\mathcal{O}_i$ to $\mathcal{O}_j$,

If the roles of i and j are reversed, then $-\mathcal{W}^{ji}$ is the nonzero submatrix of $\mathbb{X}^{ij}$,

with

$$\mathcal{W}^{ji}_{k_z nP,k'_z n'P'} = \mathcal{V}^{ji*}_{k'_z n'P',k_z nP}\frac{C_P}{C_{P'}}$$
$$= I_{n-n'}\left(|\mathbf{X}_{ji,\perp}|\sqrt{k_z^2+\kappa^2}\right)e^{+ik_z X_{ji,z}-i(n-n')\theta_{ji}}(-1)^{n+n'}\delta_{P,P'}\tfrac{2\pi}{L}\delta(k_z-k'_z). \tag{C.2.3}$$

Since the matrix is diagonal in P, the factor $\frac{C_P}{C_{P'}}$ cancels.

C.3 Spherical wave basis

The TE vector wave functions are orthogonal to the radius vector $\mathbf{x}$. Since the same vector wave function cannot also be orthogonal everywhere to the radius vector of a shifted coordinate system, TE and TM polarizations mix under translation.

Suppose object i and its origin are outside a spherical separating surface, which encloses j. The nonzero submatrix of $\mathbb{X}^{ij}$ is $-\mathcal{U}^{ji}$, with

$$\mathcal{U}^{ji}_{l'm'M,lmM} = (-1)^{m+l}\sum_{l''}\left[l(l+1)+l'(l'+1)-l''(l''+1)\right]\sqrt{\frac{\pi(2l+1)(2l'+1)(2l''+1)}{l(l+1)l'(l'+1)}}$$
$$\times\begin{pmatrix} l & l' & l'' \\ 0 & 0 & 0\end{pmatrix}\begin{pmatrix} l & l' & l'' \\ m & -m' & m'-m\end{pmatrix}k_{l''}(\kappa|\mathbf{X}_{ji}|)Y_{l''m-m'}(\hat{\mathbf{X}}_{ji}),$$
$$\mathcal{U}^{ji}_{l'm'E,lmM} = -\frac{i\kappa}{\sqrt{l(l+1)l'(l'+1)}}\mathbf{X}_{ji}\cdot\left[\hat{\mathbf{x}}\frac{1}{2}\left(\lambda^+_{lm}A_{l'm'lm+1}(\mathbf{X}_{ji})+\lambda^-_{lm}A_{l'm'lm-1}(\mathbf{X}_{ji})\right)\right.$$
$$\left.+\,\hat{\mathbf{y}}\frac{1}{2i}\left(\lambda^+_{lm}A_{l'm'lm+1}(\mathbf{X}_{ji})-\lambda^-_{lm}A_{l'm'lm-1}(\mathbf{X}_{ji})\right)+\hat{\mathbf{z}}\,m\,A_{l'm'lm}(\mathbf{X}_{ji})\right],$$
$$\mathcal{U}^{ji}_{l'm'M,lmE} = -\mathcal{U}^{ji}_{l'm'E,lmM}, \qquad \mathcal{U}^{ji}_{l'm'E,lmE} = \mathcal{U}^{ji}_{l'm'M,lmM},$$

where

$$A_{l'm'lm}(\mathbf{X}_{ji}) = (-1)^{m+l}\sum_{l''}\sqrt{4\pi(2l+1)(2l'+1)(2l''+1)}$$
$$\times\begin{pmatrix} l & l' & l'' \\ 0 & 0 & 0\end{pmatrix}\begin{pmatrix} l & l' & l'' \\ m & -m' & m'-m\end{pmatrix}k_{l''}(\kappa|\mathbf{X}_{ji}|)Y_{l''m-m'}(\hat{\mathbf{X}}_{ji}) \tag{C.3.1}$$

and $\lambda_{lm}^{\pm} = \sqrt{(l \mp m)(l \pm m + 1)}$.

The translations between regular waves are described by the matrix elements

$$\begin{aligned}
\mathcal{V}^{ij}_{l'm'M,lmM} &= (-1)^m \sum_{l''} \left[l(l+1) + l'(l'+1) - l''(l''+1)\right] \sqrt{\frac{\pi(2l+1)(2l'+1)(2l''+1)}{l(l+1)l'(l'+1)}} \\
&\quad \times \begin{pmatrix} l & l' & l'' \\ 0 & 0 & 0 \end{pmatrix} \begin{pmatrix} l & l' & l'' \\ m & -m' & m'-m \end{pmatrix} i_{l''}(\kappa|\mathbf{X}_{ij}|)(-1)^{l''} Y_{l''m-m'}(\hat{\mathbf{X}}_{ij}), \\
\mathcal{V}^{ij}_{l'm'E,lmM} &= -\frac{i\kappa}{\sqrt{l(l+1)l'(l'+1)}} \mathbf{X}_{ij} \cdot \left[\hat{\mathbf{x}} \frac{1}{2} \left(\lambda^+_{lm} B_{l'm'lm+1}(\mathbf{X}_{ij}) + \lambda^-_{lm} B_{l'm'lm-1}(\mathbf{X}_{ij})\right)\right. \\
&\quad \left. + \hat{\mathbf{y}} \frac{1}{2i} \left(\lambda^+_{lm} B_{l'm'lm+1}(\mathbf{X}_{ij}) - \lambda^-_{lm} B_{l'm'lm-1}(\mathbf{X}_{ij})\right) + \hat{\mathbf{z}}\, m\, B_{l'm'lm}(\mathbf{X}_{ij})\right], \\
\mathcal{V}^{ij}_{l'm'M,lmE} &= -\mathcal{V}^{ij}_{l'm'E,lmM}, \qquad \mathcal{V}^{ij}_{l'm'E,lmE} = \mathcal{V}^{ij}_{l'm'M,lmM},
\end{aligned}$$

where

$$\begin{aligned}
B_{l'm'lm}(\mathbf{X}_{ij}) &= (-1)^m \sum_{l''} \sqrt{4\pi(2l+1)(2l'+1)(2l''+1)} \\
&\quad \times \begin{pmatrix} l & l' & l'' \\ 0 & 0 & 0 \end{pmatrix} \begin{pmatrix} l & l' & l'' \\ m & -m' & m'-m \end{pmatrix} i_{l''}(\kappa|\mathbf{X}_{ij}|)(-1)^{l''} Y_{l''m-m'}(\hat{\mathbf{X}}_{ij})
\end{aligned} \tag{C.3.2}$$

and $\lambda_{lm}^{\pm} = \sqrt{(l \mp m)(l \pm m + 1)}$.

The matrix $\mathcal{W}^{ji}$ is related to $\mathcal{V}^{ji}$,

$$\mathcal{W}^{ji}_{l'm'P',lmP} = \mathcal{V}^{ji\dagger}_{l'm'P',lmP} \frac{C_{P'}(\kappa)}{C_P(\kappa)}. \tag{C.3.3}$$

$\mathcal{V}^{ji}$, of course, is the same as $\mathcal{V}^{ij}$ with $\mathbf{X}_{ij}$ replaced by $\mathbf{X}_{ji}$. To be more specific, the elements correspond in the following way,

$$\begin{aligned}
\mathcal{W}^{ji}_{l'm'M,lmM} &= \mathcal{V}^{ji*}_{lmM,l'm'M}, \quad \mathcal{W}^{ji}_{l'm'E,lmM} = -\mathcal{V}^{ji*}_{lmM,l'm'E}, \\
\mathcal{W}^{ji}_{l'm'M,lmE} &= -\mathcal{V}^{ji*}_{lmE,l'm'M}, \quad \mathcal{W}^{ji}_{l'm'E,lmE} = \mathcal{V}^{ji*}_{lmE,l'm'E}.
\end{aligned} \tag{C.3.4}$$

Appendix D

Wave conversion matrices

It is not necessary to express all the objects' scattering amplitudes in the same basis. Here, we supply the matrices that convert modified vector plane wave functions to spherical or cylindrical vector wave functions.

D.1 Vector plane wave functions to spherical vector wave functions

$$\begin{aligned}\mathbf{M}^{\mathrm{reg}}_{\mathbf{k}_\perp}(\kappa,\mathbf{x}) &= \sum_{lm} D_{lmM,\mathbf{k}_\perp M}\mathbf{M}^{\mathrm{reg}}_{lm}(\kappa,\mathbf{x}) + D_{lmE,\mathbf{k}_\perp M}\mathbf{N}^{\mathrm{reg}}_{lm}(\kappa,\mathbf{x})\,,\\ \mathbf{N}^{\mathrm{reg}}_{\mathbf{k}_\perp}(\kappa,\mathbf{x}) &= \sum_{lm} D_{lmM,\mathbf{k}_\perp E}\mathbf{M}^{\mathrm{reg}}_{lm}(\kappa,\mathbf{x}) + D_{lmE,\mathbf{k}_\perp E}\mathbf{N}^{\mathrm{reg}}_{lm}(\kappa,\mathbf{x}).\end{aligned} \tag{D.1.1}$$

The conversion matrices are obtained from the decomposition of a plane wave in spherical coordinates,

$$\begin{aligned}D_{lmM,\mathbf{k}_\perp M} &= \sqrt{\frac{4\pi(2l+1)(l-m)!}{l(l+1)(l+m)!}}\frac{|\mathbf{k}_\perp|}{\kappa}e^{-im\phi_{\mathbf{k}_\perp}}P_l'^m\left(\sqrt{\mathbf{k}_\perp^2+\kappa^2}/\kappa\right)\,,\\ D_{lmE,\mathbf{k}_\perp M} &= \sqrt{\frac{4\pi(2l+1)(l-m)!}{l(l+1)(l+m)!}}im\frac{\kappa}{|\mathbf{k}_\perp|}e^{-im\phi_{\mathbf{k}_\perp}}P_l^m\left(\sqrt{\mathbf{k}_\perp^2+\kappa^2}/\kappa\right)\,,\\ D_{lmE,\mathbf{k}_\perp E} &= D_{lmM,\mathbf{k}_\perp M}, \qquad D_{lmM,\mathbf{k}_\perp E} = -D_{lmE,\mathbf{k}_\perp M},\end{aligned} \tag{D.1.2}$$

where P_l^m is the associated Legendre polynomial and prime indicates the derivative of P_l^m with respect to its argument.

D.2 Vector plane wave functions to cylindrical vector wave functions

The cylindrical vector wave functions are defined as before, but now we consider regular vector plane wave functions that decay along the $-\hat{\mathbf{x}}$ axis instead of the $-\hat{\mathbf{z}}$ axis,

$$\begin{aligned}\mathbf{M}^{\mathrm{reg}}_{\mathbf{k}_\perp}(\kappa,\mathbf{x}) &= \frac{1}{\sqrt{k_y^2+k_z^2}}\boldsymbol{\nabla}\times e^{\sqrt{\kappa^2+k_y^2+k_z^2}x+ik_y y+ik_z z}\hat{\mathbf{x}},\\ \mathbf{N}^{\mathrm{reg}}_{\mathbf{k}_\perp}(\kappa,\mathbf{x}) &= \frac{1}{\kappa\sqrt{k_y^2+k_z^2}}\boldsymbol{\nabla}\times\boldsymbol{\nabla}\times e^{\sqrt{\kappa^2+k_y^2+k_z^2}x+ik_y y+ik_z z}\hat{\mathbf{x}}.\end{aligned} \tag{D.2.1}$$

The vector plane wave functions can be decomposed in vector cylindrical wave functions,

$$\begin{aligned}\mathbf{M}^{\mathrm{reg}}_{\mathbf{k}_\perp}(\kappa,\mathbf{x}) &= \sum_n D_{k_z nM,\mathbf{k}_\perp M}\mathbf{M}^{\mathrm{reg}}_{k_z n}(\kappa,\mathbf{x}) + D_{k_z nE,\mathbf{k}_\perp M}\mathbf{N}^{\mathrm{reg}}_{k_z n}(\kappa,\mathbf{x}),\\ \mathbf{N}^{\mathrm{reg}}_{\mathbf{k}_\perp}(\kappa,\mathbf{x}) &= \sum_n D_{k_z nM,\mathbf{k}_\perp E}\mathbf{M}^{\mathrm{reg}}_{k_z n}(\kappa,\mathbf{x}) + D_{k_z nE,\mathbf{k}_\perp E}\mathbf{N}^{\mathrm{reg}}_{k_z n}(\kappa,\mathbf{x}),\end{aligned} \tag{D.2.2}$$

using the conversion matrix elements

$$\begin{aligned}D_{k_z nM,\mathbf{k}_\perp M} &= -i\frac{k_z}{\sqrt{k_y^2+k_z^2}}\sqrt{1+\xi^2}\left(\sqrt{1+\xi^2}+\xi\right)^n,\\ D_{k_z nE,\mathbf{k}_\perp M} &= i\frac{\kappa}{\sqrt{k_y^2+k_z^2}}\xi\left(\sqrt{1+\xi^2}+\xi\right)^n,\\ D_{k_z nE,\mathbf{k}_\perp E} &= D_{k_z nM,\mathbf{k}_\perp M}, \qquad D_{k_z nM,\mathbf{k}_\perp E} = -D_{k_z nE,\mathbf{k}_\perp M},\end{aligned} \tag{D.2.3}$$

where $\xi = \frac{k_y}{\sqrt{\kappa^2+k_z^2}}$ and $\mathbf{k}_\perp = (k_y, k_z)$.

D.3 Vector plane wave functions to parabolic cylinder vector wave functions

To agree with the coordinate choices in Ref. [80], we must convert the outgoing vector plane wave functions,

$$\begin{aligned}
\mathbf{M}^{\text{out}}_{\mathbf{k}'_\perp}(\kappa,\mathbf{x}') &= \frac{1}{\sqrt{k_x'^2+k_z'^2}}\boldsymbol{\nabla}'\times e^{ik'_x x'-\sqrt{\kappa^2+k_x'^2+k_z'^2}y'+ik'_z z'}\hat{\mathbf{y}}'\,,\\
\mathbf{N}^{\text{out}}_{\mathbf{k}'_\perp}(\kappa,\mathbf{x}') &= \frac{1}{\kappa\sqrt{k_x'^2+k_z'^2}}\boldsymbol{\nabla}'\times\boldsymbol{\nabla}'\times e^{ik'_x x'-\sqrt{\kappa^2+k_x'^2+k_z'^2}y'+ik'_z z'}\hat{\mathbf{y}}'\,,
\end{aligned} \tag{D.3.1}$$

to regular vector parabolic cylinder wave functions,

$$\begin{aligned}
\mathbf{M}^{\text{out}}_{\mathbf{k}'_\perp}(\kappa,\mathbf{x}') &= \sum_{\nu=0}^{\infty} D_{k_z\nu M,\mathbf{k}'_\perp M}\mathbf{M}^{\text{reg}}_{k_z\nu}(\kappa,\mathbf{x}) + D_{k_z\nu E,\mathbf{k}'_\perp M}\mathbf{N}^{\text{reg}}_{k_z\nu}(\kappa,\mathbf{x})\,,\\
\mathbf{N}^{\text{reg}}_{\mathbf{k}'_\perp}(\kappa,\mathbf{x}') &= \sum_{\nu=0}^{\infty} D_{k_z\nu M,\mathbf{k}'_\perp E}\mathbf{M}^{\text{reg}}_{k_z\nu}(\kappa,\mathbf{x}) + D_{k_z\nu E,\mathbf{k}'_\perp E}\mathbf{N}^{\text{reg}}_{k_z\nu}(\kappa,\mathbf{x})\,,
\end{aligned} \tag{D.3.2}$$

using the conversion matrix elements

$$\begin{aligned}
D_{k_z\nu M,\mathbf{k}'_\perp M} &= \frac{ik'_z\sqrt{\kappa^2+k_x'^2+k_z'^2}}{\sqrt{\kappa^2+k_z'^2}\sqrt{k_x'^2+k_z'^2}}\frac{\sqrt{2}}{\nu!\sqrt{1+k_y/\sqrt{\kappa^2+k_z'^2}}}\left(i\sqrt{\frac{k_y/\sqrt{\kappa^2+k_z'^2}-1}{k_y/\sqrt{\kappa^2+k_z'^2}+1}}\right)^{\nu}\,,\\
D_{k_z\nu E,\mathbf{k}'_\perp M} &= \frac{-i\kappa k'_x}{\sqrt{\kappa^2+k_z'^2}\sqrt{k_x'^2+k_z'^2}}\frac{\sqrt{2}}{\nu!\sqrt{1+k_y/\sqrt{\kappa^2+k_z'^2}}}\left(i\sqrt{\frac{k_y/\sqrt{\kappa^2+k_z'^2}-1}{k_y/\sqrt{\kappa^2+k_z'^2}+1}}\right)^{\nu}\,,\\
D_{k_z\nu E,\mathbf{k}'_\perp E} &= D_{k_z\nu M,\mathbf{k}'_\perp M}\,,\qquad D_{k_z\nu M,\mathbf{k}'_\perp E} = -D_{k_z\nu E,\mathbf{k}'_\perp M}\,,
\end{aligned} \tag{D.3.3}$$

where $\mathbf{k}'_\perp = (k'_x, k'_z)$. The coordinate system has been rotated by θ around the $\hat{\mathbf{z}}$ axis so that $\mathbf{x} = (x, y, z)$ and $\mathbf{x}' = (x', y', z')$ are related by $x = x'\cos\theta + y'\sin\theta$, $y = -x'\sin\theta + y'\cos\theta$, and $z = z'$. The momenta labels are related by $k_y = \sqrt{\kappa^2 + k_x'^2 + k_z'^2}\cos\theta + ik'_x\sin\theta$ and $k_z = k'_z$.

Bibliography

[1] S. K. Lamoreaux, Phys. Rev. Lett. **78**, 5 (1997).

[2] U. Mohideen and A. Roy, Phys. Rev. Lett. **81**, 4549 (1998).

[3] A. Roy, C.-Y. Lin, and U. Mohideen, Phys. Rev. D **60**, 111101(R) (1999).

[4] T. Ederth, Phys. Rev. A **62**, 062104 (2000).

[5] H. B. Chan, V. A. Aksyuk, R. N. Kleiman, D. J. Bishop, and F. Capasso, Science **291**, 1941 (2001).

[6] F. Chen, U. Mohideen, G. L. Klimchitskaya, and V. M. Mostepanenko, Phys. Rev. Lett. **88**, 101801 (2002).

[7] V. Druzhinina and M. DeKieviet, Phys. Rev. Lett. **91**, 193202 (2003).

[8] D. M. Harber, J. M. Obrecht, J. M. McGuirk, and E. A. Cornell, Phys. Rev. A **72**, 033610 (2005).

[9] F. Chen, G. L. Klimchitskaya, V. M. Mostepanenko, and U. Mohideen, Phys. Rev. Lett. **97**, 170402 (2006).

[10] D. E. Krause, R. S. Decca, D. López, and E. Fischbach, Phys. Rev. Lett. **98**, 050403 (2007).

[11] R. S. Decca, D. López, E. Fischbach, G. L. Klimchitskaya, D. E. Krause, and V. M. Mostepanenko, Phys. Rev. D **75**, 077101 (2007).

[12] F. Chen, G. L. Klimchitskaya, V. M. Mostepanenko, and U. Mohideen, Phys. Rev. B **76**, 035338 (2007).

[13] J. N. Munday and F. Capasso, Phys. Rev. A **75**, 060102(R) (2007).

[14] H. B. Chan, Y. Bao, J. Zou, R. A. Cirelli, F. Klemens, W. M. Mansfield, and C. S. Pai, Phys. Rev. Lett. **101**, 030401 (2008).

[15] W. J. Kim, M. Brown-Hayes, D. A. R. Dalvit, J. H. Brownell, and R. Onofrio, Phys. Rev. A **78**, 020101(R) (2008).

[16] G. Palasantzas, P. J. van Zwol, and J. T. M. De Hosson, Appl. Phys. Lett. **93**, 121912 (2008).

[17] J. N. Munday, F. Capasso, and V. A. Parsegian, Nature **457**, 170 (2009).

[18] F. Capasso, J. N. Munday, D. Iannuzzi, and H. B. Chan, IEEE J. Sel. Top. Quant. **13**, 400 (2007).

[19] G. L. Klimchitskaya, U. Mohideen, and V. M. Mostepanenko, Rev. Mod. Phys. **81**, 1827 (2009).

[20] H. B. G. Casimir and D. Polder, Phys. Rev. **73**, 360 (1948).

[21] H. B. G. Casimir, Proc. K. Ned. Akad. Wet. **51**, 793 (1948).

[22] G. Feinberg and J. Sucher, J. Chem. Phys. **48**, 3333 (1968).

[23] G. Feinberg and J. Sucher, Phys. Rev. A **2**, 2395 (1970).

[24] E. M. Lifshitz, Dokl. Akad. Nauk SSSR **100**, 879 (1955).

[25] E. M. Lifshitz, Sov. Phys. JETP **2**, 73 (1956).

[26] E. M. Lifshitz, Sov. Phys. JETP **3**, 977 (1957).

[27] I. E. Dzyaloshinskii, E. M. Lifshitz, and L. P. Pitaevskii, Adv. Phys. **10**, 165 (1961).

[28] E. M. Lifshitz and L. P. Pitaevskii, *Statistical Physics Part 2* (Pergamon Press, Oxford, 1980).

[29] V. A. Parsegian, *van der Waals Forces* (Cambridge University Press, Cambridge, 2005).

[30] T. Emig, N. Graham, R. L. Jaffe, and M. Kardar, Phys. Rev. Lett. **99**, 170403 (2007).

[31] T. Emig, N. Graham, R. L. Jaffe, and M. Kardar, Phys. Rev. D **77**, 025005 (2008).

[32] S. J. Rahi, T. Emig, N. Graham, R. L. Jaffe, and M. Kardar, Phys. Rev. D **80**, 085021 (2009).

[33] E. I. Kats, Sov. Phys. JETP **46**, 109 (1977).

[34] M. T. Jaekel and S. Reynaud, J. Physique I **1**, 1395 (1991).

[35] C. Genet, A. Lambrecht, and S. Reynaud, Phys. Rev. A **67**, 043811 (2003).

[36] A. Lambrecht, P. A. Maia Neto, and S. Reynaud, New J. Phys. **8**, 243 (2006).

[37] R. Balian and B. Duplantier, Ann. Phys., NY **104**, 300 (1977).

[38] R. Balian and B. Duplantier, Ann. Phys., NY **112**, 165 (1978).

[39] M. J. Renne, Physica **56**, 125 (1971).

[40] M. G. Krein, Mat. Sborn. (NS) **33**, 597 (1953).

[41] M. G. Krein, Sov. Math.-Dokl. **3**, 707 (1962).

[42] M. S. Birman and M. G. Krein, Sov. Math.-Dokl. **3**, 740 (1962).

[43] M. Henseler, A. Wirzba, and T. Guhr, Ann. Phys., NY **258**, 286 (1997).

[44] A. Wirzba, Phys. Rep. **309**, 1 (1999).

[45] A. Bulgac and A. Wirzba, Phys. Rev. Lett. **87**, 120404 (2001).

[46] A. Bulgac, P. Magierski, and A. Wirzba, Phys. Rev. D **73**, 025007 (2006).

[47] A. Wirzba, J. Phys. A: Math. Theor. **41**, 164003 (2008).

[48] N. Graham, M. Quandt, and H. Weigel, *Spectral Methods in Quantum Field Theory* (Springer-Verlag, Berlin, 2009).

[49] M. Bordag, D. Robaschik, and E. Wieczorek, Ann. Phys. (N.Y.) **165**, 192 (1985).

[50] D. Robaschik, K. Scharnhorst, and E. Wieczorek, Ann. Phys. (N.Y.) **174**, 401 (1987).

[51] H. Li and M. Kardar, Phys. Rev. Lett. **67**, 3275 (1991).

[52] H. Li and M. Kardar, Phys. Rev. A **46**, 6490 (1992).

[53] R. Golestanian and M. Kardar, Phys. Rev. Lett. **78**, 3421 (1997).

[54] R. Golestanian and M. Kardar, Phys. Rev. A **58**, 1713 (1998).

[55] T. Emig, A. Hanke, R. Golestanian, and M. Kardar, Phys. Rev. Lett. **87**, 260402 (2001).

[56] T. Emig, A. Hanke, R. Golestanian, and M. Kardar, Phys. Rev. A **67**, 022114 (2003).

[57] R. Büscher and T. Emig, Phys. Rev. Lett. **94**, 133901 (2005).

[58] O. Kenneth and I. Klich, Phys. Rev. Lett. **97**, 160401 (2006).

[59] J. Schwinger, Lett. Math. Phys. **1**, 43 (1975).

[60] O. Kenneth and I. Klich, Phys. Rev. B **78**, 014103 (2008).

[61] K. A. Milton, P. Parashar, and J. Wagner, Phys. Rev. Lett. **101**, 160402 (2008).

[62] K. A. Milton, P. Parashar, and J. Wagner (2008), `arXiv:0811.0128`.

[63] M. T. H. Reid, A. W. Rodriguez, J. White, and S. G. Johnson, Phys. Rev. Lett. **103**, 040401 (2009).

[64] R. Golestanian, Phys. Rev. A **80**, 012519 (2009).

[65] C. C. Ttira, C. D. Fosco, and E. L. Losada (2009), `arXiv:0905.4756`.

[66] M. Schaden and L. Spruch, Phys. Rev. **A58**, 935 (1998).

[67] W. C. Chew, J. M. Jin, E. Michielssen, and J. M. Song, eds., *Fast and Efficient Algorithms in Computational Electrodynamics* (Artech House, Norwood, MA, 2001).

[68] A. W. Rodriguez, J. D. Joannopoulos, and S. G. Johnson, Phys. Rev. A **77**, 062107 (2008).

[69] M. Levin, A. P. McCauley, A. W. Rodriguez, M. T. H. Reid, and S. G. Johnson (2010), `arXiv:1003.3487`.

[70] C. P. Bachas, J. Phys. A: Math. Theor. **40**, 9089 (2007).

[71] S. J. Rahi, M. Kardar, and T. Emig (2009), `arXiv:0911.5364`.

[72] B. W. Harris, F. Chen, and U. Mohideen, Phys. Rev. A **62**, 052109 (2000).

[73] R. S. Decca, D. López, E. Fischbach, and D. E. Krause, Phys. Rev. Lett. **91**, 050402 (2003).

[74] D. Iannuzzi, M. Lisanti, and F. Capasso, Proc. Natl. Acad. Sci. USA **101**, 4019 (2004).

[75] T. Emig, J. Stat. Mech. p. P04007 (2008).

[76] A. Canaguier-Durand, P. A. Maia Neto, I. Cavero-Pelaez, A. Lambrecht, and S. Reynaud, Phys. Rev. Lett. **102**, 230404 (2009).

[77] A. Canaguier-Durand, P. A. M. Neto, A. Lambrecht, and S. Reynaud, Phys. Rev. Lett. **104**, 040403 (2010).

[78] R. Zandi, T. Emig, and U. Mohideen (2010), `arXiv:1003.0068`.

[79] T. Emig, R. L. Jaffe, M. Kardar, and A. Scardicchio, Phys. Rev. Lett. **96**, 080403 (2006).

[80] N. Graham, A. Shpunt, T. Emig, S. J. Rahi, R. L. Jaffe, and M. Kardar, Phys. Rev. D **81**, 061701(R) (2010).

[81] D. A. R. Dalvit, F. C. Lombardo, F. D. Mazzitelli, and R. Onofrio, Phys. Rev. A **74**, 020101(R) (2006).

[82] S. J. Rahi, T. Emig, R. L. Jaffe, and M. Kardar, Phys. Rev. A **78**, 012104 (2008).

[83] S. Zaheer, S. J. Rahi, T. Emig, and R. L. Jaffe, Phys. Rev. A **81**, 030502(R) (2010).

[84] S. J. Rahi and S. Zaheer, Phys. Rev. Lett. **104**, 070405 (2010).

[85] K. A. Milton, J. Wagner, P. Parashar, and I. Brevik (2010), `arXiv:1001.4163`.

[86] R. P. Feynman and A. R. Hibbs, *Quantum Mechanics and Path Integrals* (McGraw-Hill, New York, 1965).

[87] N. Graham, R. L. Jaffe, V. Khemani, M. Quandt, M. Scandurra, and H. Weigel, Phys. Lett. B **572**, 196 (2003).

[88] P. M. Morse and H. Feshbach, *Methods of Theoretical Physics* (McGraw-Hill, New York, 1953).

[89] E. Merzbacher, *Quantum Mechanics* (John Wiley and Sons, New York, 1998).

[90] R. G. Newton, *Scattering Theory of Waves and Particles* (Dover, Mineola, NY, 2002).

[91] P. C. Waterman, Proceedings of the IEEE **53**, 805 (1965).

[92] P. C. Waterman, Phys. Rev. D **3**, 825 (1971).

[93] B. A. Lippmann and J. Schwinger, Phys. Rev. **79**, 469 (1950).

[94] T. H. Boyer, Phys. Rev. A **9**, 2078 (1974).

[95] O. Kenneth, I. Klich, A. Mann, and M. Revzen, Phys. Rev. Lett. **89**, 033001 (2002).

[96] S. Earnshaw, Trans. Camb. Phil. Soc. **7**, 97 (1842).

[97] W. Braunbek, Z. Phys. **112**, 753 (1939).

[98] W. Braunbek, Z. Phys. **112**, 764 (1939).

[99] A. Geim, Phys. Today **51(9)**, 36 (1998).

[100] T. B. Jones, *Electromechanics of Particles* (Cambridge University Press, Cambridge, 1995).

[101] A. Ashkin, Phys. Rev. Lett. **24**, 156 (1970).

[102] A. Ashkin and J. P. Gordon, Opt. Lett. **8**, 511 (1983).

[103] L. D. Landau and E. M. Lifshitz, *Electrodynamics of continuous media* (Pergamon Press, Oxford, 1984).

[104] F. S. S. Rosa, D. A. R. Dalvit, and P. W. Milonni, Phys. Rev. Lett. **100**, 183602 (2008).

[105] F. S. S. Rosa, J. Phys.: Conf. Ser. **161**, 012039 (2009).

[106] R. Zhao, J. Zhou, T. Koschny, E. N. Economou, and C. M. Soukoulis, Phys. Rev. Lett. **103**, 103602 (2009).

[107] F. London, Z. Physik **63**, 245 (1930).

[108] J. D. Jackson, *Classical Electrodynamics* (Wiley, New York, 1998), 3rd ed.

[109] S. J. Rahi, A. W. Rodriguez, T. Emig, R. L. Jaffe, S. G. Johnson, and M. Kardar, Phys. Rev. A **77**, 030101(R) (2008).

[110] P. A. Maia Neto, A. Lambrecht, and S. Reynaud, Phys. Rev. A **78**, 012115 (2008).

[111] A. W. Rodriguez, J. N. Munday, J. D. Joannopoulos, F. Capasso, D. A. R. Dalvit, and S. G. Johnson, Phys. Rev. Lett. **101**, 190404 (2008).

[112] T. Emig, N. Graham, R. L. Jaffe, and M. Kardar, Phys. Rev. A **79**, 054901 (2009).

[113] S. Kondrat, L. Harnau, and S. Dietrich, J. Chem. Phys. **131**, 204902 (2009).

[114] D. Peer, J. M. Karp, S. Hong, O. C. Farokhzad, R. Margalit, and R. Langer, Nat. Nano. **2**, 751 (2007).

[115] P. Mal, B. Breiner, K. Rissanen, and J. R. Nitschke, Science **324**, 1697 (2009).

[116] C. Yeh, Phys. Rev. **135**, A1193 (1964).

[117] V. A. Erma, Phys. Rev. **179**, 1238 (1969).

[118] R. F. Millar, Radio Sci. **8**, 785 (1973).

[119] I. Pirozhenko, A. Lambrecht, and V. B. Svetovoy, New J. Phys. **8**, 238 (2006).

[120] A. Milling, P. Mulvaney, and I. Larson, J. Colloid Interface Sci. **180**, 460 (1996).

[121] L. Bergström, Adv. Colloid Interface Sci. **70**, 125 (1997).

[122] H. Gies, K. Langfeld, and L. Moyaerts, J. High Energy Phys. 06 **2003**, 018 (2003).

[123] R. L. Jaffe and A. Scardicchio, Phys. Rev. Lett. **92**, 070402 (2004).

[124] M. Bordag and V. Nikolaev, J. Phys. A-Math. Theor. **41**, 164002 (2008).

[125] S. Reynaud, P. A. Maia Neto, and A. Lambrecht, J. Phys. A-Math. Theor. **41**, 164004 (2008).

[126] M. Bordag and V. Nikolaev, Phys. Rev. D **81**, 065011 (2010).

[127] H. Bateman, Trans. Amer. Math. Soc. **33**, 817 (1931).

[128] H. Gies and K. Klingmüller, Phys. Rev. Lett. **97**, 220405 (2006).

[129] A. Weber and H. Gies, Phys. Rev. D **80**, 065033 (2009).

[130] M. Antezza, L. P. Pitaevskii, S. Stringari, and V. B. Svetovoy, Phys. Rev. A **77**, 022901 (2008).

[131] G. Bimonte, Phys. Rev. A **80**, 042102 (2009).

[132] A. Ashourvan, M. Miri, and R. Golestanian, Phys. Rev. E **75**, 040103 (2007).

[133] S. Sachdev, *Quantum Phase Transitions* (Cambridge University Press, Cambridge, 1999).

[134] L. D. Landau and E. M. Lifshitz, *Statistical Physics I*, vol. 5 (Pergamon Press, Oxford, 1980).

[135] A. A. Abrikosov, L. P. Gorkov, and I. E. Dzyaloshinski, *Methods of Quantum Field Theory in Statistical Physics* (Dover, New York, 1975).

[136] F. M. Schulz, K. Stamnes, and J. J. Stamnes, Appl. Optics **37**, 7875 (1998).

[137] N. Graham and K. D. Olum, Phys. Rev. D **72**, 025013 (2005).

[138] F. Alhargan, ACM T Math Software **26**, 390 (2000).

[139] F. Alhargan, ACM T Math Software **26**, 408 (2000).